The role of RIPK1 signaling in liver injury and cancer

Inaugural-Dissertation

zur Erlangung des Doktorgrades
der Mathematisch-Naturwissenschaftlichen Fakultät
der Universität zu Köln

vorgelegt von
Trieu My Van
aus Köln

Köln 2017

Köln, 2017

Berichterstatter: Prof. Dr. Manolis Pasparakis
                             Prof. Dr. Kay Hofmann

Tag der mündlichen Prüfung: 23.05.2017

Zusammenfassung

Die Serin/Threonin Rezeptor-interagierende Protein Kinase (RIPK)1 ist ein zentrales Protein, welches den Ausgang von TNF Rezeptor 1 (TNFR1)- und Toll-ähnlicher Rezeptor (TLR)-vermittelten Signalen durch Kinase-abhängigen und Kinase-unabhängigen Funktionen determiniert. Bis heute ist es unklar, in wie fern RIPK1 in der Regulierung von Leberfunktionen agiert. Deshalb wurde ein konditionales RIPK1-Allel erzeugt, welches die Cre-Recombinase vermittelte Deletion von RIPK1 in Leber-parenchymalen Zellen (LPZ) ermöglicht. Zusätzlich wurden RIPK1-Mutanten verwendet, welche, aufgrund eines Aminosäureaustausches an der Position 138 von Asparaginsäure zu Asparagin, eine mutierte Form von RIPK1 exprimieren (RIPK1D138N) und deshalb keine Kinaseaktivität besitzen. Mit Hilfe dieser Mutanten sollten die Kinase-abhängigen und Kinase-unabhängigen Funktionen von RIPK1 in der Regulierung bzw. Induzierung von Leberschäden und in der Initiierung von Leberkrebs untersucht werden. Die LPZ-spezifische Deletion von RIPK1 beeinflusste weder die Leberentwicklung noch die Leber Homöostase unter normalen Konditionen, sensibilisierte RIPK1-defiziente Hepatozyten jedoch zu spontaner Apoptose *in vitro*. RIPK1^LPZ-KO Mäuse zeigten eine erhöhte Sensitivität gegenüber einer Lipopolysaccharid (LPS)-Injektion aufgrund von erhöhter Apoptose von Hepatozyten. Die LPZ-spezifische Deletion von TNFR1, Fas-assoziiert via *Death Domain* (FADD) oder TNFRSF1A-assoziiert via *Death Domain* (TRADD) schützte RIPK1-defiziente Hepatozyten vor Zelltod, wodurch die hohe Sensitivität von RIPK1^LPZ-KO Mäusen nach einer LPS-Injektion vermindert werden konnte. Die Inaktivierung der Kinase Aktivität von RIPK1 schützte Mäuse vor LPS/D-Galactosamin (D-GalN) induzierten Leberschäden. Die LPZ-spezifische Deletion von RIPK1, aber nicht die Inaktivierung der Kinase Aktivität in Mäusen reduzierte Diethylnitrosamin (DEN)-induzierten Leberkrebs, was auf eine Kinase-unabhängige Funktion von RIPK1 in der Initiierung von Leberkrebs hindeutet. Darüber hinaus reduzierte die LPZ-spezifische Deletion von RIPK1 zum Teil DEN-induzierte Tumorentstehung in einem Mausmodel mit induzierter Adipositas. Eine reduzierte Entstehung von DEN-induziertem Leberkrebs korrelierte mit einer erhöhten Anzahl von frühzeitiger Caspase-8-vermittelter Apoptose und reduzierten DNS Schäden in RIPK1^LPZ-KO Mäusen. Die Inhibierung des frühzeitigen Zelltodes durch die zusätzliche LPZ-spezifische Deletion von TNFR1 stellte die volle Entstehung von DEN-induziertem Leberkrebs in RIPK1^LPZ-KO Mäusen wieder her. Zusammenfassend kann geschlussfolgert werden, dass die Resultate dieser Arbeit eine neue, wichtige Kinase-unabhängige Funktion von RIPK1 für die Expression von Überlebenssignalen enthüllen wodurch das Überleben von Hepatozyten beeinflusst wird. Durch diese Funktion reduziert RIPK1 durch LPS Injektion induzierte akute Leberschäden und verhindert somit Leberversagen. Wohingegen RIPK1 durch seine Überlebensfunktion erhöhten Zelltod nach DEN Injektion blockiert und dadurch zu erhöhter Tumorentstehung nach einer DEN Injektion führt.

Summary

The serine/threonine kinase receptor-interacting protein kinase (RIPK) 1 with pro-death kinase-dependent and pro-survival kinase-independent functions has emerged as an important regulator of cell death, survival and inflammation downstream of death receptors (DR) and Toll-like receptors (TLR), including tumor necrosis factor receptor (TNFR) 1 and TLR4 respectively. The functions of RIPK1 in regulating liver homeostasis, inflammation and cell death are poorly understood and remain to be elucidated. In this study we aimed to investigate the biological significance of the kinase-dependent and -independent functions of RIPK1 specifically in maintaining liver homeostasis and in the regulation of acute liver injury and carcinogenesis using well-established murine models. Accordingly, mice lacking RIPK1 or its kinase activity specifically in liver-parenchymal cells (LPC) were generated using the Cre/LoxP system. LPC-specific RIPK1 deficiency did not affect normal liver development and homeostasis but sensitized RIPK1-deficient hepatocytes to spontaneous apoptotic death *in vitro*. *In vivo*, RIPK1^{LPC-KO} mice were highly sensitive to lipopolysaccharide (LPS)-induced injury showing massive hepatocyte apoptosis that resulted in early death of mice. LPC-specific TNFR1, Fas-Associated via Death Domain (FADD) or TNFRSF1A-Associated via Death Domain (TRADD) ablation prevented LPS-induced liver injury in RIPK1^{LPC-KO} mice, identifying TNFR1-TRADD-FADD-induced hepatocyte apoptosis as the cause of liver damage. Inactivation of RIPK1 kinase activity (D138N) did not phenocopy the high sensitivity of RIPK1^{LPC-KO} mice to LPS-induced liver injury suggesting a RIPK1 scaffolding function in preventing LPS-induced toxicity. However, inactivation of RIPK1 kinase activity partially prevented TNFR1-induced cell death caused by LPS/D-Galactosamine (D-GalN) suggesting a RIPK1 kinase-dependent function in mediating LPS/D-GalN-induced death.

LPC-specific RIPK1 knockout but not loss of its kinase activity reduced Diethylnitrosamine (DEN)-induced liver carcinogenesis in mice suggesting a kinase-independent function of RIPK1 in promoting liver tumorigenesis. Moreover, LPC-specific RIPK1 deficiency also reduced liver tumor formation in a model of dietary obesity-driven DEN-induced hepatocarcinogenesis. Reduced liver tumor development correlated with increased early DEN-induced Caspase-8-mediated hepatocyte apoptosis and reduced γH2AX levels in the liver of RIPK1^{LPC-KO} mice. LPC-specific TNFR1 deficiency prevented increased early hepatocyte apoptosis and restored liver tumor development in DEN-injected RIPK1^{LPC-KO} TNFR1^{LPC-KO} mice.

Taken together, the results presented in this work reveal a novel, important kinase-independent scaffolding function of RIPK1 in the regulation of liver cell survival, acute liver damage and liver cancer development.

Table of Content

Abbreviations

ABC	Avidin-Biotin-Complex
ALF	Acute liver failure
Alfp	α-fetoprotein
ALS	Amyotrophic lateral sclerosis
ALT	Alanine aminotransferase
ANK	Ankyrin repeats
APAF-1	Apoptotic protease activating factor 1
APAP	Acetaminophen
AST	Aspartate aminotransferase
ATM	Ataxia telangiectasia mutated
ATR	Ataxia telangiectasia and Rad3-related protein
BAFF	B-cell activating factor of the TNF family
BCL-2	B-cell lymphoma 2
Bid	BH3 interacting domain death agonist
BILTS	Total bilirubin special
BMDMs	Bone marrow derived macrophages
BSA	Bovine Serum Albumin
BW	Body weight
CC3/8/9	Cleaved Caspase 3/8/9
CD40L	Cluster of differentiation 40L
cDNA	Complementary DNA
cFLIP	Cellular FLICE-like Inhibitory Protein
Chk	Checkpoint kinase
CHX	Cycloheximide
cIAP1/2	Cellular Inhibitor of Apoptosis Protein 1/2
ConA	Concanavalin A
Cre	Causes recombination
CYLD	Cylindromatosis (Protein)
DAI/Zbp1	DNA-dependent activator of IFN-regulatory factors
DAB	Diaminobenzidine

DD	Death Domain
ddH$_2$O	Double-distilled water
DED	Death effector domain
DEN	Diethylnitrosamine
D-GalN	D-Galactosamine
DISC	Death-Inducing Signaling Complex
DMEM	Dulbecco's Modified Eagle Medium
DMSO	Dimethyl sulfoxide
DNA	Desoxyribonucleic acid
dNTPs	Desoxyribonucleotides
DR	Death Receptor
DTT	Dithiothreithol
ECL	Enhanced Chemiluminescence
EDTA	Etylene Diamine Tetraacetate
ERK	Extracellular signal related kinases
FADD	Fas (TNFRSF6)-Associated via Death Domain
FAS	TNF Receptor Superfamily Member 6
FasL	Fas ligand
FCS	Fetal Calf Serum
GTP	Guanosintriphosphate
GTT	Glucose-tolerance test
HBV	Hepatitis B virus
HCC	Hepatocellular carcinoma
HCL	Hydrochloride acid
HCV	Hepatitis C virus
HE	Hematoxylin and Eosin
HEPES	4-2-hydroxyethyl-1-piperazineethanesulfonic acid
HFD	High-fat diet
HOIL-1	Heme-Oxidized IRP2 Ubiquitin Ligase 1 Homolog
HOIP	HOIL-1 Interacting Protein
HRP	Horseradish peroxidase

HRP	Horseradish peroxide	**NF-κB**	Nuclear Factor kappa light polypeptide gene enhancer in B-cells
ID	Intermediate domain		
IFN-γ	Interferon-γ		
IHC	Immunhistochemistry	**NIK**	NF-κB inducing kinase
IL	Interleukin	**NOXA**	phorbol-12-myristate-13-acetate-induced protein 1
(p-)IκBα	(phospho-) Inhibitor of NF-κB alpha		
IKK1	Inhibitor of κB Kinase 1	**NP-40**	Nonident P40
IKK2	Inhibitor of κB Kinase 2	**PAMP**	Pathogen Associated Molecular Pattern
IKK2ca	Inhibitor of κB Kinase 2 constitutively active	**PARP-1**	poly(ADP-ribose)-polymerase 1
IRAK	interleukin-1 receptor-associated kinase	**PBS(T)**	Phosphate Buffered Saline (Tween)
i.p.	Intraperitoneal	**PCR**	Polymerase Chain Reaction
ITT	Insulin-tolerance test	**PFA**	Paraformaldehyde
JNK	c-Jun N-terminal kinase	**PUMA**	p53 upregulated modulator of apoptosis
KD	Kinase dead		
KO	knock-out	**RHIM**	Receptor (TNFRSF)-Interacting Protein Homotypic Interaction Motif
LDH	Lactatedehydrogenase		
LDL-C	Low–density-lipoprotein-cholesterol		
LPC	Liver parenchymal cell	**RIPK1**	Receptor (TNFRSF)-Interacting Serine-Threonine Protein Kinase 1
LPS	Lipopolysaccharide		
LRR	Leucine rich repeat		
LoxP	Locus of X-over P1	**RIPK3**	Receptor (TNFRSF)-Interacting Serine-Threonine Protein Kinase 3
LUBAC	Linear Ubiquitin Chain Assembly Complex		
MAPK	Mitogen-Activated Protein Kinases	**RNA**	Ribonucleic acid
		ROS	Reactive Oxygen Species
MCL-1	Myeloid leukemia cell differentiation protein	**RT**	Room temperature
		qRT-PCR	Quantitative Real-Time PCR
MEF	Murine Embryoinc Fibroblasts	**SDS**	Sodium Dodecyl Sulfate
MLKL	Mixed-lineage kinase domain like	**SEM**	Standard error of the mean
		SHARPIN	SHANK-Associated RH Domain Interacting Protein SI
MyD88	Myeloid Differentiation Primary Response Gene 88	**SMAC**	Second mitochondria derived activator of Caspases
NCD	Normal-chow diet	**TAB1**	TAK1-Binding Protein 1
nec-1	Necrostatin-1	**TAB2**	TAK1-Binding Protein 2
NEMO	Nuclear Factor-kappa B essential modulator	**TAK**	TGF-β-Activated Kinase 1
		Tbp	TATA-binding protein

TE	Tris EDTA Buffer		**TRAF6**	TNF Receptor-Associated Factor 6
TEMED	N,N,N',N' Tetra methylenediamine		**TRAIL(R)**	TNF-related apoptosis-inducing ligand (receptor)
Tg	Transgenic		**TRIF**	TIR Domain-Containing Adaptor Inducing IFN-β
TLR	Toll-Like Receptor			
TNF	Tumor Necrosis Factor		**TWEAK**	TNF-like weak inducer of apoptosis
TNFR1/2	TNF Receptor 1/2			
TRADD	TNFRSF1A-Associated via Death Domain		**UV**	Ultraviolett
TRAF2	TNF Receptor-Associated Factor 2		**WT**	Wildtype
			XIAP	X-linked Inhibitor of Apoptosis
TRAF5	TNF Receptor-Associated Factor 5		**zVAD-fmk**	Carbobenzoxy-valyl-alanyl-aspartyl-[O-methyl]-fluoromethylketone

Abbreviations of units

bp	Base pair		**mM**	millimol
cm	centimetre		**µM**	micromol
µm	micrometer		**nM**	nanomol
cm	centimeter		**mA**	milliampere
nm	nanometre gram		**mol**	mole
g	gram		**rpm**	revolutions per minute
mg	milligram		**V**	Volts
µg	microgram		**W**	Watt
ng	nanogram		**°C**	degree celsius
kDa	kilodalton			
l	litre		**%**	percentage
ml	millimetre		**h, min, s**	hours, minutes, seconds
µl	microlitre		**x g**	G force
M	mole			

Table of Figures

List of Tables

1. Introduction

1.1. Receptor-interacting protein kinases (RIPKs)

The RIPK family consists of seven known family members, which are classified as serine-threonine kinases due to their highly conserved kinase domain (KD) (Figure 1) (Zhang, Lin, and Han 2010; Festjens et al. 2007). A number of different domain structures such as the intermediate domain (ID) and the Caspase activation and recruitment domain (CARD) are found in different RIPK family members defining the specific function and the interaction partners of each protein (Figure 1). RIPKs participate in different biological processes implicated in the regulation of cell survival and cell death in response to a variety of stimuli (Zhang, Lin, and Han 2010; Pasparakis and Vandenabeele 2015).
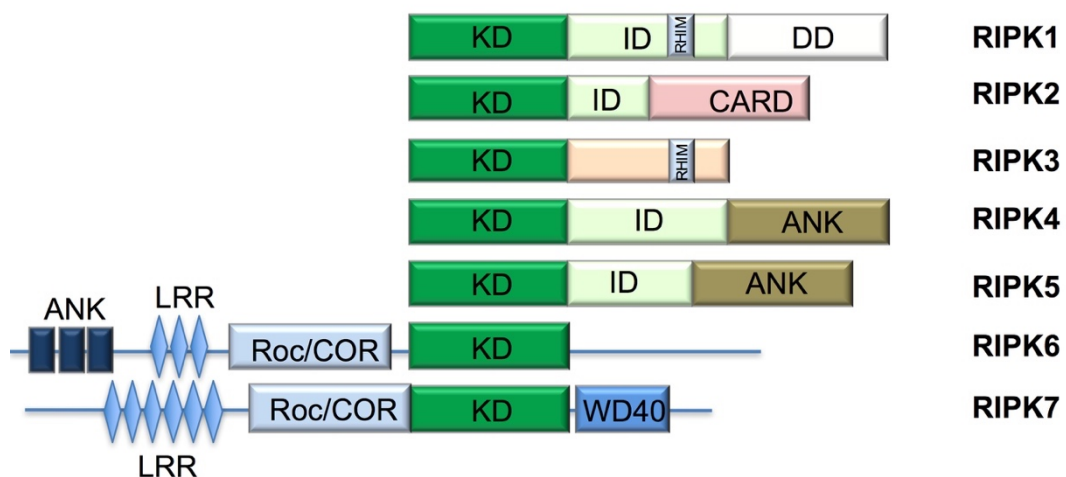
Figure 1. Schematic representation of the structure of the RIPK family members
(adapted from Zhang, Lin and Han 2010)
The RIPK family consists of seven family members with all of them sharing a conserved KD. In addition to the KD each RIPK displays additional domain structures which defines their additional function or interaction partners. RIPK1, RIPK2, RIPK4 and RIPK5 contain in addition to the KD an ID. Only RIPK1 has a death domain (DD). Together with RIPK3 it contains a receptor homotypic interacting motif (RHIM). RIPK2 has an additional CARD domain. RIPK4 and RIPK5 contain a C-terminal ankyrin repeats (ANK) domain, which is also present in RIPK6. Like RIPK7, RIPK6 has a leucine-rich repeat (LRR) motif and a Ros of complex proteins/C-terminal of Roc (Roc/COR) domain. RIPK7 further harbors a C-terminal WD40 motif.

1.1.1   RIPK1

RIPK1 was initially identified in 1995 as an interaction partner of the death receptor (DR) Fas (CD95) using a yeast-two hybrid screen and was described to be activated downstream of other DRs, such as tumor necrosis factor receptor 1 (TNFR1), and toll-like receptors (TLRs) including TLR4 (Stanger et al. 1995; Zhang, Lin, and Han 2010). Human and murine RIPK1 proteins share 68% homology with the highest similarity in

the DD. Human *RIPK1* is located on chromosome 6 whereas mouse *Ripk1* has been mapped to chromosome 13 (Hsu, Huang et al. 1996; Stanger et al. 1995). RIPK1 consists of an N-terminal KD, an ID and a C-terminal DD (Figure 2) (Festjens et al. 2007; Stanger et al. 1995; Kelliher et al. 1998).

Until now, the kinase-dependent cellular functions of RIPK1 are still not fully understood. So far, only RIPK1 is known to be a target of its kinase activity. Degterev et al. identified various serine, threonine and tyrosine residues as phosphorylation sites (Degterev et al. 2008). Accumulating evidence suggests that the KD of RIPK1 enables its autophosphorylation on Ser14/15, Ser20, Ser161 and Ser166 and that site-specific autophosphorylation of RIPK1 defines its function (Degterev et al. 2008; de Almagro et al. 2017; Zhang et al. 2017)

In addition to the KD, RIPK1 consists of an ID, which harbors a Caspase-8 cleavage site, ubiquitination sites, and a receptor homotypic interacting motif (RHIM) domain (Zhang, Lin, and Han 2010). Like autophosphorylation, site-specific ubiquitination of RIPK1 was recently reported to promote specific functions of RIPK1 (de Almagro et al. 2017). Moreover, the RHIM domain of RIPK1 is required for the interaction with other RHIM domain containing proteins, such as RIPK3, TIR domain-containing adaptor inducing IFN-beta (TRIF) and DNA-dependent activator of IFN-regulatory factors (DAI/ZBP1) (Sun et al. 2002; Kaiser and Offermann 2005; Rebsamen et al. 2009; Lin et al. 2016; Newton et al. 2016).

Furthermore, the DD of RIPK1 mediates homotypic interactions with other DD-containing proteins, including TNFR1, TNFR superfamily 1A-associated via death domain (TRADD) and Fas (TNFRSF6)-associated via death domain (FADD) thus promoting tumor necrosis factor (TNF)-induced cell death or nuclear factor kappa light polypeptide gene enhancer in B-cells (NF-κB) activation (Zhang, Lin, and Han 2010) (Figure 2).
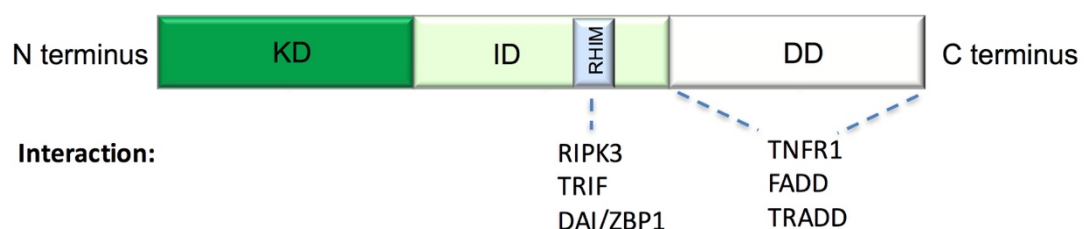
Figure 2. Schematic representation of the RIPK1 domain structure
RIPK1 is composed of a N-terminal KD, an ID, containing a RHIM domain, and a C-terminal DD. RIPK1 interacts with RIPK3, TRIF and DAI/ZBP1 via its RHIM domain while its DD allows its interaction with TNFR1, FADD and TRADD.

1.2. NF-κB signaling

NF-κB was identified as a transcription factor that binds to the intronic enhancer of the kappa light chain gene in B cells (Sen and Baltimore 1986a, 1986b). The NF-κB transcription factor family consists of p50, its precursor p105, p52, its precursor p100, RelA (p65), c-Rel and RelB with all of them sharing a Rel homology domain (Mitchell, Vargas, and Hoffmann 2016; Hayden and Ghosh 2014). The Rel domain allows NF-κB family members to homo- or heterodimerize and sequence-specific DNA binding. p50 and p52 rely on dimerization with RelA, c-Rel and RelB, which contain a transactivation domain, to positively induce transcription (Mitchell, Vargas, and Hoffmann 2016; Hayden and Ghosh 2014; Rothwarf and Karin 1999; Chen and Greene 2004). In resting cells, NF-κB transcription factors remain in an inactive state in the cytoplasm through the binding to inhibitor of κB proteins (IκBs) (IκBα, IκBβ and IκBγ) and the precursor proteins p100 and p105 (Hayden and Ghosh 2014).

NF-κB signaling can be distinguished between canonical and non-canonical pathway (Figure 3). TNF, interleukin (IL)-1, lipopolysaccharide (LPS) and cluster of differentiation (CD)40L are potent inducers of canonical NF-κB involving p50/RelA heterodimerization (Figure 3) (Ghosh and Hayden 2008; Hayden and Ghosh 2008). Binding of the ligands to their receptor induces the ubiquitination of RIPK1 which serves as a platform for the recruitment of the inhibitor of κB kinase (IKK) complex consisting of the regulatory subunit nuclear factor kappa B essential modulator (NEMO) and the kinases IKK1 and IKK2. The IKK complex triggers the phosphorylation of IκBα on Ser32 and 36 and thereby targets it for K48-ubiquitination and subsequently proteasomal degradation (Woronicz et al. 1997; Mercurio et al. 1997; Wang et al. 2001). Degradation of IκBα induces rapid translocation of the canonical NF-κB heterodimer p65(RelA):p50 to the nucleus initiating the transcription of target genes such as pro-inflammatory cytokines including *Tnf* and *Il-6* and the anti-apoptotic/anti-necroptotic gene *Cflar* (Mitchell, Vargas, and Hoffmann 2016; Hayden and Ghosh 2014). In contrast, binding of B cell activating factor of the TNF family (BAFF), TNF-like weak inducer of apoptosis (Tweak) and CD40L to their respective receptors induces non-canonical NF-κB activation. In the non-canonical NF-κB pathway, NF-κB inducing kinase (NIK)-dependent activation of IKK1 mediates processing of p100 to p52 leading to the formation of a transcriptionally active p52-RelB complex. In summary, RIPK1, IKK1/2 and NEMO are key drivers of the canonical NF-κB pathway while the non-canonical NF-κB pathway acts independently of RIPK1, IKK2 and NEMO but exclusively relies on NIK and IKK1 (Figure 3) (Senftleben et al. 2001).
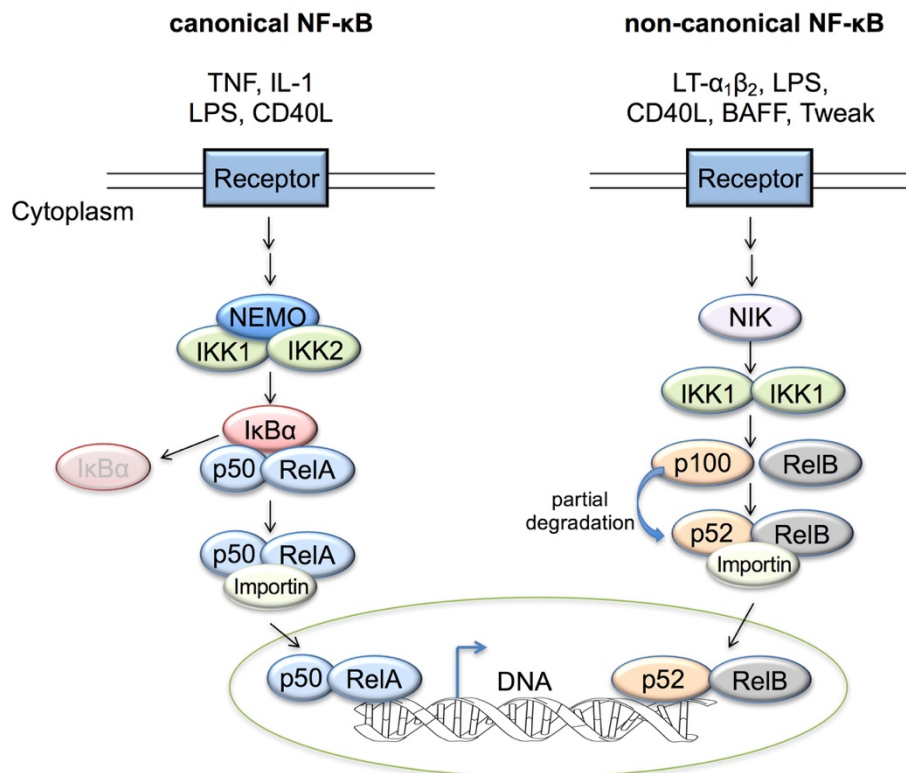
Figure 3. Canonical and non-canonical pathways of NF-κB activation
(adapted from Horie and Umezawa 2012)
Under resting conditions, NF-κB dimers are bound to an IκB protein. Binding of a ligand to its receptor mediates the degradation of the inhibitor resulting in the release of the NF-κB dimer, which translocates to the nucleus mediating transcription of pro-inflammatory cytokines. There are two types of pathways that can induce NF-κB activation, the canonical and the non-canonical. The canonical NF-κB pathway can be induced by ligation of TNF, IL-1, LPS and CD40L with their respective receptor triggering the degradation of the IκB protein in a NEMO/IKK1/2-dependent manner resulting in the nuclear translocation of the NF-κB heterodimer mostly consisting of p65/RelA. In contrast, the non-canonical pathway is activated by the binding of CD40L, BAFF and lymphotoxin-β, LPS and TWEAK to their receptors, involving NF-κB inducing kinase (NIK)-dependent IKK1-mediated phosphorylation of p100, which associates with RelB. This induces a partial degradation of p100 to p52 leading to the formation of the transcriptionally active p52-RelB complex.

1.3. Death receptor signaling

The TNF receptor superfamily consists of various family members important for the regulation of cell survival and cell death in response to inflammatory cytokines and infectious particles (Locksley, Killeen, and Lenardo 2001). DRs, which are a subgroup of the TNF receptor superfamily, are characterized by their DD motif (Wajant 2003; Wilson, Dixit, and Ashkenazi 2009). The DR family consists of 6 family members that are activated by distinct ligands. Tumor necrosis factor superfamily member (Tnfrs) 1a (TNFR1) is activated by ligation with TNF or lymphotoxin α (LTα), Tnfrsf6 (Fas or CD95) is activated by FasL/CD95L, TNF-related apoptosis-inducing ligand receptor 1 and 2 (TRAILR1 and TRAILR2) are activated by TRAIL while DR3 (Tnfrsf25) and DR6

are activated by TLA1 and amyloid precursor protein (APP) respectively (Silke and Hartland 2013; Wilson, Dixit, and Ashkenazi 2009). In contrast to the other DRs, DR3 and DR6 are not efficient in inducing cell death (Wajant 2003). Activation of DRs by binding to their ligands induces the recruitment of DD-containing adapter proteins via homotypic interactions. This interaction results in the formation of a receptor associated signaling complex mediating downstream signaling including cell death or inflammatory gene expression (Wilson, Dixit and Ashkenazi 2009).

1.3.1. TNF signaling pathway

TNF is a cytokine produced by immune, epithelial and endothelial cells and binds to two plasma membrane receptors, TNFR1 and TNFR2. Unlike TNFR1, which recognizes soluble and membrane-bound TNF, TNFR2 binds with a much higher affinity to the membrane-bound TNF precursor and is likely to be restricted to T cells (Brockhaus et al. 1990; Dembic et al. 1990; Schall et al. 1990; Zheng et al. 1995; Kim and Teh 2001; Depuydt et al. 2005). Until now, TNFR1 is the most well-studied receptor with respect to cell death or cell survival pathways. TNF ligation to TNFR1 induces inflammatory, cell survival and anti-microbial processes via complex-I but in addition also mediates apoptosis via complex-IIa/-IIb and necroptosis through the necrosome (Figure 4) (Micheau and Tschopp et al 2003; Li et al. 2012; Varfolomeev and Vucic 2016). TNF alone is not sufficient to induce cell death in most cell types while in combination with inhibitors of transcription (e.g. D-Galactosamine) or translation (e.g. cycloheximide) TNF potently triggers cell death suggesting that NF-κB-dependent gene expression negatively regulates TNF-induced cell death (Morikawa et al. 1996; Wang, Du and Wang 2008).
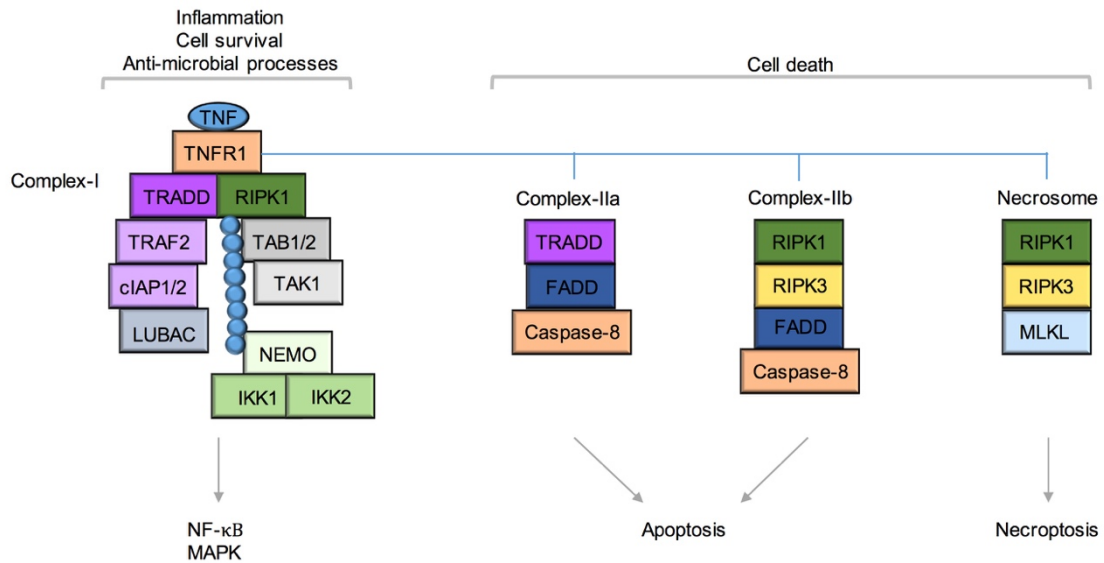
Figure 4. TNFR1 signaling induces cell survival, inflammation, anti-microbial processes and cell death.
TNF ligation to TNFR1 results in formation of a receptor-bound complex (complex-I) that activates NF-κB and mitogen-activated protein kinase (MAPK) signaling triggering inflammation, cell survival and anti-microbial processes. Under certain conditions, TNF causes complex-IIa or IIb-mediated TRADD or RIPK1-dependent apoptotic death. However, inhibition of complex-IIa and IIb TNF mediates necroptosis through the necrosome formation. (for details see 1.3.1.1-3)

1.3.1.1. TNFR1-induced pro-inflammatory and pro-survival signaling

Binding of TNF to TNFR1 induces pro-inflammatory and anti-apoptotic functions by inducing canonical activation of the transcription factor NF-κB and mitogen-activated protein kinase (MAPK) pathways (Varfolomeev and Vucic 2016; Baud and Karin 2001). TNF induces the trimerization of TNFR1 resulting in a rapid formation of a receptor proximal complex-I consisting of RIPK1, TRADD, TNF receptor-associated factor 2 (TRAF2), cellular Inhibitor of Apoptosis Protein 1/2 (cIAP1/2) and linear ubiquitin chain assembly complex (LUBAC) (Figure 4 and 5) (Legler et al. 2003; Hayden and Ghosh 2014; Hsu, Huang, et al. 1996). RIPK1 and TRADD are recruited via their DD to the intracellular DD of TNFR1. TRADD in turn recruits the E3 ubiquitin ligase TRAF2 via interaction through their TRAF binding domain (Hsu, Huang, et al. 1996; Hsu, Shu, et al. 1996; Hsu, Xiong, and Goeddel 1995; Pobezinskaya et al . 2008). TRAF2 further binds the E3 ligases, cIAP1 and cIAP2, and recruits them to the TNFR1 complex (Shu, Takeuchi, and Goeddel 1996). The recruitment of the E3 ligases cIAP1/2 to complex-I promotes K11-, K63- and K48-linked ubiquitination of themselves and RIPK1 (Figure 5) (Park, Yoon and Lee 2004; Varfolomeev et al. 2008; Dynek et al. 2010; Mahoney et al. 2008). K63-specific modification of cIAP1/2 supports the engagement of LUBAC consisting of haem-oxidized IRP2 ubiquitin ligase-1 (HOIL-1L), HOIL-1 interacting

protein (HOIP) and SHANK-associated RH domain-interacting protein (SHARPIN) (Ikeda et al. 2011; Tokunaga et al. 2011). K63-specific modification of RIPK1 supports the recruitment of transforming growth factor b activated kinase (TAK1) and TAK1 binding protein 1 and 2 (TAB1/TAB2) (Wang et al. 2001; Kanayama et al. 2004). LUBAC in turn promotes linear ubiquitination (M1) of TNFR1, TRADD, RIPK1 and NEMO (Haas et al. 2009; Tokunaga et al. 2009). NEMO together with the IKKs are recruited to the TNFR1 complex through the interaction of NEMO with M1-, K11- and K63-linked ubiquitin chains, with the highest affinity for M1-ubiquitin chains, via its Ub binding in ABIN and NEMO (UBAN) domain (Wu et al. 2006; Rahighi et al. 2009; Dynek et al. 2010). Trans-autophosphorylation of TAK1 induces the activation of IKK2 which mediates the activation of the NF-κB signaling pathway (for details see 1.2) (Wang et al. 2001).
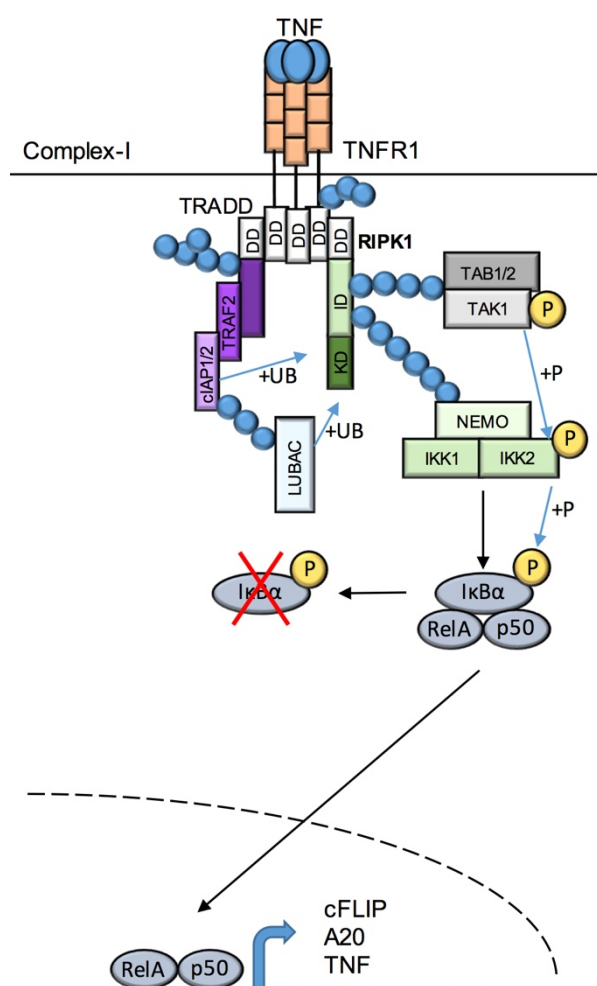
Figure 5. TNF-induced complex-I signaling
Upon TNF ligation to TNFR1 a receptor-associated complex-I is being assembled, which mediates NF-κB activation resulting in pro-inflammatory and pro-survival signaling. For details see text.

Ub   Ubiquitination (blue circles)
P   Phosphorylation

Stabilization of complex-I signaling is mediated by the modification of several complex-I members with ubiquitin chains (O'Donnell et al. 2007; Mollah et al. 2007; Tokunaga et al. 2009) (Figure 6). Genetic studies in mice revealed impaired canonical NF-κB activation in response to TNF in absence of HOIL-1 and HOIP or after mutation of *Sharpin* (Mollah et al. 2007; Tokunaga et al. 2009). RIPK1 displays multiple

ubiquitination sites, however, it remains controversial whether ubiquitination of RIPK1 is fundamental for NF-κB activation. Several studies indicated that ubiquitination of RIPK1 was indeed essential for NF-κB activation since mutation of the ubiquitination site at K377 abolished the recruitment of the TAK1- and IKK-complex to complex-I as well as IκBα phosphorylation after TNF stimulation (Ea et al. 2006; Hsu, Huang, et al. 1996; Li et al. 2006). On the contrary, an independent study reported that mutated ubiquitin, which could not engage K63 chains, did not result in reduced IκBa phosphorylation upon TNF stimulation suggesting a ubiquitin-dependent, K63-independent mechanism of TNF-induced NF-κB activation (Xu et al. 2009). In contrast to ubiquitination, autophosphorylation of RIPK1 is largely dispensable for TNF-induced NF-κB activation (Lee et al. 2004). However, unlike autophosphorylation, phosphorylation of RIPK1 by IKK1/IKK2 within complex-I was recently described to be important to restrain RIPK1 in complex-I in order to suppress its pro-death function and stabilize complex-I signaling (Dondelinger et al. 2015; Koppe et al. 2016).

Positive and negative regulation of NF-κB by TNF is partially achieved through the transcription of A20 (Mevissen et al. 2013; Ritorto et al. 2014; Wertz et al. 2004). A20 recruitment to complex-I requires the M1-chain forming function of LUBAC since absence of HOIP or M1-ubiquitin chains abolishes A20 recruitment to complex-I (Draber et al. 2015). Through its Zinc finger domains 4 and 7, A20 binds to K63- and M1 linkages respectively (Bosanac et al. 2010; Tokunaga et al. 2012; Verhelst et al. 2012). A20 has been so far implicated in the hydrolysis of K11-, K63- and K48- but not M1-ubiquitin chains to positively and negatively regulate NF-κB activation (Figure 6). On the one hand, A20 stabilizes complex-I and favors signal transduction that leads to gene transcription by binding M1-ubiquitin chains. On the other hand, A20 negatively regulates TNF-induced NF-κB activation by hydrolyzing K63-ubiquitin chains via its OTU domain, leading to K48-ubiquitination and proteasomal degradation of RIPK1 (Wertz et al. 2004; Zilberman-Rudenko et al. 2016). In addition, accumulation of M1-ubiquitin-bound A20 can switch from positive to negative regulation of NF-κB activation by restricting NEMO/IKK complex binding to M1-ubiquitin chains (Zilberman-Rudenko et al. 2016). Together, A20 exhibits dual functions in NF-κB regulation by acting as an ubiquitin-stabilizing protein promoting NF-κB activation and as an ubiquitin hydrolyzing protein impairing NF-κB activation.

In addition to A20, the deubiquitinase cylindromatosis (CYLD) is recruited to TNFR1-associated signaling complex-I by associating with HOIP-1 induced by SPATA2 at which it regulates gene activator signaling and cell survival/death (Figure 6) (Takiuchi et al. 2014; Draber et al. 2015). Unlike A20, CYLD recruitment most probably depends

on its interaction with HOIP but is independent of LUBAC's M1-chain-forming capacity. CYLD antagonizes and hydrolyzes K63-ubiquitin and M1 chains via its USP domain sensitizing cells to TNF-induced cell death (Figure 6) (Trompouki et al. 2003; Wright et al. 2007; Ritorto et al. 2014; Sato et al. 2015). In summary, controlled regulation of complex-I mediated signaling is achieved by A20 and CYLD. A20 positively regulates complex-I by binding to M1-ubiquitin chains but like CYLD it also negatively regulates complex-I signaling by hydrolyzing K63-ubiquitin chains.
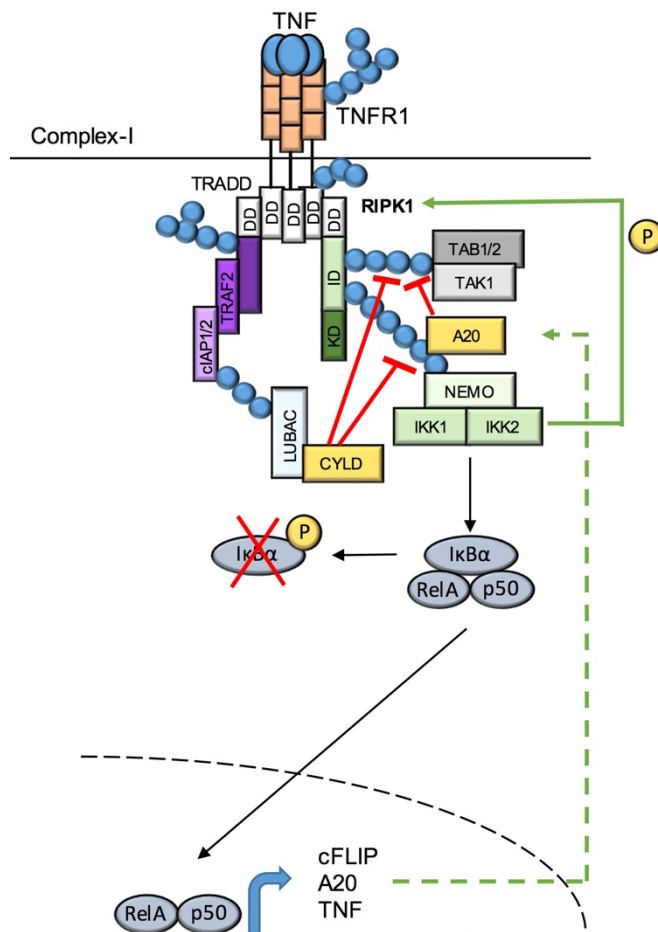
Figure 6. (De-)Ubiquitination events regulating proximal TNF signaling. TNF-induced NF-κB activation is tightly regulated by (de)ubiquitination events. Ubiquitination of several complex-I members including TNFR1, TRADD and RIPK1 is mediated by cIAP1/2 and LUBAC resulting in the stabilization of complex-I promoting NF-κB activation. A20 stabilizes complex-I by binding to M1-ubiquitin chains but together with CYLD it also negatively regulates complex-I signaling by hydrolyzing K63-ubiquitin chains.

P   Phosphorylation

In addition to NF-κB signaling, TNF ligation to TNFR1 also activates MAPKs such as c-Jun n-terminal kinases (JNK), extracellular signal-related kinases (ERK) and p38 via TAK1-mediated activation. TAK1 acts as a MAP3K and consequently starts the phosphorylation cascade (Sabio and Davis 2014; Sakurai et al. 2000). MAPKs are evolutionarily conserved serine-threonine kinases regulating cellular processes such as cell proliferation, differentiation, survival, death and regulation of gene expression. They are activated by phosphorylation cascades or by interaction with small guanosintriphosphate (GTP)-proteins of the Ras/Rho family in response to oxidative and osmotic stress, heat shock and pro-inflammatory cytokines including TNF (Figure 7) (Pearson et al. 2001; Treisman 1996).
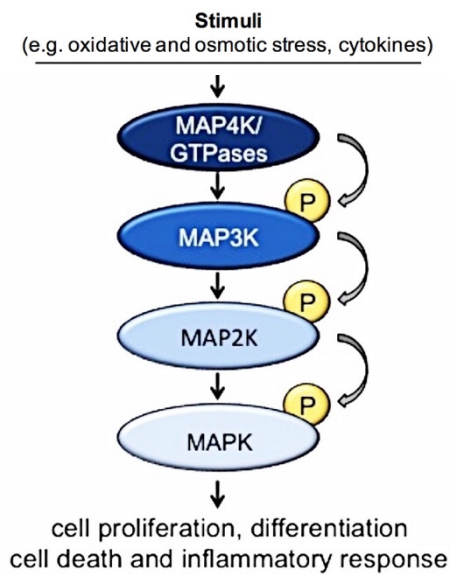
Figure 7. Various stimuli activate MAPK by inducing a phosphorylation cascade.
Various stimuli such as oxidative or osmotic stress and cytokines activate MAP4K or GTPases. Activation of MAP4K and GTPases induces the activation of downstream kinases by a phosphorylation cascade. MAPK activation results consequently in cell proliferation, differentiation, cell death and inflammatory response.

1.3.1.2. TNF-induced complex-IIa/-IIb-mediated apoptosis

In addition to complex-I, binding of TNF to TNFR1 also results in apoptosis mediated by complex-IIa and IIb. Formation of complex-IIa through the association of TRADD and FADD via homotypic DD-DD interactions is induced e.g. after inhibition of pro-survival protein translation caused by cycloheximide (CHX) (Hsu et al. 1996; Hsu, Xiong and Goeddel 1995; Wang, Du and Wang 2008; Micheau and Tschopp 2003). FADD then recruits the initiator Caspase, Caspase-8, via its death effector domain (DED) (Figure 8) (Micheau and Tschopp 2003; Wang, Du, and Wang 2008). Alternatively, under conditions such as TNF stimulation in the presence of an IAP inhibitor, knockout of IAPs, TAK1 inhibition or knockdown, and NEMO knockout, a cytosolic complex-IIb can be formed consisting of RIPK1, FADD and Caspase-8 to execute RIPK1-kinase-dependent apoptosis (Figure 8) (Dondelinger et al. 2013; Moulin et al. 2012; Legarda-Addison et al. 2009; Wang, Du, and Wang 2008; Wilson, Dixit, and Ashkenazi 2009). This complex mediates apoptosis in a RIPK1 kinase-activity dependent manner (Kondylis et al. 2015). Accumulating evidence suggests that deubiquitination of RIPK1 is crucial for the execution of TNF-induced apoptosis (de Almagro et al. 2017; O'Donnell et al. 2007). Moreover, cleavage of RIPK1 at the Caspase cleavage site located in its ID by Caspase-8 is believed to prevent NF-κB activation and necroptosis but promotes complex IIa-dependent apoptotic death in response to DR signaling (Lin et al. 1999; Rajput et al. 2011).
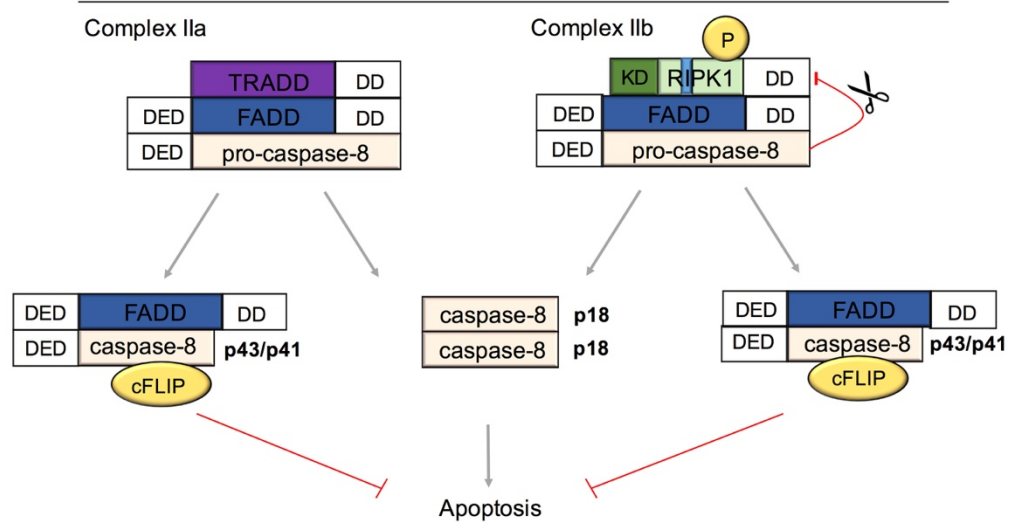
Figure 8. TNF-induced complex-IIa and -IIb formation
Destabilization of complex-I results in the assembly of complex-IIa and -IIb in response to TNF. Assembly of complex-IIa and -IIb promotes Caspase-dependent apoptotic death. TNF-induced complex-IIa signaling is TRADD dependent whereas complex-IIb signaling is RIPK1-kinase activity dependent.

In both complexes, homodimerization of pro-Caspase-8 results in a conformational change inducing the autocatalytic cleavage at Asp374 and the generation of multiple Caspase-8 fragments such as p43/p41 and p10 (Figure 8). After an additional cleavage at Asp216 the catalytic active p18 fragment and the inactive p26/24 prodomain are produced (Medema, Scaffidi, et al. 1997; Medema, Toes, et al. 1997). The p18 fragment forms a homodimer which induces the cleavage and activation of the effector Caspases such as Caspase-3, -6 and -7 mediating extrinsic apoptosis. Moreover, activated Caspase-8 also triggers the activation of the pro-apoptotic BH3 interacting domain death agonist (Bid) resulting in the mitochondrial-mediated amplification of the apoptotic signal induced by extrinsic stimuli (Figure 9) (Li et al. 1998; Luo et al. 1998). Bid induces the release of mitochondrial proteins such as cytochrome C and second mitochondrial derived activator of Caspases (SMAC) leading to APAF-1-dependent apoptosome formation and pro-Caspase-9 activation (Luo et al. 1998; Gross et al. 1999). Activated Caspase-9 activates effector Caspases such as Caspase-3 and consequently amplifies apoptotic signaling also in cells with low levels of Death-Inducing Signaling Complex (DISC) components (Wilson, Dixit, and Ashkenazi 2009). Independent of Caspase-8, the mitochondria-mediated form of apoptosis is induced among others by DNA-damage and ER-stress and is classified as intrinsic apoptosis.
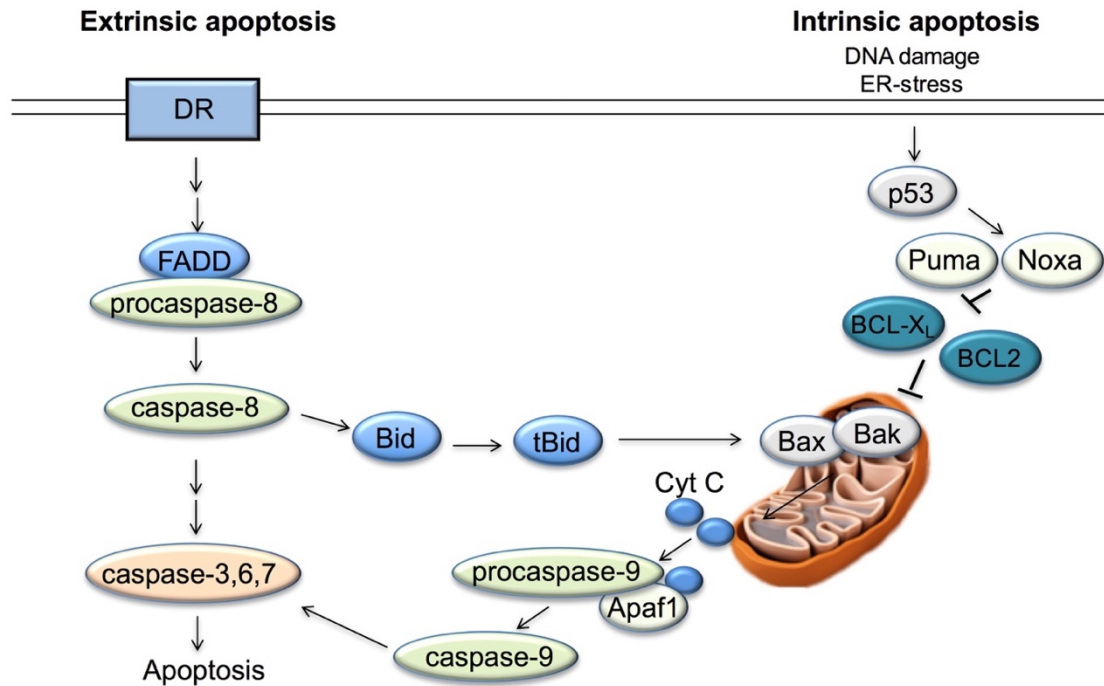
Figure 9. The extrinsic and intrinsic apoptotic pathways
Apoptosis is induced via mitochondrial (intrinsic) or via DR-mediated (extrinsic) pathways. The extrinsic apoptotic pathway is dependent on FADD-pro-Caspase-8 interaction resulting in the processing of pro-Caspase-8 to catalytically active Caspase-8, which consequently activates Caspase-3/6/7. In contrast, intrinsic apoptosis is activated in response to DNA-damage and ER-stress that induces p53 activation. p53 signaling activation results in the upregulation of p53 upregulated modulator of apoptosis (PUMA) and phorbol-12-myristate-13-acetate-induced-protein 1 (NOXA) that neutralizes the anti-apoptotic BCL-2 proteins, B-cell lymphoma (BCL)-2 and BCL-XL resulting in the activation of Bid (tBid). tBid in turn activates Bax and Bak resulting in the disruption of mitochondrial integrity causing the release of cytochrome C and SMAC and consequently resulting in apoptosome-dependent activation of Caspase-9. This leads to the activation of Caspase-3/6/7 and ultimately to apoptosis. However, extrinsic apoptosis induces also intrinsic apoptosis via Caspase-8-dependent activation of Bid to tBid.

Effector Caspases activate cytoplasmic endonucleases and proteases to induce the degradation of nuclear material and cytoskeletal proteins, respectively. These processes influence the morphological characteristics of apoptosis characterized by cell shrinkage and pyknosis, a result of chromatin condensation (Kerr, Wyllie, and Currie 1972). Moreover, extensive plasma membrane blebbing followed by karyorrhexis, separation of cell fragments into apoptotic bodies and nuclear fragmentation are characteristics of apoptosis (Kerr, Wyllie, and Currie 1972). Apoptotic bodies are subsequently phagocytosed by macrophages, parenchymal cells or neoplastic cells and degraded within phagolysosomes (Poon et al. 2014).

Due to the immediate clearance of apoptotic bodies, apoptosis is considered to be non-immunogenic (Lamkanfi and Dixit 2010; Green et al. 2009). Conversely, current

studies also identified a pro-inflammatory role of apoptosis under cancerous conditions (Poon et al. 2014).

Apoptotic death has to be tightly regulated since inappropriate apoptosis is involved in neurodegenerative diseases, autoimmune disorders and many types of cancer including hepatocellular carcinoma (HCC) (Poon et al. 2014; Kondylis et al. 2015). Accordingly, a study using a genetic model of HCC formation revealed that the liver-parenchyma cell (LPC)-specific deficiency of NEMO triggered apoptotic death resulting in an inflammatory response inducing spontaneous HCC development in mice (Kondylis et al. 2015). Furthermore, IKK1/IKK2^{LPC-KO} mice developed increased RIPK1-dependent cholangiocyte death resulting in strong hepatocellular damage, severe biliary destructions and cholestasis, which are fatal at 7-9 months of age (Luedde et al. 2008; Koppe et al. 2016). Conversely, inhibition of extrinsic apoptosis also results in a developmentally fatal outcome since Caspase-8 deficiency is embryonically lethal accompanied by embryonic vascular, cardiac and haematopoietic defects (Varfolomeev et al. 1998; Kaiser et al. 2011). Similarly, inhibition of intrinsic apoptosis by Caspase-9 deficiency resulted in embryonic/neonatal lethality showing enlarged and malformed cerebellum (Kuida et al. 1998; Hakem et al. 1998). Taken together, both extensive but also diminished apoptosis strongly affect tissue homeostasis and the viability of mice. Therefore, tight regulation of Caspase-dependent apoptosis is essential for development and tissue homeostasis.

NF-κB-dependent expression of cellular FLICE-like inhibitory protein (cFLIP) is considered to negatively regulate extrinsic apoptotic signaling through modulation of Caspase-8 activity (Dillon et al. 2012; Feoktistova et al. 2011). cFLIP is a catalytically inactive homolog of Caspase-8 with two isoforms, cFLIP$_L$ and cFLIP$_S$ in humans and cFLIP$_L$ and cFLIP$_R$ in mice. Caspase-8 cFLIP heterodimerization results in primary Caspase-8 cleavage and the generation of a p10-fragment but lacks secondary cleavage inhibiting p18-fragment generation (Pop et al. 2011). Interaction between the p43/p41 Caspase-8 fragment and cFLIP$_L$ negatively regulates apoptosis and is thought to inhibit necroptosis. In detail, a Caspase-8-cFLIP heterodimer has been suggested to cleave CYLD, RIPK1 and RIPK3 degrading key drivers of TNF-induced necroptosis (see 1.3.1.3.). There is evidence suggesting that low levels of cFLIP$_L$ stabilize complex IIa by binding to Caspase-8 allowing its oligomerization to execute apoptosis and block necroptosis while high levels of cFLIP$_L$ prevent Caspase-8 oligomerization and thereby block apoptosis (Hughes et al. 2016; Fu et al. 2016). This hypothesis is based on data obtained by Fas/FasL signaling and yet needs to be confirmed in a TNFR1-dependent setting (Pop et al. 2011; Wachter et al. 2004; Hughes et al. 2016; Fu et al. 2016).

1.3.1.3. TNF-induced complex-IIc mediated necroptosis

When the formation of complex-IIa and-IIb are blocked by FADD, Caspase-8 deficiency or inhibition of Caspase-8 activity by zVAD-fmk, TNF induces the assembly of a third death-inducing complex, called complex-IIc/ necrosome, consisting of RIPK1, RIPK3 and mixed lineage kinase domain-like (MLKL) (Figure 10) (Newton et al. 2014; Pasparakis and Vandenabeele 2015). Accordingly, *Fadd⁻ᐟ⁻* or *Caspase-8⁻ᐟ⁻* mice showed embryonic lethality that was prevented by additional deletion of the necroptosis mediator RIPK3 or MLKL (Kaiser et al. 2011; Dillon et al. 2012; Alvarez-Diaz et al. 2016) To date, necroptotic death is considered to occur independently of Caspases in cells with elevated levels of RIPK3 and MLKL. TNF-induced necroptotic death is dependent on RIPK1 kinase activity as several studies reported that mutation of the kinase activity or using the allosteric inhibitor of the kinase activity of RIPK1, necrostatin-1 (nec-1), prevented necroptotic death (Ni et al. 2016; Polykratis et al. 2014; Degterev et al. 2008; Degterev et al. 2005; Kondylis et al. 2015; Vlantis et al. 2016; Newton et al. 2014). Indeed, autophosphorylation of RIPK1 on Ser161 or Ser166 was recently reported to be important for necroptotic death (de Almagro et al. 2017; Zhang et al. 2017). Autophosphorylation at the residue Ser161 was shown to be triggered in response to TNF-induced ROS (Zhang et al. 2017). However, it remains to be elucidated whether only autophosphorylation or phosphorylation by other kinases at one or multiple residues are crucial for RIPK1 functions particularly in the necrosome. It was recently identified that not only phosphorylation, but coordinated ubiquitination and phosphorylation of RIPK1 within complex-IIc are crucial for the induction of necroptosis (Figure 10) (de Almagro et al. 2017 and 2015). Mutation of the ubiquitination site of RIPK1 at K115 prevented K63- and linear ubiquitination of RIPK1 and thereby reduced RIPK1 phosphorylation, necrosome formation and consequently necroptosis (de Almagro et al. 2017). However, the precise molecular mechanisms controlling RIPK1 activation in the necrosome are still unclear.

Activation of RIPK1 results in conformational changes allowing an interaction between RIPK1 and RIPK3 through their RHIM domains (Chan, Luz, and Moriwaki 2015; Cho et al. 2009). The heterodimeric interaction between RIPK1 and RIPK3 mediates the recruitment of another RIPK3 molecule to form a RIPK3-RIPK3 amyloid complex allowing RIPK3 autophosphorylation (Cho et al. 2009; He et al. 2009; Li et al. 2012; Zhang et al. 2009; Sun et al. 2002). RIPK3 phosphorylation at Ser232 is crucial for the recruitment and activation of its downstream target MLKL (Zhao et al. 2012; Sun et al. 2012; Murphy et al. 2013). The activation of the pseudokinase MLKL is mediated by its phosphorylation by RIPK3 at different phosphorylation sites including Ser345, Ser347,

Ser 352 and Thr 349 (Chen et al. 2013; Li et al. 2012; McQuade, Cho, and Chan 2013; Cai et al. 2014). This phosphorylation of MLKL results in a conformational change that exposes the 4-helical bundle domain allowing its oligomerization (Cai et al. 2014; Chen et al. 2013; Dondelinger et al. 2014; Sun et al. 2012; Wang et al. 2014; Xie et al. 2013). It is still highly debated how MLKL executes necroptotic death. The current model suggests that MLKL binds to phospholipids of the cell membrane through its 4-helical bundle domain resulting in the influx of Ca^{2+} and Na^+ that likely contribute to cell death (Cai et al. 2014; Chen et al. 2013; Dondelinger et al. 2014; Su et al. 2014; Wang et al. 2014).

Morphologically, necrotic cell death is characterized by organelle swelling and loss of plasma membrane integrity (Festjens et al. 2007; Krysko et al. 2008; Vanden Berghe et al. 2010). In contrast to apoptotic death, necroptotic death is currently believed to be highly immunogenic by releasing factors collectively described as damage-associated molecular patterns (DAMPs) (Kono and Rock 2008; Krysko et al. 2008; Lamkanfi and Dixit 2010). Consistently, FADD deficiency in both intestinal epithelial cells (IECs) and keratinocytes induces necroptotic death and tissue inflammation that was both prevented by RIPK3 deficiency (Welz et al. 2011; Bonnet et al. 2011).
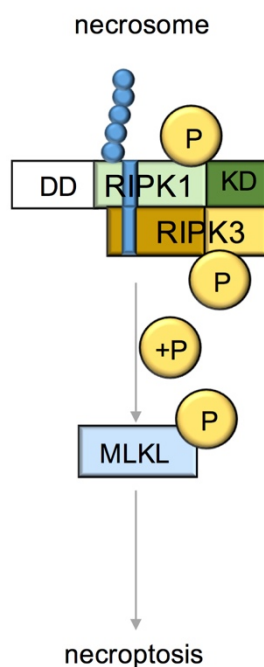
Figure 10. TNF-induced necrosome formation.
TNF induces the assembly of a necrosome mediating Caspase-independent necroptotic death in a RIPK1-RIPK3 kinase activity dependent manner. Coordinated ubiquitination and phosphorylation of RIPK1 was reported to induce the complex formation between RIPK1 and RIPK3, which interact via their RHIM domain, resulting in the phosphorylation and activation of MLKL.

1.4. TLR signaling

TLRs are receptors involved in the activation of innate immune cells recognizing specific patterns of microbial components (PAMPs) including bacteria, mycobacteria and viruses or altered host-derived DAMPs that under specific conditions may trigger

an immunological response (Akira, Takeda and Kaisho 2001; Akira, Uematsu and Takeuchi 2006; Janeway and Medzhitov 2002). All TLRs share a conserved cytoplasmic TIR domain with which they can interact with TIR domain-containing adaptors such as myeloid differentiation primary response gene 88 (MyD88) and TRIF. In addition to their TIR domain, TLRs contain a leucine-rich repeat (LRR) ectodomain which enables recognition of PAMPs and DAMPs (Kawai and Akira 2010). Until now, 12 TLRs have been identified in humans and 10 in mice. Unlike MyD88, which is implicated in the signaling induced by all TLRs except for TLR3, TRIF is implicated only in TLR3 and TLR4 signaling (Kawai and Akira 2010).

TLR4 induces an inflammatory response against gram-negative bacteria after recognizing lipopolysaccharide (LPS) on their outer-surface (Figure 11) (Hoshino et al. 1999; Poltorak et al. 1998; Qureshi et al. 1999). TLR4 is the only TLR that mediates signaling via both MyD88 and TRIF adaptors. After LPS stimulation, TLR4 recruits the intracellular adapter MyD88 and TRIF via TIRAP/TRAM. MyD88 induces inflammatory cytokine production through NF-κB activation mediated by interleukin-1 receptor-associated kinase (IRAK) and TRAF6 interaction. TRIF associates with either TANK-binding kinase (TBK)1 or activates IFN regulatory factor 3 (IRF3) mediating type I IFN expression. In addition, TRIF interacts with RIPK1 via their RHIM domains to mediate MAPK and NF-κB activation (Figure 11). Similar to its role in TNF signaling, recruitment of RIPK1 to TLR4 via TRIF is followed by its polyubiquitination, which is possibly mediated by TRAF6. Polyubiquitination of RIPK1 mediates the recruitment of TAB1/2 and TAK1 resulting in MAPK activation and in the recruitment of the IKK1/2/NEMO complex inducing NF-κB activation (Cusson-Hermance et al. 2005). TLR4-mediated TRIF-dependent cell death occurs in order to eliminate infected host-cells. Therefore, a death-inducing complex containing TRIF, RIPK1, RIPK3, FADD, Caspase-8 and cFLIP induces RIPK1 kinase-activity-dependent apoptosis and necroptosis (He et al. 2011; Kaiser et al. 2005; Polykratis et al. 2014).
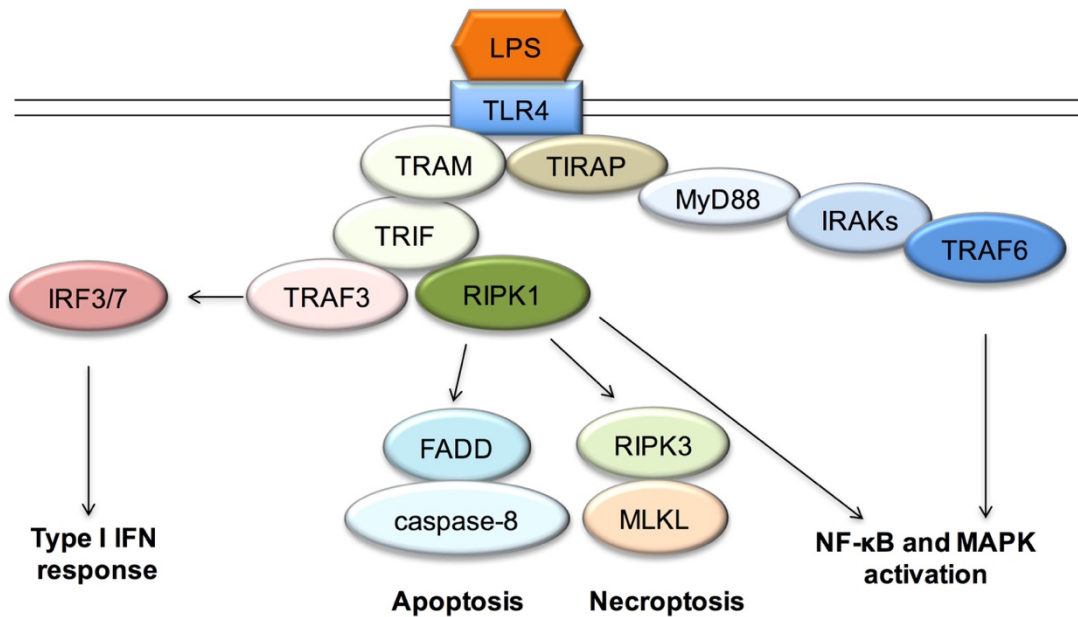
Figure 11. LPS-mediated TLR4 signaling activation
Binding of LPS to TLR4 induces the engagement of TIR domain-containing adaptor proteins TIRAP/MyD88 or TRAM/TRIF. This mediates the interaction between MyD88 with IRAKs and the adapter molecule TRAF6. Together they mediate NF-κB and MAPK activation. Via TRAM and TRIF TLR4 interacts with RIPK1 and TRAF3. Through TRAF3 TLR4 triggers IRF3/7-mediated Type-I-Interferon response while via RIPK1 TLR4 induces either NF-κB/ MAPK activation or cell death (apoptosis or necroptosis).

1.5. Anatomy and function of the liver

The liver is an essential organ in vertebrates consisting of two main lobes in humans and four main lobes in mice (Abdel-Misih and Bloomston 2010). The liver is a heterogeneous organ that is predominantly composed of the liver parenchyma cell compartment consisting of 60-65% hepatocytes and 3.5% biliary epithelial cells and the non-parenchymal cell compartment including 15-20% endothelial cells, as well as 8-12% liver-resident macrophages (Kupffer cells) and 3-8% lymphocytes and hepatic stellate cells (Racanelli and Rehermann 2006; Kmiec 2001). The liver mediates various functions that are implicated in fat and glucose metabolism, detoxification, protein synthesis, hormone production and glycogen storage (van den Berghe 1991; Dietschy, Turley, and Spady 1993). Deregulation of liver homeostasis can result in acute liver failure (ALF), in chronic liver diseases or in HCC (Dietschy, Turley, and Spady 1993; Kmiec 2001; van den Berghe 1991; Wullaert et al. 2007).

The maintenance of liver homeostasis is dependent on the tight regulation of inflammation and cell death. Although under physiological conditions the turnover rate of differentiated hepatocytes is relatively low (200-400 days in mice/rats) compared to other epithelial or epidermal cells, liver regeneration capacity is highly increased upon extensive tissue loss during surgical resection or injury caused by massive alcohol

consumption, metabolic toxicity and viral or other microbial infections (Martins, Theruvath and Neuhaus 2008; Fausto 2004). Massive hepatocyte death exceeding the regenerative capacity of the liver mediates acute liver injury which can ultimately result in ALF causing high mortality rates of patients (Bantel and Schulze-Osthoff 2012). Moreover, massive hepatocyte death or chronic inflammation coupled with compensatory liver regeneration induced by hepatocyte proliferation is thought to greatly increase the risk of HCC (Luedde, Kaplowitz, and Schwabe 2014; Guicciardi et al. 2013). HCC is one of the most frequent and difficult to treat types of cancer constituting the second most common cause of cancer-related deaths worldwide (Shariff et al. 2009; El-Serag 2011). Understanding the mechanisms regulating chronic inflammation and cell death in the liver is essential to find new therapeutic strategies against liver diseases such as ALF and HCC.

1.5.1. Murine models of liver inflammation and liver injury

Several murine models of liver injury provide distinct approaches to elucidate the inflammatory response and cell death signaling in the liver upon damage. A well-characterized murine model to study inflammatory signaling is the LPS-induced systemic inflammation model. A single intraperitoneal injection (i.p.) of sub-lethal doses of the gram-negative bacteria derived endotoxin LPS induces a TLR4-dependent acute inflammatory response, which resembles to a large extent those occurring during the early stages of septic shock (Martich, Boujoukos, and Suffredini 1993). LPS toxicity is associated with activation of KCs in the liver and the release of inflammatory cytokines such as TNF resulting in a strong inflammatory response that can ultimately lead to death by septic shock without inducing liver injury (Bautista et al. 1994; Luster et al. 1994; Bradham et al. 1998). Combined injection of LPS with a hepatic transcription inhibitor D-galactosamine (D-GalN), which is metabolized into an active metabolite exclusively in hepatocytes and blocks transcription by depleting uridine nucleotides, sensitizes hepatocytes to death resulting in hepatic damage caused by TNF resembling viral hepatitis accompanied by focal cell death and periportal inflammation (Keppler, Pausch, and Decker 1974; Freudenberg, Keppler, and Galanos 1986; Morikawa et al. 1996; Xiong et al. 1999; Van Dien et al. 2001; Liu et al. 2008). Besides the LPS/TNF-induced murine model, ConA-induced hepatic inflammation reflects the overall physiopathological conditions observed in human viral-induced or autoimmune hepatitis. ConA is an effective activator of T-cells resulting in the activation of cytotoxic effectors such as TNF that trigger hepatocyte death consequently resulting in hepatitis development (Mizuhara et al. 1994; Tiegs et al. 1992). Moreover, α-galactosylceramide (α-GalCer), a potent NKT cell stimulator, causes liver injury through a pronounced

cytokine response, including TNF, IFNγ and IL-2/-4/-6. In addition, acetaminophen (APAP)-mediated toxicity is a model of induced hepatocyte death and hepatotoxicity (Nelson et al. 1990; Hinson et al. 1995). APAP is metabolized to NAPQI via Cyp450, which is highly electrophilic and covalently binds intracellular proteins inducing hepatocyte toxicity (Mitchell et al. 1973). APAP induces liver damage resembling histological characteristics of necrosis independently of TNFR1 signaling (Boess et al. 1998). Together these murine models mimic human liver diseases and therefore enable the studies of disease initiation and progression in mice.

1.5.2. Murine model of hepatocellular carcinoma

The chemical compound diethylnitrosamine (DEN) has been widely used to mimic HCC in experimental animal models by causing DNA-damage (Tolba et al. 2015). DEN-induced HCC has histological and genetic similarities to that of human HCC, which allows studying the molecular mechanisms of hepatocarcinogenesis. In 1961, the hepatotoxic and carcinogenic effect of DEN was first reported in rats inducing high incidences of hepatic tumors upon a single application (Thomas 1961). Intraperitoneal injection of DEN results in the bioactivation of DEN by cytochrome P450 enzymes including CYP2E1 in the liver resulting in DNA-adducts formed through an alkylation mechanism further leading to the induction of carcinogenesis (Figure 12). These alkylated adducts activate the DNA-damage repair which is coupled to the DNA damage response resulting in cell cycle arrest, NF-κB activation or cell death (Rao and Vesselinovitch 1973; Li et al. 2001). Sensing DNA damage occurs through ataxia telangiectasia mutated (ATM) or Ataxia telangiectasia and Rad3-related protein (ATR) kinase (Teoh et al. 2010; Piret, Schoonbroodt, and Piette 1999). DNA damage sensing by ATM results in the formation of a cytoplasmic complex containing ATM, RIPK1, TAK1 and NEMO (Figure 12) (Yang et al. 2011). Within this complex RIPK1 is modified by ubiquitin resulting in the activation of the NF-κB pathway (Hur et al. 2003; Piret, Schoonbroodt, and Piette 1999). DNA-damage-induced NF-κB activation is dependent on RIPK1 since DNA-damage failed to activate NF-κB in $Ripk1^{-/-}$ fibroblasts. Additionally, this complex mediates cell cycle control and DNA repair via p53 and the checkpoint kinase (Chk) 2. Cell cycle arrest as well as NF-κB activation enables the cell to repair DNA lesions and avoid further damage until the DNA damaging agent is cleared. However, excessive damage that cannot be repaired properly leads to the induction of apoptotic death. It was suggested in a previous report that ATM induced apoptotic death via TNF feedfoward signaling (Biton and Ashkenazi 2011). Nevertheless, accumulation of excessive DNA-damage without proper clearance could

result in tumorigenesis. The majority of liver tumors, which are generated by a single injection of DEN, are mutated either in the *Ha-ras* or the *B-raf* gene (Jaworski et al. 2005).

Similar to human HCC, DEN-induced HCC is also more prominent and extensive in males. This gender disparity was reported and shown extensively to depend on the serum IL-6 level that is produced to a greater extent in males. In females the hormone estrogen inhibits the secretion of IL-6 from KCs and therefore reduces the risk of HCC in females (Naugler et al. 2007).
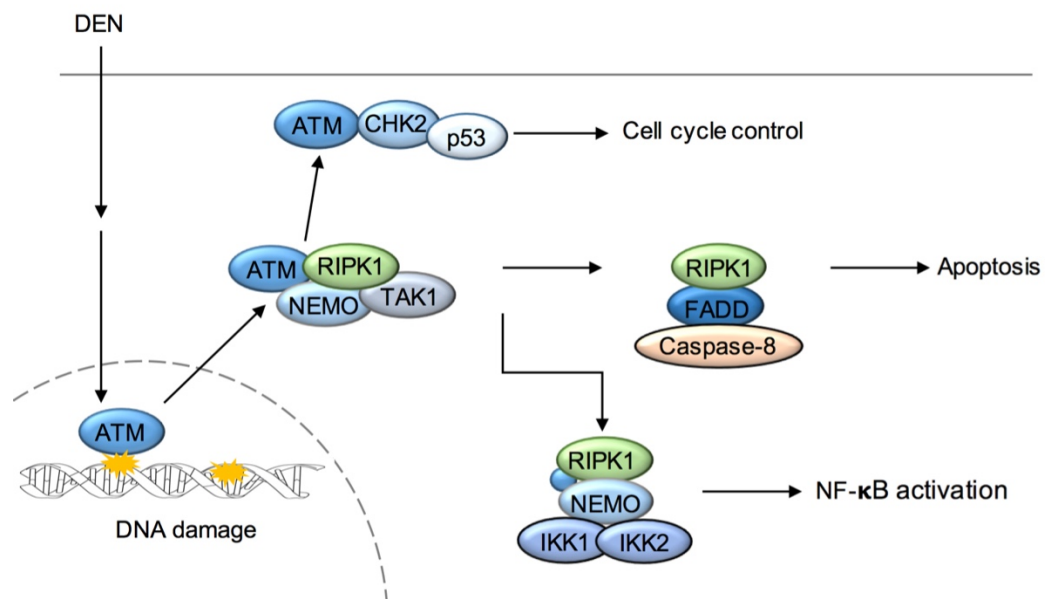
Figure 12. DEN-induced DNA-damage response
The carcinogen DEN needs to be bioactivated by cytochrome P450 in order to cause DNA adducts. DNA adducts are recognized by ATM resulting in either p53-dependent cell cycle control or in the formation of a death-inducing complex consisting of ATM, RIPK1, NEMO and TAK1 mediating NF-κB activation or cell death. Accumulation of DNA-damage without sufficient clearance results in DNA-damage-induced cancer.

The mechanism of tumor initiation after DEN administration has not been fully solved. However, the current model implicates a combined effect of continuous hepatocyte death leading to high regenerative and proliferative capacity of hepatocytes induced by inflammation resulting in steatosis and fibrosis that can progress to cirrhosis. This is consistent with the mechanism involved in the onset of spontaneous HCC in mouse models such as NEMO^{LPC-KO} and tumor initiations in human HCC (Bisgaard and Thorgeirsson 1996; Kondylis et al. 2015). In fact, TLR4-deficient, Bid liver-specific deficient and PUMA-deficient mice showed reduced apoptosis, proliferation and inflammatory markers resulting in reduced HCC development (Weber et al. 2016; Yu et al. 2016; Qiu et al. 2011). In independent reports, it was demonstrated that IKK2^{Δhep} mice developed more HCC than control mice due to enhanced DEN-induced

hepatocyte death and increased hepatocyte proliferation capacity due to increased JNK activation (Koch et al. 2009; Sakurai et al. 2006; Maeda et al. 2005). Furthermore, BCL-2, an anti-apoptotic protein, was reported to delay HCC development upon DEN by interfering with hepatocyte proliferation induced by transforming growth factor alpha (TGFα) signaling (Vail, Pierce, and Fausto 2001). In contrast to these results, *Atm*^{-/-} mice remained protected from DEN-induced HCC up to 15 months although *Atm*^{-/-} mice revealed increased p53 expression-dependent CC3 levels (Teoh et al. 2010). ATM deficiency at the same time upregulated markers of senescence resulting in cell cycle arrest that could protect mice from tumor development (Teoh et al. 2010). Moreover, Gruber et al. reported elevated apoptosis and compensatory levels but reduced HCC formation in IL-6Rα-deficient mice (Gruber et al. 2013). The current model of DEN-induced HCC development highly depends on the correlation between increased cell death and compensatory proliferation. However, the data on DEN-injected *Atm*^{-/-} and IL-6Rα-deficient mice suggest an additional mechanism independent of cell death and compensatory proliferation.

1.5.2.1. Diet-induced obesity and its role in DEN-induced HCC

Epidemiological studies have identified obesity as a major risk factor for several cancer types including HCC (Bianchini, Kaaks, and Vainio 2002; Calle and Kaaks 2004). Under obese conditions, mice develop HCC with higher tumor numbers and tumor size (Calle and Kaaks 2004; Hill-Baskin et al. 2009). Obesity is known to induce a chronic low-grade inflammatory state resulting in immune cell infiltration in the white adipose tissue and the liver. The most prominent cytokines that are chronically expressed under obese conditions are TNF and IL-6 (Park et al. 2010). Blocking TNFR1 signaling reduces DEN/obesity-induced HCC development (Park et al. 2010). It was suggested that constant TNF production under obese conditions may promote an inflammatory environment inducing TNF-mediated cell death and compensatory proliferation resulting in higher tumor formation (Park et al. 2010). In contrast to TNF, IL-6 promotes DEN-induced HCC in lean mice by suppressing myeloid leukemia cell differentiation protein (MCL-1), a Bcl-2 family member, and consequently inhibit cell death. However, under obese conditions Mcl-1 was stabilized and in turn inhibits apoptosis of damaged hepatocytes contributing to the induction and progression of tumors independent of IL-6 signaling (Gruber et al. 2013).

1.6. The role of RIPK1 in tissue homeostasis, liver injury and HCC

Ripk1$^{-/-}$ mice die shortly after birth showing excessive cell death and inflammation in various tissues including gut, skin and the liver (Kelliher et al. 1998; Dillon et al. 2014; Kaiser et al. 2014). Unlike *Ripk1$^{-/-}$*, deficiency of RIPK1 kinase activity alone did not result in extensive cell death or obvious pathological features suggesting that a kinase-independent function of RIPK1 regulates cell survival and tissue homeostasis (Polykratis et al. 2014). Moreover, RIPK1 kinase inactive mutants prevent TNF-induced necroptosis and apoptosis in mouse models with increased cell death implying an essential role for autophosphorylation-mediated activation of RIPK1 in DR-induced cell death (Polykratis et al. 2014; Kondylis et al. 2015; Vlantis et al. 2016). In contrast to RIPK1 KD deficiency, deficiency of RIPK1 RHIM domain largely resembled the perinatal death of *Ripk1$^{-/-}$* mice showing epidermal hyperplasia and immune cell infiltrations suggesting a pro-survival function of the RHIM domain of RIPK1. Genetic studies revealed a pivotal role of the RHIM domain of RIPK1 in regulating skin inflammation and DAI/ZBP1-induced necroptotic death (Lin et al. 2016; Newton et al. 2016).

Similar to *Ripk1$^{-/-}$* mice, intestinal epithelial cell (IEC)-specific or epidermis-specific deficiency of RIPK1 resulted in premature death of mice due to massive IEC/ keratinocyte death and extensive inflammation emphasizing a pro-survival scaffolding function of RIPK1 in the gut and the skin (Dannappel et al. 2014; Takahashi et al. 2014). The gut or the skin resembles the most important barrier protecting from harmful bacteria and viruses. Disruption of either of these barriers enables the invasion of harmful bacteria allowing direct contact with resident immune cells triggering an inflammatory response and might consequently result in the pathology observed in RIPK1^{E-KO} and RIPK1^{IEC-KO} mice. Accordingly, Takahashi et al. identified a MyD88/microbiota-dependent mechanism of RIPK1 in mediating gut pathology using antibiotic treatments or by performing germ-free housing of mice (Takahashi et al. 2014). This finding was challenged by the finding of Dannappel et al. that showed a MyD88/microbiota-independent mechanism of RIPK1 using similar approaches (Dannappel et al. 2014). However, ablation of TNFR1 signaling partially reduced cell death in RIPK1^{IEC-KO} and RIPK1^{E-KO} mice improving tissue homeostasis suggesting a partial role of RIPK1 in negatively regulating TNF-dependent cell death (Takahashi et al. 2014; Dannappel et al. 2014). Moreover, ablation of TNFR1 and TRIF prolonged the survival of *Ripk1$^{-/-}$* mice suggesting a combined effect of TNFR1 and TRIF in mediating cell death, inflammation and the premature death of these mice (Dillon et al. 2014).

Since complete or IEC/keratinocyte specific-deficiency of RIPK1 in mice result in premature death, limited data are available about the kinase-dependent or kinase-independent functions of RIPK1 in response to LPS or in cancer development. Increasing evidence suggests a crucial role for RIPK1 in LPS/TLR-induced toxicity due to its important regulatory role in inflammation and cell death. Vivarelli et al. reported an involvement of RIPK1 in TLR4-mediated signaling by activating PI3K/AKT signaling (Vivarelli et al. 2004). *Ripk1*^{-/-} mouse splenocytes failed to proliferate and show impaired AKT activation in response to LPS resulting in increased apoptotic death suggesting an essential pro-survival function of RIPK1 in TLR4 signaling (Vivarelli et al. 2004).

Despite increasing evidence for an involvement of RIPK1 in the DNA-damage response, evidences for the importance of RIPK1 in DNA-damage-induced carcinogenesis are limited. Recent reports revealed a pro-survival role of RIPK1 in melanoma cells resulting in tumorigenesis and metastasis. Consistently, knockdown of RIPK1 in melanoma cells was reported to sensitize cells to death and consequently in less tumor formation in a xenograft model (Liu et al. 2015; Luan et al. 2015).

Nevertheless, the *in vivo* function of RIPK1 in regulating TLR4-dependent signaling or carcinogenesis remains unaddressed, mainly due to the perinatal lethality of RIPK1 knockout mice (Kelliher et al. 1998; Dillon et al. 2014; Kaiser et al. 2014).

1.7. Project description

RIPK1 is a critical regulator of cell death and inflammation downstream of death receptors (DR)s and toll-like receptors (TLRs) with kinase-dependent and kinase-independent functions. Deregulation of cell death and inflammation are characteristics in the pathogenesis of liver diseases including acute liver failure (ALF) and hepatocellular carcinoma (HCC). ALF and HCC are still life-threatening diseases without effective and efficient long-term therapeutic strategies due to their severity and heterogeneity, which limits the finding of effective medications (Bantel and Schulze-Osthoff 2012; Kim et al. 2016). Therefore, with its dual-function RIPK1 might be a crucial regulator of liver homeostasis, ALF and HCC.

Here we aimed at studying the biological significance of RIPK1 kinase-dependent and -independent functions in the liver using well-established genetic mouse models of ALF or HCC that would allow us to specifically decipher the initiation, promotion and progression of HCC and the processes resulting in ALF.

2. Material and Methods

2.1. Chemicals and biological materials

Kits and chemicals used in this work were purchased from the depicted companies. All solutions were prepared with double-distilled water (ddH$_2$O).

Table 1. Reagents/Chemicals used in this study

Reagents/ Chemicals	Supplier (Catalog number)
Acrylamid/Bis solution	Serva (10688.01)
Ammonium persulphate (APS)	Sigma (A3678-100G)
β-mercaptoethanol	Sigma (M7522)
4-2-hydroxyethyl-1-piperazineethanesulfonic acid (HEPES)	Invitrogen (15630-056)
Agarose ultra-pure	Biozym (840004)
Albumine bovine fraction (BSA)	Biorad (500-0006)
Bromophenol blue	KMF
Complete (Protease EDTA-free Inhibitor Cocktail Tablets	Roche (11836145001)
Diethylnitrosamine (DEN)	Sigma (N0766-10ml)
D-Galactosamine (D-GalN)	Sigma (G0500)
DMEM	Gibco (41965-062)
dimethyl sulfoxide (DMSO)	AppliChem (A3672,0050)
ECL Detection Reagents	GE Healthcare (RPN2132)
ECL Detection Reagents (femto)	Thermo Scientific (34095)
Ethylenediaminetetraacetic acid (EDTA)	JT-Baker (8993-01)
Ethanol absolute	AnalR Normapur (20821-321)
Fetal calf serum (FCS)	PAA (A15-101)
Fluoromount-G	Southern Biotech (0100-01)
Glucose 20%	Fresenius Kabi
100x L-Glutamine (200mM)	Invitrogen (25030123)
Glycerol	VWR (24386-298)
Hydrochloride acid (HCl) 37%	AppliChem (A2427-2500)
Insulin	Sanofi-Aventis (08923023)
Isopropanol (2-Propanol)	AppliChem (A3928)
Ketamin 10mg/ml	Ratiopharm
Lactate Dehydrogenase Assay	Sigma (MAK066-1KT)

Reagents/ Chemicals	Supplier (Catalog number)
Methanol	Sigma (494437)
Nitrogen (liquid)	Sigma (N4638)
Paraformaldehyde (PFA)	AppliCHem (A3813)
PBS (without Ca2+ and Mg2+)	Gibco (14190-094)
100x Penicillin (10000U/ml)/Streptomycin (10000ug/ml)	Invitrogen (15140163)
Phosphatase inhibitor cocktail tablets, PhosSTOP	Roche (04906837 001)
Phosphate buffered saline (PBS)	Gibco (14190-094)
Pierce	ThermoScientific (22660)
Proteinase K	Roche (3115852)
Proteinmarker PeqGold	Peqlab (27-2210)
Rompun 2%	Bayer (321350-RX)
Sodium dodecyl sulfate (SDS)	Millipore (817034.1000)
100x Sodium pyruvate (100mM)	Gibco (11360-039)
Stripping buffer	ThermoScientific (21059)
N,N,N',N' Tetra methylenediamine (TEMED)	Serva (35925)
Tris HCL/Base	VWR (443864E)
Triton X-100	AppliChem (A4975-0500)
Trizol reagent	Invitrogen (15596-018)
Trypsin EDTA	Gibco (12603-010)
Tween-20	Sigma (P1379-500)

Table 2. Kits used in this study

Kits	Supplier (Cat. No.)
ABC Kit Vectastain Elite	Vector (PK 6100)
Avidin/Biotin Blocking Kit	Vector (no. SP-2001)
Liquid DAB Substrate Chromogen System	DakoCytomation (Code K3466)
RNA extraction RNeasy mini Kit	Qiagen (74106)
RNase-free DNase set	Qiagen (79254)
SuperScriptIII cDNA synthesis Kit	Invitrogen (18080-044)
TaqMan® Gene expression Master Mix	Applied Biosystems (4369542)

Table 3. Buffers and solutions used in this study

Buffers and solutions	Composition	
Western blot blocking buffer	PBS	
	Tween-20	0,1%
	BSA (w/v)	5%
	Non-fat dry milk	5%
Cytoplasmic and nuclear protein Extraction buffers	Hypotonic lysis buffer	
	HEPES (pH 7.6)	10 mM
	KCl	10 mM
	$MgCl_2$	1 mM
	EDTA	0.1 mM
	After the swelling step 0.8% (v/v) Nonident P-40, Protease and Phosphatase inhibitors were added prior to use.	
	High salt nuclear lysis buffer	
	HEPES (pH 7.8)	50 mM
	KCl	50 mM
	NaCl	300 mM
	EDTA	0.1 mM
	Glycerol	10% (v/v)
	Protease and Phosphatase inhibitors were added prior to use.	
Endogenous peroxidase blocking buffer (for IHC)	NaCitrate	0.04 M
	Na_2HPO_4	0.121 M
	NaN_3	0.03 M
	H_2O_2	3% (v/v)
High salt RIPA lysis buffer	HEPES (pH 7.6)	20 mM
	NaCl	350 mM
	$MgCl_2$	1 mM
	EDTA	0.5 mM
	EGTA	0.1 mM
	Glycerol	20 %(v/v)
	1% Nonident P-40, Protease and Phosphatase inhibitors were added prior to use	
5x Laemlli loading buffer	Tris-HCL (pH 6.8)	250 mM
	SDS	10% (w/v)
	Glycerol	50% (v/v)
	Bromphenolblue	0.01% (w/v)
	β-Mercaptoethanol	10% (v/v)

Buffers and solutions	Composition
PBS (1x), pH 7.3	NaCl 137 mM KCl 2.7 mM Na2HPO4 – 7H2O 4.3 mM KH2PO4 1.4 mM
Primary and secondary antibody dilution buffer for immunoblots	PBS Tween 0.1% Sodium azide
TAE Buffer (25x) for 10l	Tris-Base 1210 g 0.5 M EDTA (pH 8.0) 500 ml Acetic acid 285.5 ml
Tail lysis Buffer	Tris-HCl (pH 8.5) 100 mM EDTA 5 mM NaCl 200 mM SDS 0.2% (w/v) 0.01mg Proteinase K (1mg/ml in 50 mM Tris, pH 8.0) per 200 µl lysis buffer was added prior to use.
TE Buffer	Tris-HCl (pH 8.0) 10 mM EDTA (pH 8.0) 1 mM
TEX Protease K buffer, pH 8.0	Tris-base 50 mM EDTA 1 mM Triton X-100 0.5% (v/v)
Tris-Glycine electrophoresis	Tris-Base 25 mM Glycine 250 mM SDS 0.1% (w/v)
SDS polyacrylamid gel	<u>10% resolving gel (for 20ml)</u> H_2O 7.9 ml 30% acrylamid mix 6.7 ml 1.5 M Tris (pH 8.8) 5.0 ml 10% (w/v) SDS 0.2 ml 10% (w/v) APS 0.2 ml TEMED 0.008 ml <u>5% stacking gel (for 10ml)</u> H_2O 6,8 ml 30% acrylamid mix 1.7 ml 1 M Tris (pH 6.8) 1.25 ml 10% (w/v) SDS 0.1 ml 10% (w/v) APS 0.1 ml TEMED 0.01 ml
Western blot Transfer Buffer	Tris-Base 25 mM Glycine 192 mM Methanol 20%

2.2. Molecular biology

2.2.1. Isolation of genomic DNA

Genotyping is a process to determine the genetic makeup of mice. For this, mouse tail biopsies were incubated overnight in lysis buffer (s. table 3) in a thermomixer (Eppendorf, Hamburg, Germany) at 56°C and 1100 rounds per minute (rpm). The genomic DNA was precipitated by adding 1 volume of isopropanol. After centrifugation, the DNA pellet was washed with 70% (v/v) ethanol, dried at room temperature (RT) for approximately 10 minutes (min) and subsequently resuspended in TE buffer (s. table 3).

2.2.2. PCR for genotyping

PCR was used to genotype mice using specific primer listed in table 4. PCR is a technique to amplify a piece of deoxyribonucleic acid (DNA)-fragment, generating million copies of this DNA sequence. To amplify this DNA sequence, a mixture containing amongst others water, $MgCl_2$ and Taq was added to 2 µl of the DNA template that was amplified by using a thermal cycler. The first step was an initialization step that heated up the reaction to 95-98°C, which was held for 4 minutes, to activate the DNA polymerase followed by a denaturation step also around 95-98°C for 20-30 seconds. This step is required to melt the double stranded DNA template by disrupting the hydrogen bonds between complementary bases. After that an annealing step at 50-65°C (depending on the primers) was started for 20-40 seconds. This temperature allows the annealing of the primers, which are single stranded nucleic acids acting as a starting point for DNA synthesis, to the single-stranded DNA template. When stable hydrogen bonds between the primer and the DNA template were formed, the polymerase binds to the primer-DNA hybrid and started the DNA synthesis. Finally, an extension and elongation step was performed at 72-80°C (depends on the temperature optimum of the polymerase). At this step the DNA polymerase uses dNTPs that are complementary to the template and synthesizes a complementary DNA chain to the template DNA. To amplify the DNA template, the thermal cycler repeats the denaturation, annealing and extension/elongation step 35 times. After that the final elongation step, which is usually performed at 70-74°C for around 4 minutes, was used to ensure that every single stranded DNA is elongated.

Table 4. Primer-sequences for genotyping PCRs and PCR-amplified fragment sizes

Typing for	Primer Sequence (5'- 3')	Band size
Alfp-Cre	TCC AGA TGG CAA ACA TAC GC	Tg: 300 bp
	GTG TAC GGT CAG TAA ATT GGA C	WT: no band
Fadd floxed	TCA CCG TTG CTC TTT GTC TAC	WT: 208 bp
	GTA ATC TCT GTA GGG AGC CCT	FL: 280 bp
	CTA GCG CAT AGG ATG ATC AGA	DEL: 331 bp
Ripk1 floxed	CAT GGC TGC AAA CAC CTA AAC	WT: 320 bp
	GTT ACA ACA TGC AAA TCA AC	FL: 380 bp
Ripk1 deleted	GAGGAAGACATCACTGAAGA	DEL: 230 bp
	CAGAGGGCTGGATCTGGTGG	
Ripk1$^{D138N/D138N}$	TACCTTCTAACAAAGCTTTCC	WT: 220 bp
	AATGGAACCACAGCATTGGC	D138N: 180 bp
	CCCTCGAAGAGGTTCACTAG	
Tnfr1 floxed	CAA GTG CTT GGG GTT CAG GG	WT: 134 bp
	CGT CCT GGA GAA AGG GAA AG	FL: 195 bp
Tradd floxed	GGC CAG ACA TCT CCA CCG TAG	WT: 400 bp
	TTT GCC TTC AGC CTA AGT TCC	FL: 440 bp
R26ikk2ca$^{sFL/sFL}$	AAAGTCGCTCTGAGTTGTTATC	WT: 570bp
	GATATGAAGTACTGGGCTCTT	sFL: 450bp
	GCATCGCCTTCTATCGCCT	

Table 5. PCR-programes for genotyping PCRs

Typing for	PCR program		Cycles
	Temperature	Time	
Alfp-Cre	94°C	3 min	
	94°C 60°C 72°C	30 sec 30 sec 30 min	35
	72°C	10 min	
Fadd floxed	94°C	3 min	
	94°C 60°C 72°C	30 sec 45 sec 30 sec	35

	72°C	3 min	
Typing for	**PCR program**		**Cycles**
Ripk1 floxed	94°C	2 min	
	94°C 58°C 72°C	30 sec 30 sec 30sec	35
	72°C	5 min	
Ripk1$^{D138N/D138N}$	94°C	2 min	
	94°C 60°C 72°C	30 sec 30 sec 30 sec	40
	72°C	5 min	
Tnfr1 floxed	94°C	3 min	
	94°C 60°C 72°C	30 sec 1 min 2 min	29
	72°C	5 min	
Tradd floxed	95°C	3 min	
	95°C 57°C 72°C	30 sec 30 sec 1.30 min	35
	72°C	5 min	
R26ikk2ca$^{sFL/sFL}$	94°C	3 min	
	94°C 56°C 72°C	30 sec 30 sec 30 sec	35
	72°C	5 min	

2.2.3. Agarose gel electrophoresis

Agarose gel electrophoresis is used to separate the DNA fragments according to their sizes. For this, products of the PCR reaction were analyzed using a 2% agarose gel containing 0.5 mg/ml ethidium bromide. 10 µl of the PCR product containing loading dye was loaded on to the gel and gels were run in 1xTAE buffer for 30 min at 120 mV. DNA was visualized using ultraviolet (UV) light and the size of the PCR product was compared to a standard DNA marker (Peqlab).

2.2.4. Isolation of RNA

RNA extraction from hepatocytes or liver tissues was performed using the Qiagen RNeasy kit following manufacturer's guidelines. For tissue samples, livers were homogenized in 1ml Trizol reagent (Invitrogen). Samples were centrifuged for 10 min

at 13000 rpm to pellet cell debris. The supernatant was transferred into a new tube and in order to extract nucleic acids 200 µl chloroform per 1 ml Trizol was added. Samples were mixed vigorously for 15 sec and were centrifuged for 15 min at 13000 rpm to separate the aqueous and organic phase. The upper aqueous phase was mixed with an equal volume of 70% (v/v) ethanol. Samples were loaded on Qiagen RNeasy columns and centrifugation for 1min at 9000 rpm allows binding of nucleic acids to the filter of the column. Afterwards to digest genomic DNA RNase-free DNase diluted in RDD buffer (provided by the manufacturer) was added to the filter of the column for 20 min. Filters of the columns were washed twice with 500 µl of washing buffer (provided by the manufacturer). RNA was eluted in nuclease free water by centrifugation for 1 min at 13000 rpm. Finally, the concentration and purity of extracted RNA were measured by photometric analysis using a NanoDrop.

2.2.5. cDNA synthesis

Synthesis of cDNA from extracted RNA was performed using the Superscript III kit (Invitrogen) according to manufacturer's instructions. For 10 µl final reaction volume, 1µg RNA was added to 1 µl of 50 ng/µL random hexamer primers and 1 µl of 10 mM dNTPs. The reaction mixture was first incubated at 65°C for 5 min to allow primer annealing and subsequently cooled down on ice for 1 min. Meanwhile, 10 µl cDNA reaction mix containing 2 µl 10x RT-reaction buffer, 4 µl 25 mM MgCl2, 2 µl 0.1 M DTT, 1µl RNase OUT (40 U/µl) and 1 µl of SuperScript III polymerase (200 U/µL) were prepared and added to the samples. Reverse transcription was performed for 10 min at 25°C, 50 min at 50°C for cDNA synthesis and heat-inactivation was performed for 5 min at 85°C in a PCR cycler. To digest the remaining RNA 1 µl RNaseH was added to the reaction and the samples were incubated for 20 min at 37°C. The cDNA reaction mix was diluted 10-fold in nuclease-free water and 2 µl of cDNA was used for an actin-PCR, to check successful cDNA synthesis, and for quantitative real time-PCR (qRT-PCR).

2.2.6. qRT-PCR

Gene expression was quantified by performing probe-based Taqman qRT-PCR. qRT–PCR was performed with TaqMan probes (Table 6) in duplicates for each sample (Life Technologies) with TATA-box-binding protein (*Tbp*) as reference gene. qRT-PCR was performed in a final volume of 10 µl, consisting of 2 µl cDNA, 5 µl Mastermix (Applied Biosystems), 0.5 µl primer-probe mix (Applied Biosystems) and 2.5 µl nuclease-free

water. All reactions were carried out in 384-well plates. Relative expression of gene transcripts was analyzed by using the 2-ΔCt method.

Table 6. Taqman probes used for qRT-PCR

Gene	Taqman probe
A20	Mm00437121_m1
Bax	Mm00432051_m1
Birc2	Mm00431811_m1
Birc3	Mm00431800_m1
Bcl-xl	Mm00437783_m1
cflip	Mm01255580_m1
Fas	Mm00433237_m1
FasL	Mm00438864_m1
Iκbα	Mm00477798_m1
Il-1b	Mm00434228_m1
Il-6	Mm00446190_m1
Il-10	Mm00439616_m1
Il-18	Mm00434225_m1
Il-27	Mm00461162_m1
Noxa	Mm00451763_m1
p53	Mm01731290_g1
p21	Mm00432448_m1
Puma	Mm00519268_m1
Tbp	Mm00446973_m1
Tnf	Mm00443258_m1
Tnfr1	Mm01182929_m1
Trail	Mm01283606_m1
Trailr	Mm00457866_m1
Xiap	Mm00776505_m1

2.2.7. Multiplex assay

(Assay was performed in collaboration with the Papadopoulos lab, Cologne)

The expression of TNF was measured using a bead-based multiplex immunoassay. 50 µl of serum from $Ripk1^{FL/FL}$ and RIPK1^{LPC-KO} mice were analyzed using the Bio-Rad kit (Bio-Rad Laboratories, Hercules, CA, USA) in a multiplex analyzer (Bio-plex200, Bio-Rad Laboratories, Hercules, CA, USA) according to the manufacturer's instructions.

The concentration was calculated from the standard curve and presented as pg/ml of serum.

2.3. Cellular biology

2.3.1. Haematoxylin and Eosin staining of liver tissue sections

Architecture and histology were determined using 5-µm-thick paraffin-embedded liver sections stained with haematoxylin and eosin (H&E). To stain with haematoxylin and eosin paraffin sections were de-paraffinized by incubating for 20 min in xylol followed by rehydration in ethanol-solutions. Thereafter, sections were incubated for 3 min in heamatoxylin solution, differentiated in tap water for 15 min and were subsequently incubated for 1 min in Eosin staining solution. Afterwards sections were dehydrated and fixated using xylol. Slides were finally mounted with Entellan.

2.3.2. Immunhistochemistry

Paraffin sections were rehydrated and heat-induced antigen retrieval was performed in citrate, TRIS buffer, pH 6 (Table 3). Sections were incubated with primary antibodies listed in table 7. Biotinylated secondary antibodies were purchased from Perkin Elmer and Dako. Stainings were visualized with ABC Kit Vectastain Elite (Vector Laboratories) and DAB substrate (DAKO and Vector Laboratories). Incubation times with DAB substrate were equal for all samples.

Table 7. Primary antibodies used for IHC in this study

Antibodies	Company	Cat. No.
anti-B220	home made	clone RA3 6B2
anti-CD3	Abcam	Ab 5690
anti-cleaved Caspase-3	Cell Signaling	9661
anti-cleaved Caspase-8	Cell Signaling	8592
anti-cleaved Caspase-9	Cell Signaling	9509
anit-Ki-67	Dako	M724901
α-SMA	Sigma Aldrich	A2547
anti-F4/80	AbD Serotec	clone A3-1
anti-γH2AX	Millipore	05-636
anti-p53	Leica	NCL-p53-CM5p

2.3.2.1. Quantification of positively stained cells

IHC quantification was performed on 5-10 randomly selected fields (10x magnification) per liver section. Liver sections from 3-7 mice per genotype per timepoint (after LPS or DEN) were analyzed. Quantifications of cleaved Caspase-3+, Caspase-8+ and Caspase-9+ cells were performed manually. γH2AX+ cells were quantified using Image J software (Version 1.48;http://rsbweb.nih.gov/ij/) by applying the appropriate pixel threshold equally on all selected images. Graphs are indicating the average number of γH2AX+ cells of 5 randomly selected fields per mouse.

2.4. Biochemistry

2.4.1. Preparation of protein extracts

Liver tissues of mice were collected and snap frozen at −80 °C until processing. Tissues were homogenized using Precellys and homogenized lysates or hepatocytes were lysed in protein lysis buffer supplemented with protease and phosphatase inhibitor tablets (Table 3). Protein concentration was assessed using the Pierce dye-binding method kit (Bio-rad).

2.4.2. Subcellular fractionation

Primary hepatocytes were treated with 20ng/ml murine TNF for 30,60,120, 240 min or left untreated. Cells were directly lysed in hypotonic buffer (Table 3) for 10 min on ice followed by centrifugation for 5 min, 2300g at 4°C. The supernatants were collected as cytoplasmic extracts. The pellets were washed twice with hypotonic buffer and lysed in high salt nuclear lysis buffer including phosphatase inhibitors (Roche) and complete protease inhibitors (Roche) (Table 3) for 30 min on ice. Cell lysates were centrifuged for 10 min at 16000 g at 4°C, and the supernatants were collected as nuclear extracts.

2.4.3. Western blot analysis

Protein lysates (50µg Protein/20µl) were separated on SDS-PAGE and transferred to PVDF membranes (IPVH00010, Millipore). Membranes were blocked with 5% milk/0.1% PBST and were probed with primary antibodies against the proteins indicated in table 8 for 16h at 4°C. Membranes were washed thrice with 0.1% PBST and were incubated with a horseradish peroxidase conjugated secondary antibody indicated in table 9 for 1h at RT. Proteins were detected with enhanced chemiluminescent detection substrate (GE Healthcare and Thermo Scientific).

Table 8. Primary antibodies and conditions used for immunoblot analysis

Antibodies	Company	Cat. No.	Source	Dilution
β-Actin	Santa Cruz	I19	Goat	1:1000
cFLIP	Alexis	ADI-AAP-440-E	Rabbit	1:1000
cIAP1	Enzo	ALX-803-335-C100	Rat	1:1000
Cleaved Caspase-3	Cell Signaling	9661	Rabbit	1:1000
PARP1	Cell Signaling	9542	Rabbit	1:1000
p-ERK	Cell Signaling	9101	Rabbit	1:1000
ERK	Cell Signaling	9102	Rabbit	1:1000
FADD	Upstate	05-486	Rabbit	1:1000
p-IκBα	Cell Signaling	9246	Mouse	1:1000
IκBα	Santa Cruz	Sc-371	Rabbit	1:1000
p-JNK	Cell Signaling	9251	Rabbit	1:1000
JNK	Cell Signaling	9252	Rabbit	1:1000
Lamin A/C	Santa Cruz	Sc-6215	Goat	1:1000
RIPK1	BD Biosciences	610459	Mouse	1:1000
RelA	Santa Cruz	Sc-372	Rabbit	1:1000
p-p38	Cell Signaling	9211	Rabbit	1:1000
p38	Cell Signaling	9212	Rabbit	1:1000
p53	Cell Signaling	2524	Mouse	1:1000
TNFR1	Cell Signaling	13377	Rabbit	1:1000
TRADD	Santa Cruz	sc-7868	Rabbit	1:1000
TRAF2	Santa Cruz	Sc-876	Rabbit	1:1000

Table 9. Secondary antibodies and conditions used for immunoblot analysis

Antibodies	Company	Cat. No.	Source	Dilution
Rabbit IgG-HRP	GE healthcare	NA934V	Goat	1:5000
Mouse IgG-HRP	GE healthcare	NA9310V	Sheep	1:5000
Goat IgG HRP	Jackson Lab	705-035-003	donkey	1:10000
Rat IgG-HRP	Jackson Lab	112-035-003	Goat	1:10000

2.5. Mouse experiments

2.5.1. Animal care

All animal procedures and experiments were performed in compliance with protocols and licenses approved by local government authorities (Bezirksregierung Köln) and were performed according to the National Institutes of Health guidelines. All mice were

housed with 3-4 animals per cage at 22-24°C and at regular 12 hours light/dark cycle with the light on at 6 am. Unless otherwise stated, animals were allowed *ad libitum* access to regular chow diet (Teklad Global Rodent 2018, Harlan) and acidified drinking water. For obesity-induced DEN-induced HCC experiments animals were allowed *ad libitum* access to either normal chow diet (NCD) (ssniff EF acc. D12450 (l) mod.) containing 13kJ% fat or high-fat diet (HFD) (ssniff EF acc D12492 (l) mod.) containing 60kJ% fat and acidified drinking water.

For breeding, male and female mice were placed together into one cage at a minimum age of 8 weeks. Litters were marked with ear tags at 2 weeks of age and tail biopsies were taken for genotyping. At 3 weeks of age litters were weaned.

Animals requiring medical attention after LPS, LPS/D-GalN or DEN injection were receiving appropriate care and were excluded from experiments described. No other exclusion criteria existed.

2.5.2. Causes recombination (Cre)/LoxP conditional gene targeting

The Cre/LoxP mediated recombination of conditional genes allows cell type-specific deletion of genes of interest early during embryonic development enabling cell type-specific analysis of gene functions. To generate a conditional knockout allele, two LoxP sites which are specific 34 bp DNA sequences need to be inserted in the same orientation to flank the gene locus or exon of interest (Rajewsky et al. 1996; Sauer 1988). The 34bp LoxP sites consist of a 8bp spacer that is flanked by two 13bp inverted palindromes (Figure 13A). The spacer region is the only factor that contributes to the orientation of the LoxP sites. LoxP orientation is important in determine the type of recombination such as intra-molecular inversion or excision. Co-alignment of two loxP sites in the same molecule preferably induces excision of the gene of interest and circulation of the excised DNA (Figure 13B). Cre-recombinase also catalyzes the reverse reaction namely the (re-)integration of DNA into a single loxP. Nevertheless, integration is inefficient due to the fact that reinserted DNA is flanked by two loxP sites favoring re-excision (Araki et al. 1997). In addition to DNA excision, Cre-recombinase can induce DNA inversion in presence of inverted loxP sites (Figure 13C).
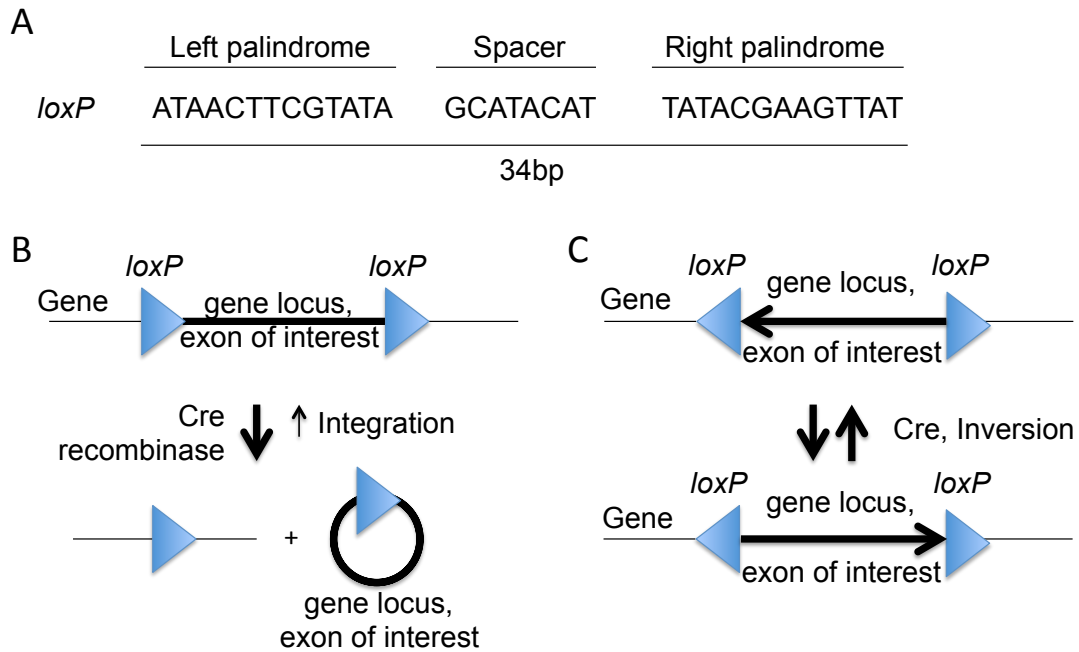
Figure 13. Cre/LoxP-mediated conditional gene targeting
(A) The 34bp loxP site is the recognition site of Cre recombinases consisting of an asymmetric 8bp sequence which is flanked by two sets of 13bp palindromic sequences. (B-C) The orientation of the loxP sites is of high importance for the type of recombination. Therefore, loxP sites in the same direction favors the excision and the circulation of the exon of interest while inverted loxP site induces inversion of the exon of interest.

An allele carrying loxP sites is referred to as ‚floxed' (FL) and consequently, mice carrying an allele with loxP sites are named floxed mice. In order to delete a loxP site flanked gene/exon of interest, floxed mice are crossed to mice expressing a bacteriophage P1-derived Cre recombinase under the control of a tissue-specific promoter. Only in Cre-expressing cells, loxP sites are recognized and recombined by Cre recombinase resulting in excision of the floxed gene fragment and consequently inactivation of the gene of interest.

2.5.3. Generation of mice

Mice with LPC-specific deletion of RIPK1 were generated by crossing *Ripk1*$^{FL/FL}$ mice with *Alfp-Cre* transgenic mice (Kellendonk et al. 2000). *Ripk1*$^{FL/FL}$ mice were generated as previously described in (Dannappel et al. 2014). RIPK1^{LPC-KO} mice were crossed to *Fadd*$^{FL/FL}$ (Mc Guire et al. 2010), *R26ikk2ca*$^{sFL/sFL}$ (Sasaki et al. 2006), *Ripk1*$^{D138N/D138N}$ (Polykratis et al. 2014), *Tnfr1*$^{FL/FL}$ (Van Hauwermeiren et al. 2013) or *Tradd*$^{FL/FL}$ (Ermolaeva et al. 2008) mice to generate double deficient mice. For all experiments littermates not carrying the *Alfp-Cre* transgene were used as control mice.

2.5.4. Serum levels of alanine (ALT), aspartate amino transferase (AST) and Low-density-lipoprotein-cholesterol (LDL-C)

Blood was collected from the caval vein during sacrifice and was spun down at 10000rpm for 15 min to collect the sera. Serum ALT, AST and LDL-C levels were measured in the sera of mice using standard assays in a Roche-Cobas C111 biochemical analyzer.

2.5.5. Intraperitoneal injection (i.p.) of LPS and D-GalN

Mice were injected i.p. at 9 weeks of age with LPS 5µg/g BW LPS (Sigma Aldrich). Mice were sacrificed 5.5h after LPS injection using CO_2 or their survival was monitored. In cases of combined LPS/D-GalN injection, 1mg/g BW D-GalN was injected 1h prior to LPS injection.

2.5.6. Isolation of hepatocytes

Primary hepatocytes were isolated from livers of 5-week-old mice by perfusing through the vena cava with EBSS supplemented with 100mM EGTA followed by a collagenase solution, containing EBSS, 15mg Collagenase type 2 and 2mg trypsin inhibitor, at 37°C. Afterwards, the liver was gently scraped in DMEM medium supplemented with 1% FCS and filtered through a 70 µm nylon filter. The flow-through was mixed with 1 volume of a 90% Percoll/HBSS solution and spun at 450g for 7 min. Hepatocytes settled at the bottom were washed twice with DMEM 1% FCS medium and were plated on collagen-coated plates. 4h after plating medium was changed.

2.5.7. Cell survival assay (Lactate Dehydrogenase assay)

Primary hepatocyte death *in vitro* was determined using a lactate dehydrogenase (LDH) release-based cytotoxicity assay (Promega) after incubating primary hepatocytes for 16h in absence or presence of 1µg/ml cycloheximide, 20 µM zVAD-fmk (Enzo LifeSciences), 10µg/ml anti-TNF (Etanercept) or 50ng/ml anti-FasL (106808, Biozol). LDH ratio (released/total LDH) was determined on cell sample supernatants using CytoTox 96 cytotoxicity assay (Promega) according to the manufacturer's protocol. The experiments were performed in triplicates (n=6 per genotype).

2.5.8. Intraperitoneal injection of DEN

2.5.8.1. DEN-induced carcinogenesis

Mice were injected i.p. at 2-weeks of age with DEN 25 mg/kg BW (Sigma Aldrich) and were sacrificed either after 3h, 6h, 12h, 24h and 48h upon DEN injection using CO_2 or were maintained until the age of 32 or 36 weeks fed with either regular chow diet or HFD. For all experiments only male mice were used.

2.5.8.2. Histopathological evaluation of HCC development in DEN-injected 32- and 36-week-old mice (Evaluation was performed by Dr. Beate Straub)

H&E stained liver sections from mice were assessed for the presence and the stage of HCC development in the following ascending order of severity: No pathology, clear cell foci, small and large cell changes (anisokaryosis), dysplastic foci, dysplastic nodules and early, small or well-differentiated HCC. Each liver sample was placed only based on the most advanced stages, despite the fact that also less advanced stages were observed in these liver samples. In the corresponding graphs, each bar represents the % of livers per genotype in which the indicated stage was identified as the most advanced disease stage.

2.5.8.3. acute dose of DEN

6-week-old mice were injected i.p. with DEN 100 mg/kg BW and were sacrificed after 3, 6, 24 and 48h after DEN injection using CO_2. For all experiments only male mice were used.

2.5.8.4. Glucose tolerance test

Glucose-tolerance tests (GTT) were performed on animals fasted for 16h overnight. Mice were injected i.p. with 10µl/g BW glucose and blood glucose levels were measured 15, 30, 60 and 120min after glucose injection. GTT was performed with 12 week-old animals fed *ad libitum* with either NCD or HFD and was repeated at 24 weeks of age.

2.6. Computer analysis

2.6.1. Software

Leica microscopy Software Leica application suite, Prism Graph, Microsoft Office, EndnoteX7

2.6.2. Statistical analysis

Data shown in graphs represent the mean, except bodyweight curves and glucose levels that show the mean ± s.e.m., as indicated in the figure legends. To determine the group size necessary for adequate statistical power, power analysis was performed using preliminary data sets. Statistical significance for two groups of nonparametric data was assessed by Mann–Whitney. For multiple group comparison, one-way Anova test was performed with a Post-hoc Tukey test for pairwise comparison of subgroups (equal variance assumed). X2-test was performed for the distribution of tumors of two groups. When two independent variables were compared, the Two-way Anova was performed. To compare the survival curves of mice the Mantel-Cox test was used. *$P \leq 0.05$, **$P \leq 0.01$, ***$P \leq 0.005$. Statistical analysis was performed with Prism version 6.0 (GraphPad).

3. Results

3.1. RIPK1 is not involved in normal liver homeostasis and development

3.1.1. Generation of mice with LPC-specific RIPK1 deficiency

To investigate the role of RIPK1 in LPCs, mice with specific deletion of RIPK1 in hepatocytes and biliary cells were generated. Therefore, mice carrying loxP-flanked RIPK1 alleles ($Ripk1^{FL/FL}$) (Dannappel et al. 2014) were crossed with mice expressing Cre recombinase under the control of an ALFP promoter. In these mice, efficient Cre recombination results in deficiency of RIPK1 specifically in hepatocytes and biliary epithelial cells but not in endothelial or KCs (hereafter referred to as RIPK1^{LPC-KO} mice). Successful deletion of RIPK1 was confirmed in isolated hepatocytes and in whole liver tissue lysates by immunoblot analysis (Figure 14).
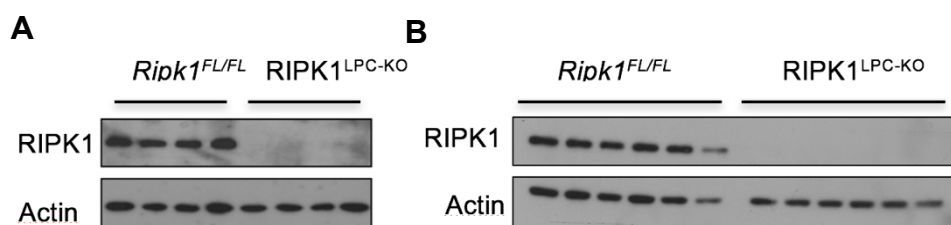
Figure 14. Conditional deletion of RIPK1 in LPCs
Immunoblot analysis for RIPK1 in whole protein extracts from primary hepatocytes (A) and liver tissues (B) from $Ripk1^{FL/FL}$ and RIPK1^{LPC-KO} mice. Actin was used as loading control.

3.1.2. LPC-specific deficiency of RIPK1 does not result in spontaneous liver pathology

RIPK1^{LPC-KO} mice were born at the expected Mendelian frequency with similar bodyweight and size compared to their floxed littermates at least up to the age of 1 year (Figure 15A). Measurement of alanine and aspartic acid aminotransferases (ALT and AST respectively), which are released into the bloodstream upon hepatocyte damage, in the sera of RIPK1^{LPC-KO} mice showed only minor elevation of ALT and AST which did not considerably affect liver homeostasis (Figure 15B). Macroscopic evaluation of the liver and histological analysis revealed similar liver morphology between RIPK1^{LPC-KO} mice and their floxed littermates even at 1 year of age (Figure 15C). Although liver morphology was not affected by RIPK1 deficiency, focal accumulations of immune cells in H&E-stained liver sections of RIPK1^{LPC-KO} mice were observed (Figure 15C). In these immune cell foci strong staining for Ki-67 and cleaved Caspase-3 (CC3) was detected indicative for high levels of immune cell proliferation and apoptosis respectively (Figure 15C). Immunohistological characterization of these

immune cell patches revealed the presence of macrophages, B- and T-cells judged by positive staining for F4/80, B220 and CD3 respectively (Figure 15D). Nevertheless, accumulation of immune cells in the liver of RIPK1[LPC-KO] mice did not result in considerable liver inflammation at least up to the age of 1 year indicated by similar *Il1b* and *Tnf* gene expression levels (Figure 15E).

Despite increased Ki-67 and CC3 levels in immune cell patches, immunohistological analysis of the liver parenchyma revealed similar levels for Ki-67 and CC3 between RIPK1[LPC-KO] and their floxed littermates suggesting similar hepatocyte proliferation and apoptosis under steady state conditions (Figure 15C). Furthermore, livers of RIPK1[LPC-KO] mice did not show signs of fibrosis as assessed by immunostaining for alpha-smooth muscle actin (αSMA), a differentiation marker of smooth muscle cells and myofibroblasts (Figure 15C). Taken together, LPC-specific ablation of RIPK1 does not affect normal liver development and homeostasis.
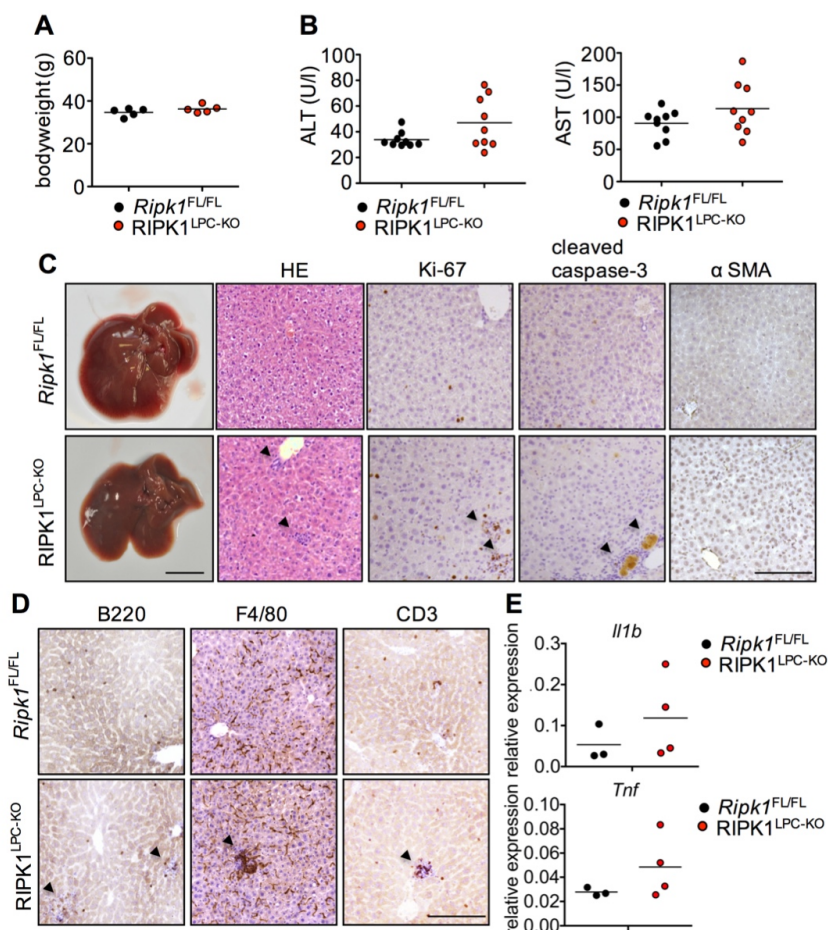
Figure 15. LPC-specific deficiency of RIPK1 did not affect normal liver homeostasis
(A) Bodyweight and (B) ALT and AST levels of *Ripk1*[FL/FL] and RIPK1[LPC-KO] mice at 1 year of age. (C) Representative picture of the liver (Scale bar, 1cm) and of liver sections stained with hematoxylin and eosin and for Ki-67, CC3 and αSMA from *Ripk1*[FL/FL] and RIPK1[LPC-KO] mice (n=4 per genotype). Scale bar 100μm. (D) Representative liver sections of *Ripk1*[FL/FL] and RIPK1[LPC-KO] mice immunostained for B220, F4/80 and CD3 (n=4 per genotype). Scale bar 100μm. Arrows indicate immune cell patches. (E) qRT-PCR analysis of *Il1b* and *Tnf* gene expression in livers from *Ripk1*[FL/FL] and RIPK1[LPC-KO] mice. Graphs show relative mRNA expression normalized to *Tbp*.

3.2. RIPK1 prevents LPS-induced liver injury by inhibiting TNF-induced hepatocyte apoptosis

3.2.1. RIPK1^{LPC-KO} mice are prone to LPS-induced liver injury

To investigate the LPC-specific role of RIPK1 in LPS-induced liver injury, groups of *Ripk1$^{FL/FL}$* and RIPK1^{LPC-KO} mice were injected i.p. with a sublethal-dose of LPS (5 µg/g of BW LPS). In contrast to *Ripk1$^{FL/FL}$* mice, LPC-specific loss of RIPK1 sensitized mice to LPS-induced liver injury resulting in death of all mice within 6h after LPS injection (Figure 16A). RIPK1^{LPC-KO} mice showed strongly elevated ALT and AST levels 5.5h after LPS injection indicative of severe liver damage (Figure 16B). Immunostaining of liver sections with antibodies against CC3 (Figure 16C) and immunoblot analysis of liver protein lysates for CC3 and cleaved PARP1 (Figure 16D) revealed increased hepatocyte apoptosis in livers of LPS-injected RIPK1^{LPC-KO} mice suggesting an anti-apoptotic role for RIPK1 in hepatocytes in response to LPS.
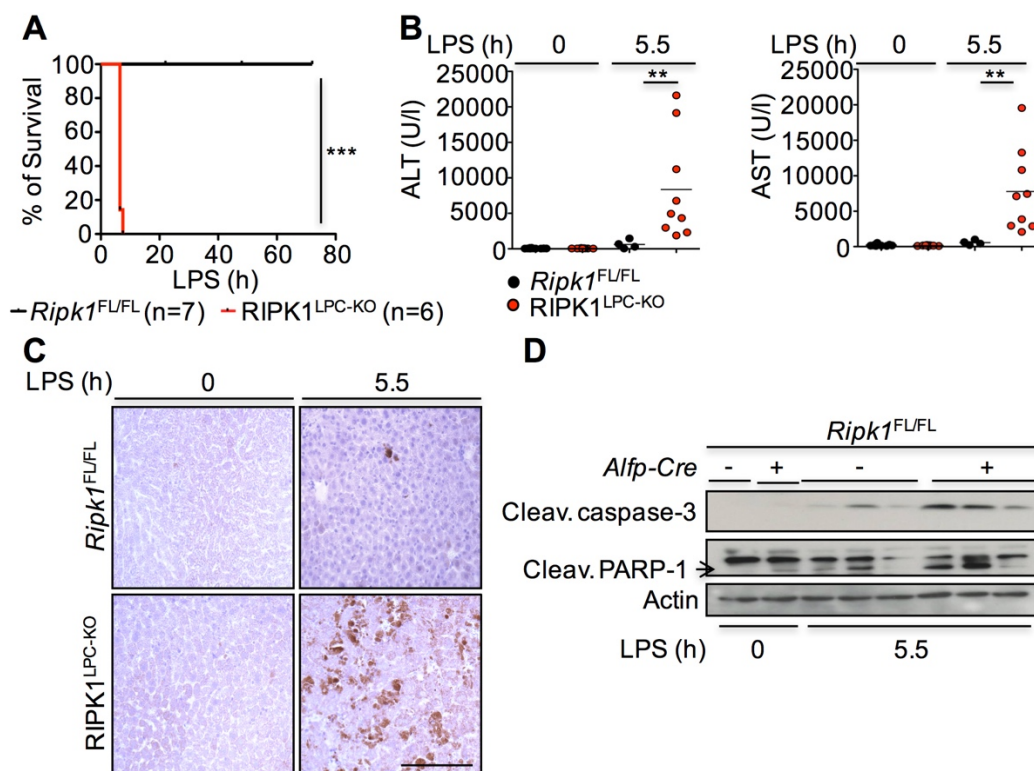
Figure 16. LPC-specific ablation of RIPK1 sensitized mice to LPS-induced liver injury
Graphs depicting survival (A) and ALT and AST levels (B) of 9-week-old non-injected or LPS-injected *Ripk1$^{FL/FL}$* and RIPK1^{LPC-KO} mice (***P<0.005 for A, **P < 0.01 for B). (C) Representative liver sections of *Ripk1$^{FL/FL}$* and RIPK1^{LPC-KO} mice immunostained for CC3 untreated or 5.5h after LPS-injection (n=4-5 per genotype). Scale bar 100µm. (D) Immunoblot analysis for cleaved Caspase-3 and cleaved PARP-1 in liver lysates from *Ripk1$^{FL/FL}$* and RIPK1^{LPC-KO} mice. Actin was used as loading control.

Given the higher susceptibility of RIPK1[LPC-KO] mice to LPS-induced liver injury, the inflammatory level in the liver of RIPK1[LPC-KO] mice was assessed compared to *Ripk1*[FL/FL] mice. At 5.5h after LPS application RIPK1[LPC-KO] mice had slightly elevated gene expression levels of pro-inflammatory cytokines suggesting mild LPS-induced inflammation in these mice (Figure 17).
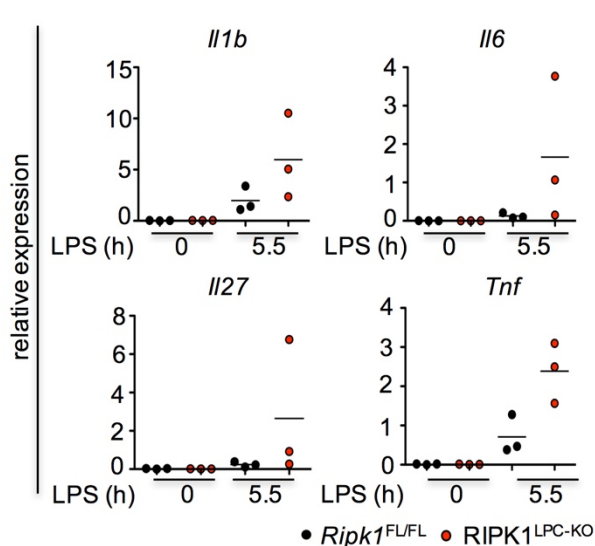
Figure 17. LPS-injected RIPK1[LPC-KO] mice showed mildly elevated cytokine expression levels in the liver
qRT-PCR analysis of cytokine gene expression in nontreated and LPS-injected livers from *Ripk1*[FL/FL] and RIPK1[LPC-KO] mice. Graphs show relative mRNA expression normalized to *Tbp*.

Measuring the level of TNF in the serum of RIPK1[LPC-KO] and *Ripk1*[FL/FL] mice at 1, 2 and 8h after LPS injection revealed similar levels of TNF between both groups (Figure 18). This result suggests that the increased liver damage in LPS-injected RIPK1[LPC-KO] mice may not be due to increased TNF release in response to LPS but rather due to a higher sensitivity of RIPK1-deficient hepatocytes to TNF.
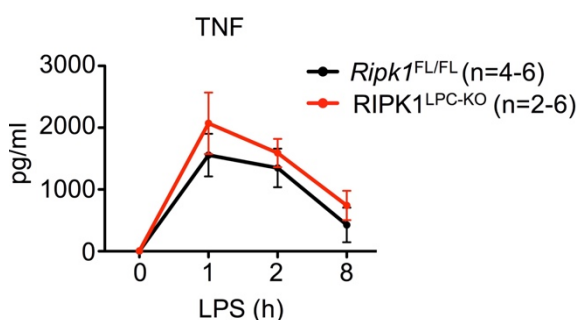
Figure 18. LPS-treated *Ripk1*[FL/FL] and RIPK1[LPC-KO] mice showed similar serum TNF levels
Graph depicting the serum TNF levels of LPS-treated *Ripk1*[FL/FL] (black, timepoint 0h, n= 4; timepoint 1h, 2h, 8h, n= 6) and RIPK1[LPC-KO] (red, timepoint 0h, 1h, 2h, n=6; timepoint 8h, n= 2) mice measured by multiplex cytokine assay (mean ± SEM).

3.2.2. RIPK1 scaffolding function protects mice from LPS- but RIPK1 kinase activity drives LPS/D-GalN induced liver injury

To explore the kinase-dependent and kinase-independent functions of RIPK1 in response to LPS or LPS/D-GalN, knock-in mice expressing a catalytically inactive kinase domain introduced by an aminoacid exchange at position 138 from aspartic acid to asparagine (hereafter referred to as *Ripk1*[D138N/D138N]) were used (Polykratis et al. 2015). *Ripk1*[FL/FL], RIPK1[LPC-KO] and *Ripk1*[D138N/D138N] mice were injected with LPS and

their survival was monitored for 72h. In contrast to RIPK1^{LPC-KO} mice, $Ripk1^{D138N/D138N}$ mice were less prone to LPS-induced toxicity as 80% of $Ripk1^{D138N/D138N}$ mice survived for at least 72h while none of RIPK1^{LPC-KO} mice survived longer than 6h suggesting that the kinase-independent scaffolding function of RIPK1 prevented liver damage in response to LPS (Figure 19A).

In order to analyze the kinase-dependent functions of RIPK1 in cell death, the hepatic transcription inhibitor D-GalN was used in addition to LPS in order to sensitize hepatocytes to death. 50% of $Ripk1^{D138N/D138N}$ mice survived in response to LPS/D-GalN injection opposed to none of the WT littermates emphasizing a death-inducing function of RIPK1 kinase activity (Figure 19B).
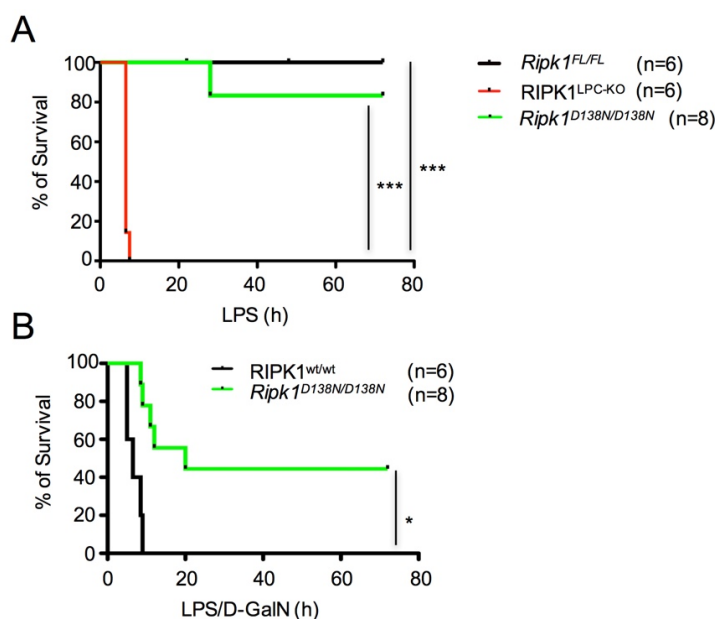
Figure 19. $Ripk1^{D138N/D138N}$ mice were protected to LPS- and LPS/D-GalN mediated liver injury
Kaplain-Meier survival curve of $Ripk1^{FL/FL}$, RIPK1^{LPC-KO} and $Ripk1^{D138N/D138N}$ mice injected with LPS (A) and LPS/D-GalN (B) (***P<0.005, *P<0.05).

3.2.3. RIPK1 prevents TNF-dependent and -independent apoptotic death of primary hepatocytes

To elucidate the mechanism of RIPK1 in preventing LPS-induced liver damage primary hepatocytes from RIPK1^{LPC-KO} and $Ripk1^{FL/FL}$ mice were isolated. Although *in vivo* RIPK1 deletion did not affect basal liver homeostasis, RIPK1-deficient primary hepatocytes died spontaneously in culture within 24h after isolation (Figure 20). Spontaneous hepatocyte death of RIPK1-deficient hepatocytes was prevented by the pan-Caspase inhibitor zVAD-fmk suggesting that RIPK1-deficient hepatocytes died predominantly by apoptosis (Figure 20). Moreover, the addition of a TNF inhibitor reduced considerably spontaneous apoptosis of RIPK1-deficient hepatocytes, while the addition of a neutralizing antibody against FasL had no measurable effect even when given together with a TNF inhibitor. Together these results suggest that RIPK1-deficient hepatocytes undergo TNF-dependent but also TNF-independent apoptosis (Figure 20).
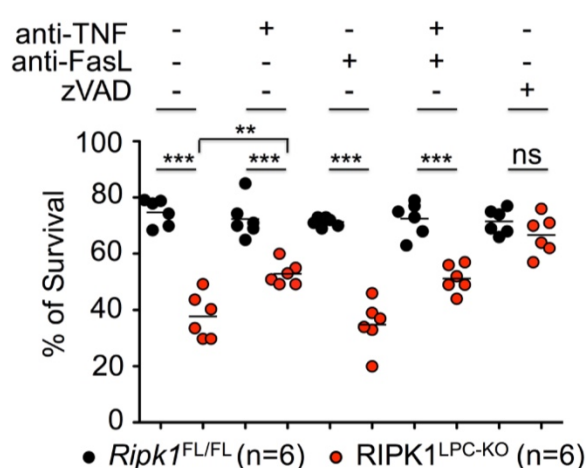
Figure 20. Loss of RIPK1 sensitized hepatocytes to TNF-dependent and –independent apoptosis
Graph depicting survival of *Ripk1*^{FL/FL} and RIPK1-deficient hepatocytes 24h after isolation. Hepatocytes were cultured for 24h in the presence or absence of a TNF inhibitor, a neutralizing antibody for FasL or zVAD-fmk (***P< 0.001, **P< 0.01, ns= not significant).

3.2.4. RIPK1 deficiency impairs TNF-induced NF-κB activation in primary hepatocytes

Since impaired NF-κB activation was reported to sensitize cells to death (Kondylis et al. 2015), NF-κB activation in RIPK1-deficient primary hepatocytes was assessed in response to TNF. To prevent spontaneous hepatocyte apoptosis, hepatocytes were cultured in presence of zVAD-fmk allowing the analysis of TNF-induced NF-κB signaling. To confirm that zVAD-fmk did not affect TNF signaling, *Ripk1*^{FL/FL} primary hepatocytes were cultured in presence or absence of zVAD-fmk and the response to TNF was compared. In presence of zVAD-fmk, NF-κB activation remained unaffected in response to TNF in *Ripk1*^{FL/FL} primary hepatocytes indicated by similar IκBα degradation by immunoblot analysis (Figure 21A). In addition, NF-κB target gene expression was similar in *Ripk1*^{FL/FL} hepatocytes in presence or absence of zVAD-fmk (Figure 21B).
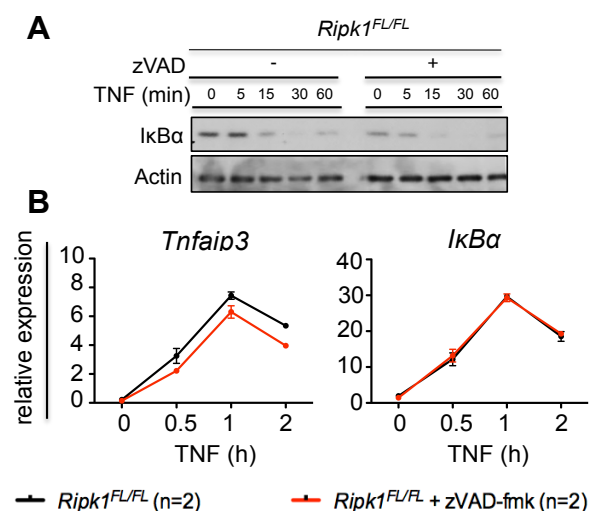
Figure 21. zVAD-fmk stimulation of hepatocytes did not affect TNF-induced NF-κB activation
(A) Immunoblot of *Ripk1*^{FL/FL} hepatocytes for IκBα after TNF stimulation for the depicted timeperiods in absence or presence of zVAD-fmk. Actin was used as loading control.
(B) Gene expression levels of *Tnfaip3* and *Ikbα* in response to TNF in absence or presence of zVAD-fmk. Graphs show relative mRNA expression normalized to *Tbp*.

To elucidate whether ablation of RIPK1 affects NF-κB activation, *Ripk1*^{FL/FL} and RIPK1-deficient primary hepatocytes were isolated and cultured with zVAD-fmk over night

before stimulation with TNF for 5, 15, 30, 60 and 120 min. TNF stimulation caused rapid phosphorylation and degradation of IκBα (Figure 22A) and robust nuclear accumulation of the NF-κB subunit RelA in *Ripk1*^{FL/FL} hepatocytes (Figure 22B) while RIPK1-deficient primary hepatocytes did not show RelA nuclear translocation, phosphorylation and degradation of IκBα. Consistently, gene expression levels of NF-κB target genes, *Tnfaip3, Birc3, Nfkbia* and *Tnf,* were significantly reduced in absence of RIPK1 (Figure 22C). Therefore, deficiency of RIPK1 strongly impaired NF-κB activation in primary hepatocytes *in vitro.*
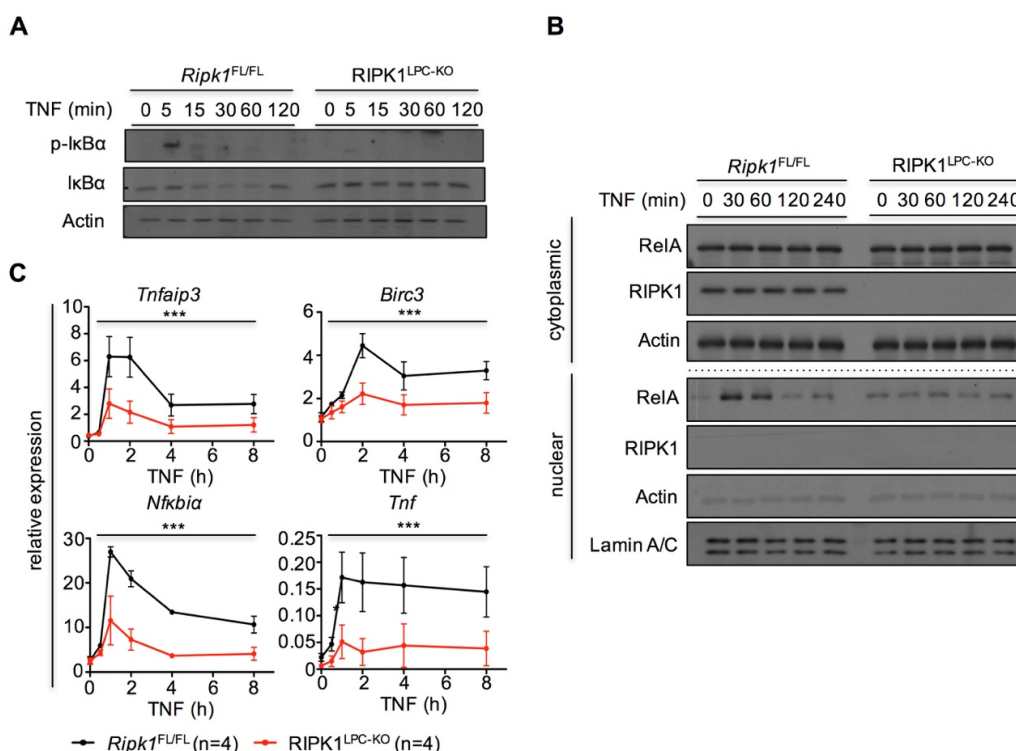
Figure 22. Loss of RIPK1 in hepatocytes impaired TNF-induced NF-κB activation
(A) Immunoblot analysis of p-IκBα and IκBα in total protein lysates of zVAD-fmk treated *Ripk1*^{FL/FL} and RIPK1-deficient primary hepatocytes stimulated with TNF for the depicted time periods. (B) Immunoblot analysis for RelA in cytoplasmic and nuclear extracts from zVAD-fmk stimulated *Ripk1*^{FL/FL} or RIPK1-deficient hepatocytes. Actin and Lamin A/C were used as loading controls. (C) qRT-PCR analysis of NF-κB target gene expression in TNF stimulated *Ripk1*^{FL/FL} and RIPK1-deficient primary hepatocytes (mean± SEM, ***P<0.005). Graphs show relative mRNA expression normalized to *Tbp*.

3.2.5. LPC-specific deficiency of RIPK1 sensitizes hepatocytes to FADD-dependent apoptosis in response to LPS

To investigate whether RIPK1 deficiency sensitizes hepatocytes to FADD-dependent apoptosis in response to LPS, RIPK1^{LPC-KO} mice were crossed to *Fadd*^{FL/FL} mice to generate RIPK1^{LPC-KO} mice that additionally lacked FADD in LPCs. Efficient deletion of FADD in RIPK1^{LPC-KO} livers was confirmed by immunoblot analysis (Figure 23A).

LPC-specific ablation of FADD fully prevented the early death of RIPK1[LPC-KO] mice upon injection with LPS (Figure 23B). Moreover, deficiency of FADD significantly reduced serum ALT and AST levels (Figure 23C) and apoptotic death indicated by immunoblot analysis of liver protein extracts for CC3 (Figure 23D) and IHC for CC3 (Figure 23E) in RIPK1[LPC-KO] FADD[LPC-KO] mice to the same extent like in LPS-injected *Ripk1[FL/FL]* mice. Taken together, these results demonstrate that the high liver damage in RIPK1[LPC-KO] mice is triggered by LPS-induced FADD-dependent apoptosis.
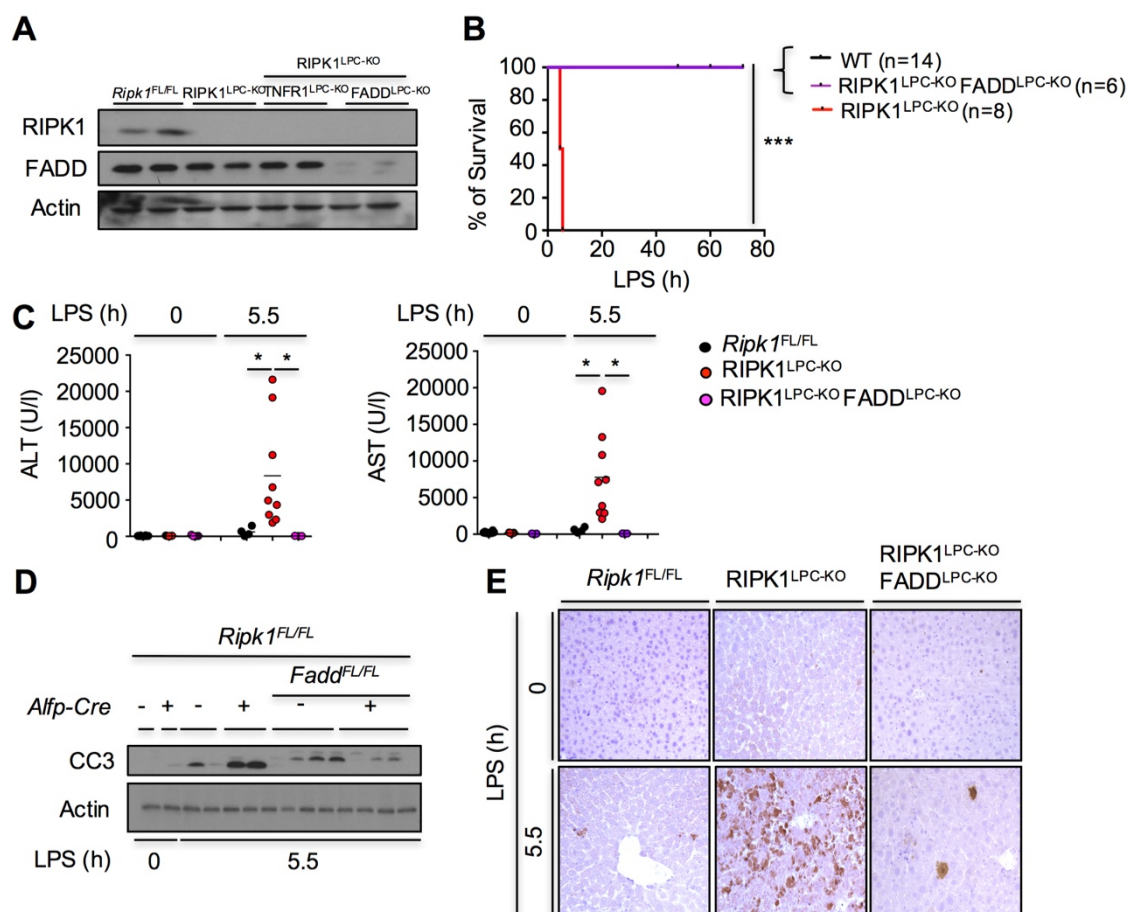
Figure 23. LPC-specific ablation of FADD prevented LPS-induced death of RIPK1[LPC-KO] mice

(A) Immunoblot analysis for RIPK1 and FADD in whole protein extracts from liver tissues of mice with depicted genotypes. Actin was used as loading control. (B) Kaplan-Meier survival curve for mice with indicated genotypes injected with LPS (***P< 0.005). (C) Graphs depicting serum ALT and AST levels in non-injected and LPS-injected mice of indicated genotypes (*P< 0.05). (D) Immunoblot analysis for CC3 in total liver protein lysates of non-injected and LPS-injected mice with depicted genotypes. Actin was used as loading control. (E) Representative liver sections of mice of indicated genotypes immunostained for CC3 untreated or 5.5h after LPS-injection (n=4 per genotype). Same RIPK1[LPC-KO] control was used in figure 16C. Scale bar 100µm.

3.2.6. LPC-specific deficiency of RIPK1 sensitizes hepatocytes to TNFR1-dependent apoptosis in response to LPS

TNFR1 signaling is implicated in LPS-induced liver injury (Filliol et al. 2017) and moreover, was shown in this study *in vitro* to be involved in spontaneous death of RIPK1-deficient hepatocytes. Therefore, to test the significance of TNF-induced apoptosis in LPS-mediated death of RIPK1^{LPC-KO} mice, mice were crossed to *Tnfr1$^{FL/FL}$* mice to generate mice that lacked RIPK1 and TNFR1 in LPCs. Efficient deletion of TNFR1 in RIPK1^{LPC-KO} livers was confirmed by immunoblot analysis (Figure 24A). Consistent with LPC-specific deletion of FADD, LPC-specific deficiency of TNFR1 fully protected RIPK1^{LPC-KO} mice against LPS-mediated liver injury (Figure 24B). LPC-specific deficiency of TNFR1 significantly reduced liver injury indicated by serum ALT and AST levels (Figure 24C) and apoptotic death indicated by immunoblot analysis of liver protein extracts for CC3 (Figure 24D) and IHC for CC3 (Figure 24E) in RIPK1^{LPC-KO} TNFR1^{LPC-KO} mice to the same extent like in LPS-injected *Ripk1$^{FL/FL}$* mice. In summary, these results show that LPS-induced FADD-mediated apoptosis in RIPK1^{LPC-KO} mice is dependent on TNFR1 signaling.
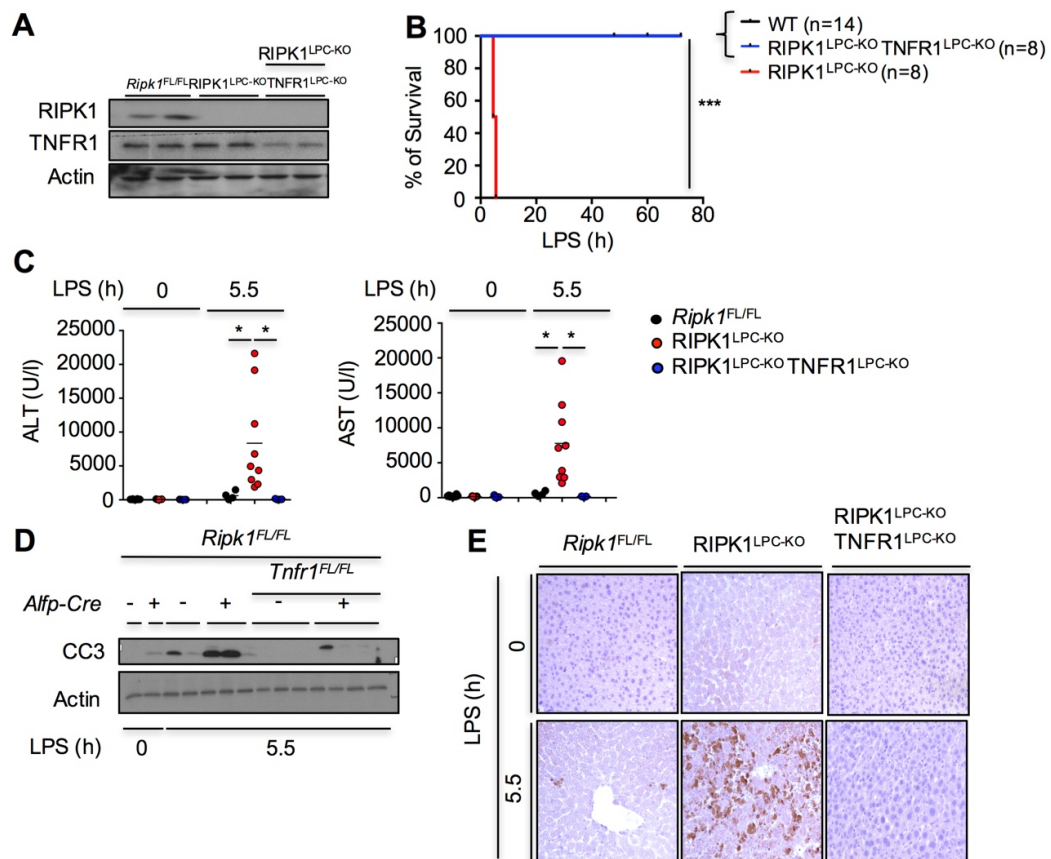
Figure 24. LPC-specific ablation of TNFR1 prevented LPS-induced death of RIPK1^{LPC-KO} mice

(A) Immunoblot analysis for RIPK1 and TNFR1 in whole protein extracts from liver tissues of mice with depicted genotypes. Actin was used as loading control. (Same blot was used to analyze FADD expression shown in Figure 23A) (B) Kaplan-Meier survival curve for mice with indicated genotypes injected with LPS (***P< 0.005). (C) Graphs depicting serum ALT and AST levels in non-injected and LPS-injected mice of indicated genotypes (*P< 0.05). (D) Immunoblot analysis for CC3 in total liver protein lysates of non-injected and LPS-injected mice of indicated genotypes. Actin was used as loading control. Same protein lysates from untreated *Ripk1$^{FL/FL}$* and RIPK1^{LPC-KO} mice were used already for the immunoblot indicated in Figure 23D. (E) Representative liver sections mice of indicated genotypes immunostained for CC3 untreated or 5.5h after LPS-injection (n=4 per genotype). Same RIPK1^{LPC-KO} control was used in figure 16C. Scale bar 100µm.

3.2.7. LPC-specific deficiency of RIPK1 sensitizes hepatocytes to TNF-induced TRADD/FADD-dependent apoptosis in response to LPS

In absence of RIPK1, cell death in response to TNFR1 is mediated by TRADD-dependent complex-IIa, which consequently recruits FADD and Caspase-8 to execute apoptosis (Pasparakis and Vandenabeele 2015). To test the importance of TRADD in triggering FADD-dependent apoptosis in response to LPS in RIPK1^{LPC-KO} mice, RIPK1^{LPC-KO} mice were crossed to *Tradd$^{FL/FL}$* mice to generate RIPK1^{LPC-KO} TRADD^{LPC-KO} mice. Efficient deletion of TRADD in RIPK1^{LPC-KO} livers was confirmed by immunoblot analysis (Figure 25A). Indeed, LPC-specific ablation of TRADD fully prevented early death of RIPK1^{LPC-KO} mice upon injection with LPS (Figure 25B).

Moreover, deficiency of TRADD significantly reduced serum ALT and AST levels (Figure 25C) and CC3 levels indicated by immunoblot (Figure 25D) and IHC analysis (Figure 25E) in RIPK1^{LPC-KO} TRADD^{LPC-KO} mice to the same extent like in $Ripk1^{FL/FL}$ mice. Taken together, LPS induces TNFR1-dependent TRADD/FADD-mediated apoptosis in RIPK1^{LPC-KO} mice.
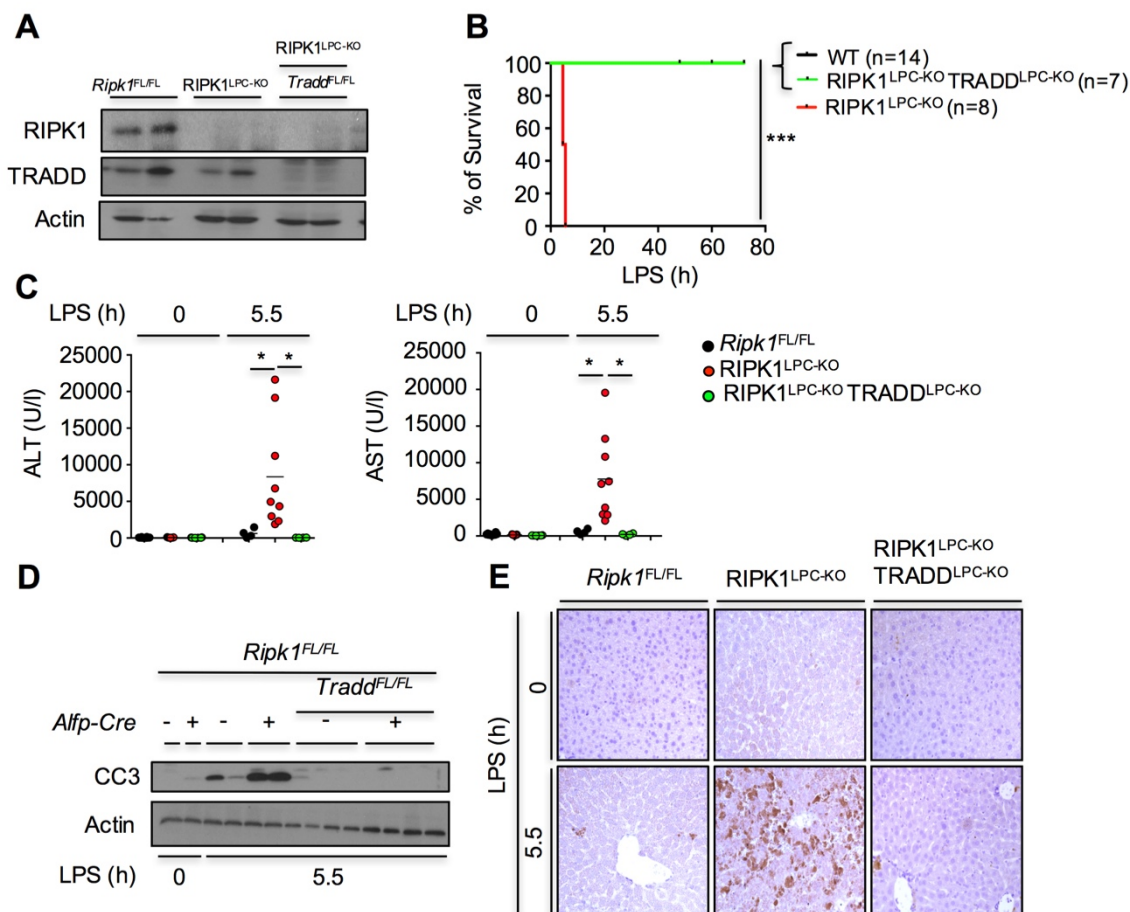
Figure 25. LPC-specific ablation of TRADD prevented LPS-induced death of RIPK1^{LPC-KO} mice

(A) Immunoblot analysis for TRADD and RIPK1 in whole protein extracts from liver tissues of mice with depicted genotypes. Actin was used as loading control. (B) Kaplan-Meier survival curve for mice with indicated genotypes injected with LPS (***P< 0.005). (C) Graphs depicting serum ALT and AST levels in non-injected and LPS-injected mice of indicated genotypes (*P< 0.05). (D) Immunoblot analysis for CC3 in total liver protein lysates of non-injected and LPS-injected mice of indicated genotypes. Actin was used as loading control. Same protein lysates from untreated $Ripk1^{FL/FL}$ and RIPK1^{LPC-KO} mice were used already for the immunoblot indicated in Figure 23/24D. (E) Representative liver sections of mice of depicted genotypes immunostained for CC3 untreated or 5.5h after LPS-injection (n=4 per genotype). Same RIPK1^{LPC-KO} control was used in figure 16C. Scale bar 100µm.

3.2.8. LPC-specific deficiency of TNFR1, FADD or TRADD protects RIPK1-deficient primary hepatocytes from spontaneous death *in vitro*

In agreement with the *in vivo* data indicated in figure 23 and 25, the lack of TRADD or FADD fully prevented spontaneous apoptosis of RIPK1-deficient hepatocytes. Ablation

of TNFR1 considerably reduced spontaneous apoptosis to a similar extent as the effect induced by the TNF inhibitor, etanercept, shown in Figure 20 (Figure 26). Collectively, these results demonstrated an anti-apoptotic role of RIPK1 in primary hepatocytes by preventing TRADD and FADD-dependent hepatocyte apoptosis that is partially triggered by TNFR1-dependent signaling.
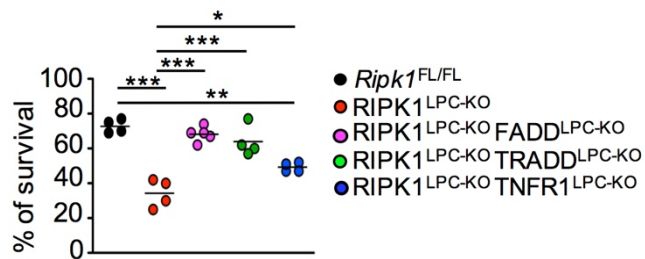
Figure 26. LPC-specific ablation of TNFR1, FADD or TRADD reduced spontaneous hepatocyte death *in vitro*
Graph depicting the % of survival of primary hepatocytes isolated from mice with depicted genotypes cultured for 24h (***P< 0.005, **P< 0.01, *P< 0.05).

3.2.9. LPC-specific deletion of RIPK1 does not sensitize to RIPK3-dependent necroptosis

LPC-specific FADD or TRADD deficiency fully prevented spontaneous death of RIPK1-deficient primary hepatocytes and hepatocyte death in LPS-injected RIPK1^{LPC-KO} mice. These results suggest a pivotal role for apoptosis in mediating death of RIPK1-deficient hepatocytes whereas necroptosis seemed to be dispensable. To analyze the impact of necroptosis in primary hepatocyte death, cells were cultured in the presence of TNF, cycloheximide (CHX) and zVAD-fmk (Figure 27A). CHX is a potent translation inhibitor and is widely used *in vitro* to sensitize cells to death. Importantly, zVAD-fmk significantly prevented TNF/CHX-induced hepatocyte death of *Ripk1$^{FL/FL}$* but also of RIPK1-deficient hepatocytes suggesting the dispensability of Caspase-independent cell death in primary hepatocytes. Furthermore, immunoblot analysis for RIPK3 protein levels, a key driver of necroptosis, was performed in whole liver lysates compared to whole epidermal skin lysates, in which necroptosis was convincingly shown before to be present (Dannappel et al. 2014) (Figure 27B). RIPK3 was expressed at very low levels in the liver under basal conditions but also 5.5h after LPS-injection compared to skin protein lysates reinforcing RIPK3-independent death of hepatocytes in RIPK1^{LPC-KO} mice.

A

B
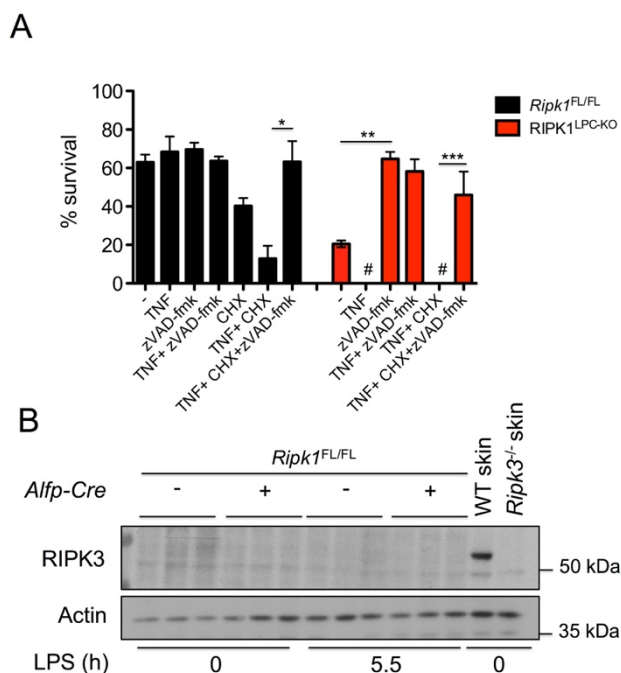
Figure 27. Primary hepatocytes underwent RIPK3-independent death *in vitro*
(A) Graph depicting survival of primary hepatocytes isolated from *Ripk1*^FL/FL^ or RIPK1^LPC-KO^ mice cultured for 24h in the presence or absence of TNF, CHX and zVAD-fmk (n=3). # indicates when all cells were dead. (*P< 0.05, **P< 0.01, ***P< 0.005) (B) Immunoblot analysis for RIPK3 in liver lysates from *Ripk1*^FL/FL^ and RIPK1^LPC-KO^ mice. Actin was used as loading control. WT and *Ripk3*^-/-^ mouse skin was used as controls.

3.2.10. LPC-specific deficiency of RIPK1 does not affect the expression of pro-survival proteins

Our *in vitro* data in figure 22 showed that impaired NF-κB signaling might cause hepatocyte death emphasizing a RIPK1-dependent role in regulating cell survival. To analyze whether impaired complex-I-dependent signaling is involved in the higher susceptibility of RIPK1^LPC-KO^ mice to LPS, 9-week old *Ripk1*^FL/FL^ and RIPK1^LPC-KO^ mice were sacrificed 5.5h upon LPS injection and gene expression of NF-κB target genes and the stabilization of pro-survival proteins were analyzed. Our analysis revealed no considerable differences in *cflip*, *Birc2* and *Birc3* gene expression levels between *Ripk1*^FL/FL^ and RIPK1^LPC-KO^ mice (Figure 28A). In addition, immunoblot analysis of cFLIP, cIAP1 and TRAF2 protein levels revealed no major differences between *Ripk1*^FL/FL^ and RIPK1^LPC-KO^ mice under untreated conditions and 5.5h after LPS injection (Figure 28B). Together these results suggest a complex-I independent role in the sensitivity of RIPK1^LPC-KO^ mice to LPS-induced liver injury.
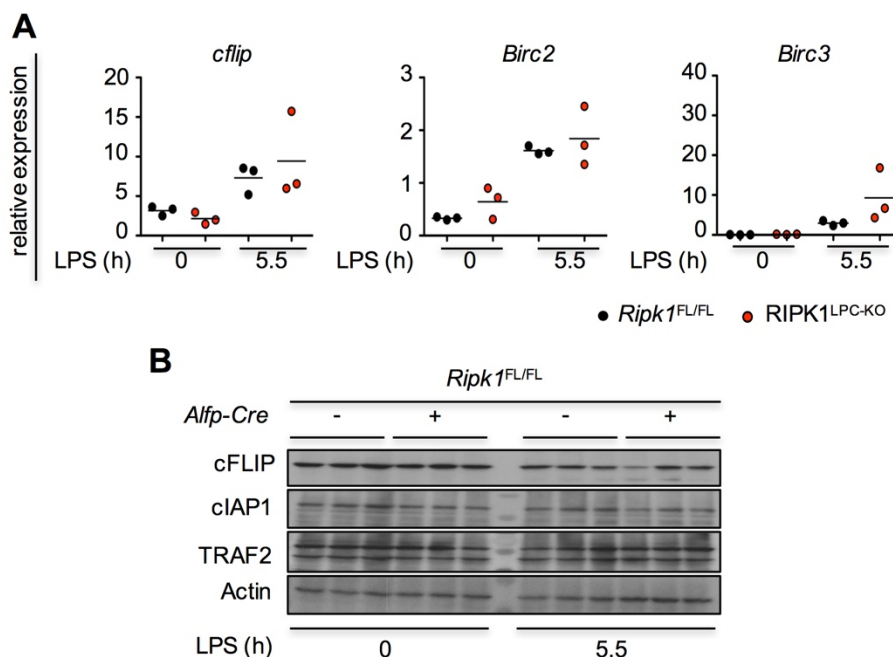
Figure 28. LPC-specific deficiency of RIPK1 did not affect gene expression and the stability of pro-survival proteins
(A) qRT-PCR analysis of NF-κB target gene expression in non- or LPS-injected $Ripk1^{FL/FL}$ and RIPK1^{LPC-KO} livers. Graphs show relative mRNA expression normalized to Tbp. (B) Immunoblot analysis for cIAP1, TRAF2 and cFLIP$_L$ in total liver protein lysates of non- or LPS-injected $Ripk1^{FL/FL}$ and RIPK1^{LPC-KO} mice. Actin was used as loading control.

3.2.11. Constitutive LPC-specific expression of IKK2 protects RIPK1^{LPC-KO} mice from LPS-induced death

To further analyze the role of NF-κB signaling in LPS-injected RIPK1^{LPC-KO} mice, mice expressing a constitutively active form of IKK2 in hepatocytes were used ($R26ikk2^{FL/FL}$; $Alfp-Cre$ tg/wt hereafter referred to as IKK2Ca^{LPC}). Constitutive LPC-specific expression of IKK2 protected 80% of RIPK1^{LPC-KO} mice from LPS-induced death but did not fully prevent liver injury indicated by elevated serum ALT and AST levels in LPS-injected RIPK1^{LPC-KO} IKK2Ca^{LPC} mice (Figure 29A, B). However, on average serum ALT and AST levels were lower compared to RIPK1^{LPC-KO} mice at 5.5h after LPS administration (Figure 29B). Unlike RIPK1^{LPC-KO} mice, where the majority of mice died within 6h after LPS injection, approximately 80% of RIPK1^{LPC-KO} IKK2Ca^{LPC} mice recovered from elevated liver damage within 48h resulting in similar serum ALT and AST levels compared to their floxed littermates (Figure 29B). Although stabilization of pro-survival proteins including TRAF2 and cIAP1 was not impaired in absence of RIPK1 (Figure 28), these data suggest that the lack of IKK2-dependent signaling might be involved in the early death of RIPK1^{LPC-KO} mice in response to LPS.
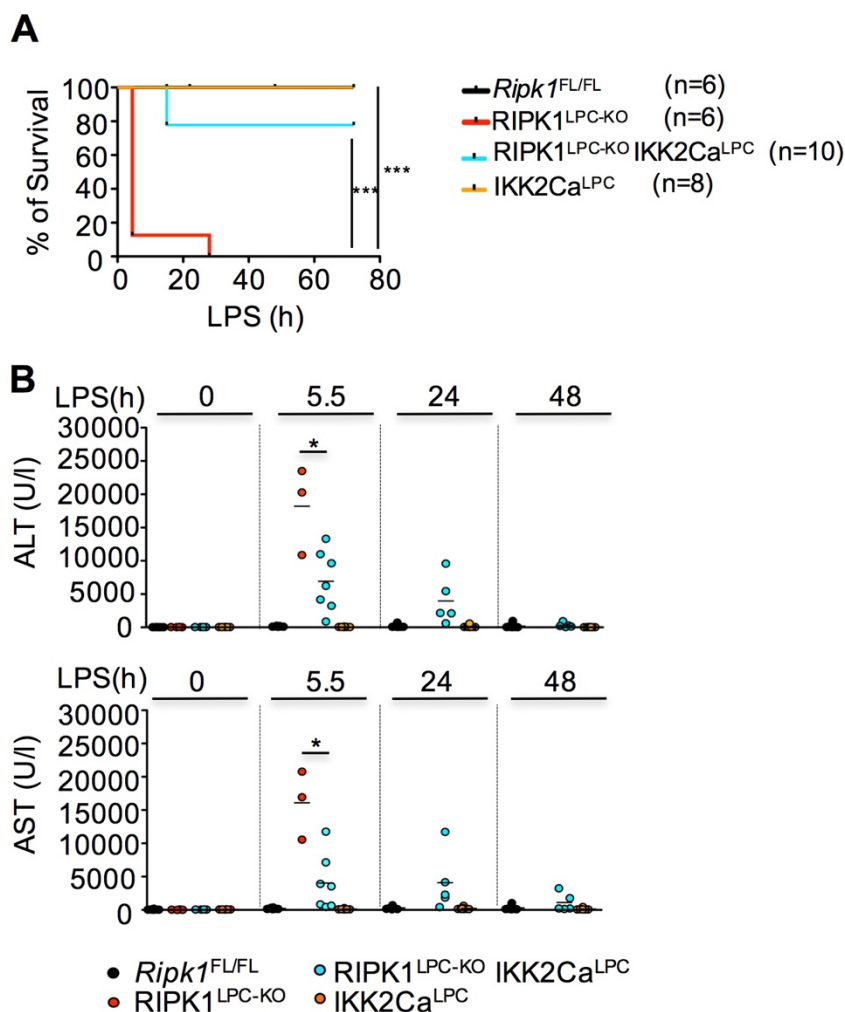
Figure 29. LPC-specific expression of constitutive active IKK2 protected RIPK1^{LPC-KO} mice from LPS-induced death

(A) Kaplan-Meier survival curve for mice with indicated genotypes injected with LPS (***P< 0.005). (B) Graphs depicting serum ALT and AST levels in mice with indicated genotypes 5.5h, 24h and 48h after LPS-injection (*P< 0.05).

3.3. LPC-specific deficiency of RIPK1 reduces DEN-induced carcinogenesis by sensitizing hepatocytes to early apoptosis

3.3.1. LPC-specific ablation of RIPK1 reduces DEN-induced tumor initiation and development

Controlled regulation of cell death and survival is essential to prevent tumorigenesis. Since RIPK1 is an important regulator of cell death and survival in response to DR signaling, many studies addressed the role of RIPK1 in survival and growth of tumors using cancer cell lines or xenograft models. Especially in xenograft models, RIPK1 deficiency was suggested to impair tumor growth emphasizing an important role of RIPK1 in tumorigenesis (Liu et al. 2015; Luan et al. 2015).

To elucidate the *in vivo* role of RIPK1 in carcinogen-induced liver tumorigenesis, an established model of DEN-induced carcinogenesis was employed. For this, groups of male RIPK1^{LPC-KO} and *Ripk1$^{FL/FL}$* mice were injected with 25 mg/kg BW DEN at 2 weeks of age. RIPK1^{LPC-KO} mice showed similar bodyweight gain and liver to bodyweight ratio compared to their control littermates up to the age of 32 weeks (Figure 30A,G). Moreover, injection of DEN did not result in elevation of serum ALT and AST levels at 32 weeks of age indicating that RIPK1 deficiency did not compromise major liver functions in response to DEN injection (Figure 30B). Strikingly, 100% of *Ripk1$^{FL/FL}$* mice displayed tumors while only 37% of RIPK1^{LPC-KO} mice had macroscopically visible tumors at the age of 32 weeks (Figure 30D). Macroscopic examination of tumors at the age of 32 weeks revealed a strong reduction in the number and size of tumors in RIPK1^{LPC-KO} mice (Figure 30C-E). Histopathological analysis of liver sections revealed that about 40% of RIPK1^{LPC-KO} mice did not show signs of liver tumorigenesis (Figure 30F). In addition, those RIPK1^{LPC-KO} mice bearing dysplastic changes in their livers generally showed less advanced tumors with about 5% of the mice showing well-differentiated HCC and 20% small HCC (Figure 30F). On the contrary to RIPK1^{LPC-KO} mice, *Ripk1$^{FL/FL}$* mice showed well-differentiated HCC in about 20% of the cases and small HCC in about 60% of the mice (Figure 30F). Chronic fatty livers and chronic inflammatory states are major factors involved in liver carcinogenesis. Nevertheless, histopathological analysis did not reveal extensive steatosis and inflammation in the liver of DEN-injected *Ripk1$^{FL/FL}$* and RIPK1^{LPC-KO} mice suggesting that a single dose of DEN did not induce an inflammatory response and steatosis in the liver 30 weeks after DEN injection (Figure 30H, I). Taken together, LPC-specific deficiency of RIPK1 negatively affects tumor initiation and tumor growth in response to DEN.
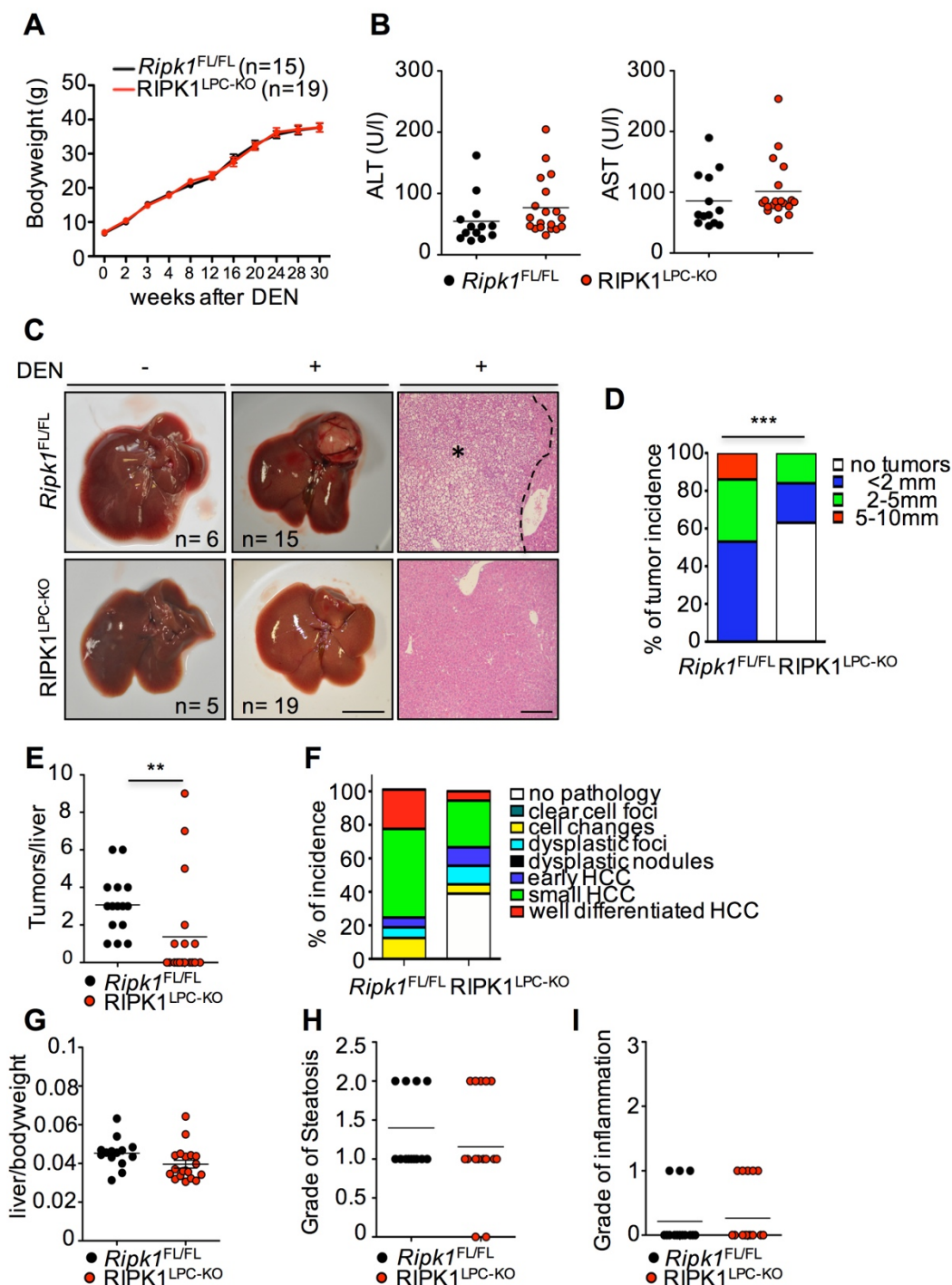
Figure 30. LPC-specific deficiency of RIPK1 reduced tumor incidences and growth
(A and B) Graphs depicting the body weight (mean ± SEM) (A) and serum ALT and AST levels at 32 weeks of age (B) of DEN-injected $Ripk1^{FL/FL}$ and RIPK1^{LPC-KO} mice. (C) Representative pictures of livers (Scale bar: 1cm) and H&E stained liver sections from DEN-injected $Ripk1^{FL/FL}$ and RIPK1^{LPC-KO} mice at the age of 32 weeks. Scale bar, 100 μm. * indicates the tumor area. (D) Tumor load in mice with indicated genotypes as estimated by quantification of the tumor size distribution (***P < 0.005) (E) Graphs depicting the number of tumors per liver (**P< 0.01) (F) Histopathological evaluation of HCC development in 32-week-old mice with the indicated genotypes. Each color bar represents the % of livers per genotype in which the indicated stage was identified as the most advanced disease stage. (G-I) Graphs depicting the liver/bodyweight ratio (G), the grade of steatosis (H), and the grade of inflammation (I) in 32-week-old mice injected with DEN.

Even at the age of 36 weeks macroscopic analysis of livers from *Ripk1$^{FL/FL}$* and RIPK1^{LPC-KO} revealed a reduction in DEN-induced tumorigenesis in RIPK1^{LPC-KO} mice, as 33% of RIPK1^{LPC-KO} mice showed no macroscopically visible tumors opposed to 8% of the control animals (Figure 31C, D, E). Similar to the results shown in figure 30 at 32 weeks, *Ripk1$^{FL/FL}$* and RIPK1^{LPC-KO} mice did not show differences in bodyweight gain, serum ALT and AST levels and liver to bodyweight ratio at 36 weeks of age (Figure 31A, B, F). In contrast to 32-week old mice, 36-week old RIPK1^{LPC-KO} mice showed a similar incidence of 5-10 mm tumors (Figure 31D). Together, these results show that RIPK1 deficiency delays DEN-induced liver tumorigenesis by decreasing overall tumor incidence and tumor numbers 30 and 34 weeks after DEN-injection.
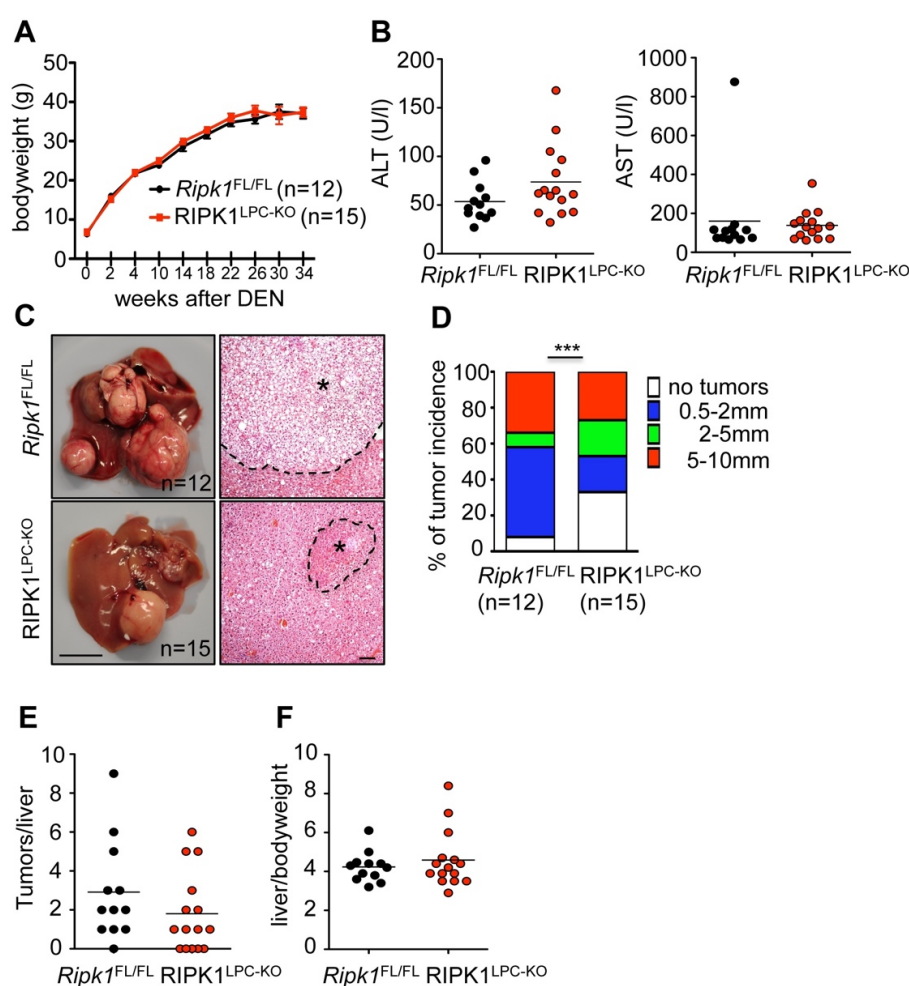
Figure 31. RIPK1^{LPC-KO} mice showed delayed tumor growth and reduced tumor numbers and incidences at 36 weeks of age
(A) Graph depicting the bodyweight of DEN-injected *Ripk1$^{FL/FL}$* and RIPK1^{LPC-KO} mice starting from DEN injection until the age of 36 weeks (mean± SEM). (B) Graph depicting serum ALT and AST level of DEN-injected *Ripk1$^{FL/FL}$* and RIPK1^{LPC-KO} mice at 36 weeks of age. (C) Representative pictures of livers (Scale bar: 1cm). * indicates the tumor area.(D) Graphs depicting the size distribution of tumors found in livers of DEN-injected *Ripk1$^{FL/FL}$* and RIPK1^{LPC-KO} mice at the age of 36 weeks (***P<0.005), (E-F) Graphs depicting the number of tumors (E) or liver/bodyweight ratio (F).

3.3.2. Loss of RIPK1 kinase activity does not affect DEN-induced carcinogenesis

RIPK1 exhibits both kinase-dependent and kinase-independent functions. To elucidate the importance of the kinase-dependent functions of RIPK1 in DEN-induced carcinogenesis, $Ripk1^{D138N/D138N}$ knock-in mice were used (Polykratis et al. 2014). To investigate the LPC-specific function of RIPK1 kinase activity, we employed mice that carry one loxP-flanked and one RIPK1D138N mutant allele crossed to *Alfp-Cre* transgenic mice (*Ripk1*$^{FL/D138N}$; *Alfp-Cre*$^{Tg/WT}$, hereafter referred to as RIPK1$^{LPC-KO/D138N}$). In these mice, Cre-mediated recombination deleted the loxP-flanked *Ripk1* allele in LPCs, therefore, these cells expressed only the kinase inactive RIPK1D138N protein whereas cells in the rest of the body remained *Ripk1*$^{FL/D138N}$. Groups of male RIPK1$^{LPC-KO/D138N}$ mice and *Ripk1*$^{FL/D138N}$ littermates were injected with 25 mg/kg BW DEN at the age of 2 weeks and their livers were examined for the presence of tumors at the age of 36 weeks. *Ripk1*$^{FL/D138N}$ and RIPK1$^{LPC-KO/D138N}$ mice did not show differences in bodyweight gain until the age of 36 weeks (Figure 32B) and did not show increased levels of the serum ALT and AST at the age of 36 weeks (Figure 32C). Unlike RIPK1^{LPC-KO} mice, RIPK1$^{LPC-KO/D138N}$ mice had similar tumor incidences, tumor numbers and also tumor size compared to their control littermates (Figure 32D-G). Furthermore, RIPK1$^{LPC-KO/D138N}$ mice showed similar liver to bodyweight ratio, steatosis and inflammation 36 weeks upon DEN-injection compared to *Ripk1*$^{FL/D138N}$ littermates (Figure 32H-J). Taken together, loss of RIPK1 kinase activity does not affect DEN-induced liver tumorigenesis suggesting that RIPK1 promotes liver tumor development via kinase-independent scaffolding functions.
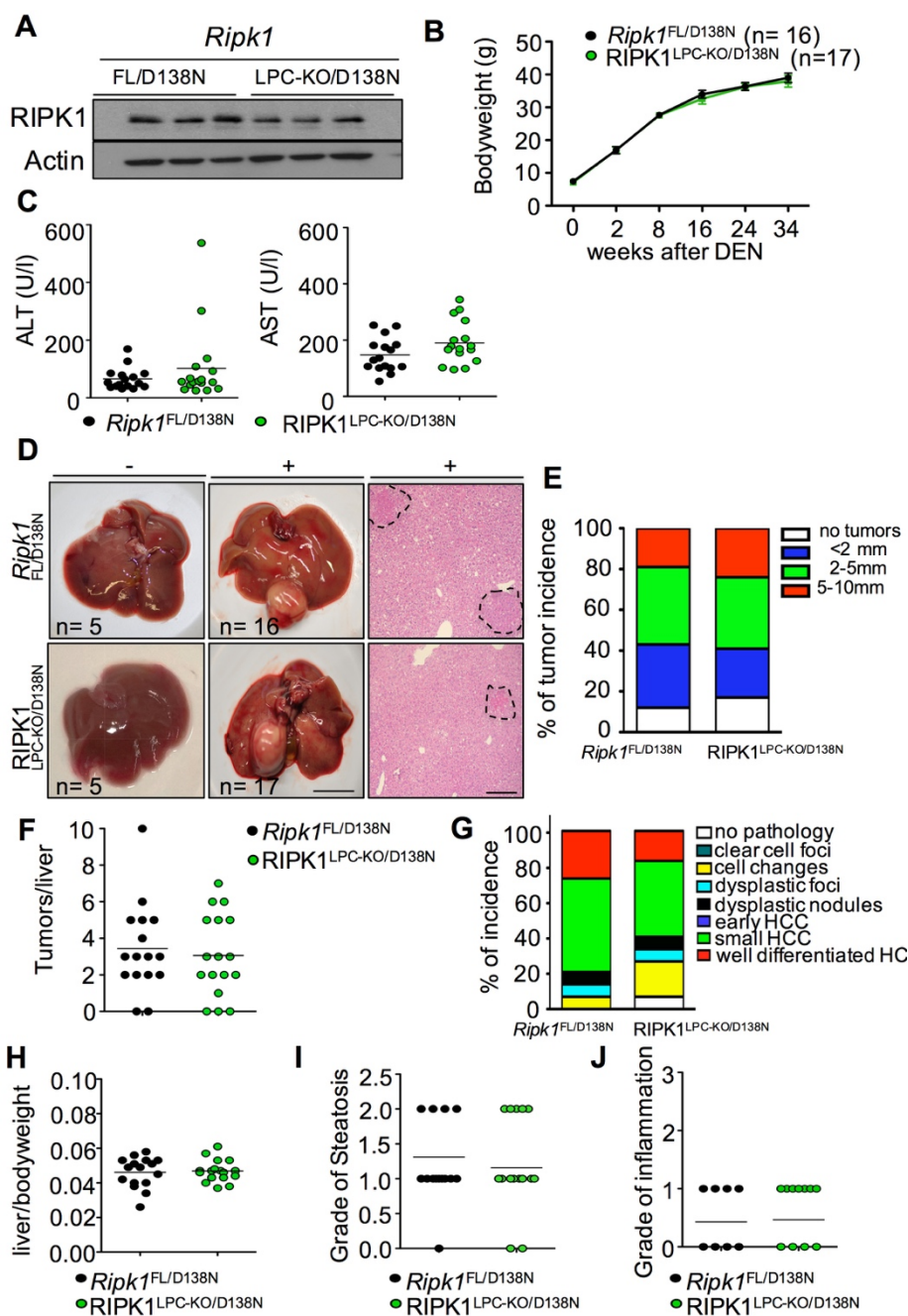
Figure 32. RIPK1[LPC-KO/D138N] **mice showed similar tumor development compared to** *Ripk1*[FL/D138N] **mice**

(A) Immunoblot analysis for RIPK1 in liver lysates of 9-week-old *Ripk1*[FL/D138N] and RIPK1[LPC-KO/D138N] mice (n=3 per genotype). (B) Bodyweight curve of DEN-injected *Ripk1*[FL/D138N] and RIPK1[LPC-KO/D138N] mice starting from DEN injection until the age of 36 weeks (mean ± SEM). (C) Graph depicting serum ALT and AST levels of 36-week-old *Ripk1*[FL/D138N] and RIPK1[LPC-KO/D138N] mice upon DEN injection. (D) Representative pictures of livers (Scale bar: 1cm) and H&E stained liver sections from DEN-injected *Ripk1*[FL/D138N] and RIPK1[LPC-KO/D138N] mice at the age of 36 weeks. Scale bar, 100 µm. Dashed lines indicate the tumor area. (E) Tumor load in 36-week-old *Ripk1*[FL/D138N] and RIPK1[LPC-KO/D138N] mice as estimated by quantification of the tumor size distribution. (F) Graph depicting the number of tumors per liver. (G) Histopathological evaluation of HCC development in 36-week-old *Ripk1*[FL/D138N] and RIPK1[LPC-KO/D138N] mice. Each color bar represents the % of livers per genotype in which the indicated stage was identified as the most advanced disease stage (n=14-15 per genotype). (H-J) Graphs depicting the liver/bodyweight ratio (H), grade of steatosis (I), and the grade of inflammation (J) in 36-week-old mice injected with DEN.

3.3.3. LPC-specific deficiency of RIPK1 reduces DEN-induced γH2AX levels

Given the fact that RIPK1^{LPC-KO} mice showed reduced tumor incidences 30- and 34-weeks after DEN injection (Figure 30 and 31) these results suggested a pivotal role of RIPK1 in the regulation of tumor initiation and growth. To interrogate the RIPK1-dependent mechanisms regulating initiation and growth of DEN-induced tumors the role of RIPK1 in the liver was analyzed in response to DEN. In order to amplify hepatocyte response to DEN groups of male RIPK1^{LPC-KO} and *Ripk1$^{FL/FL}$* mice were injected at 6 weeks of age with an acute dose of DEN (100mg/kg BW) and were analyzed after 3, 6, 24, or 48h.

To directly assess DEN-induced DNA-damage liver sections were stained with antibodies recognizing phosphorylated histone H2AX (γH2AX), which is generated in the vicinity of DNA-damage lesions (Lukas et al. 2011). DEN administration induced the appearance of γH2AX in the liver already 3h after injection, which persisted up to 24h and declined thereafter (Figure 33A). Quantification of γH2AX+ hepatocytes revealed slightly reduced levels at 3 and 6h but significantly reduced numbers of γH2AX stained hepatocytes at 24h in RIPK1^{LPC-KO} mice compared to *Ripk1$^{FL/FL}$* littermates (Figure 33B). DNA-damage induces the stabilization and activation of the tumor suppressor p53, which maintains genomic stability by controlling the expression of genes regulating cellular senescence, cell-cycle progression, cell death and DNA repair (Bieging et al. 2014). Immunoblot analysis of liver protein extracts revealed p53 stabilization in the liver starting at 6h, peaked at 24h and subsided 48h after DEN administration in both RIPK1^{LPC-KO} and *Ripk1$^{FL/FL}$* littermates (Figure 33C). Furthermore, qRT-PCR analysis of the expression of key p53 target genes did not reveal considerable differences in p53-dependent gene expression between RIPK1^{LPC-KO} and *Ripk1$^{FL/FL}$* mice (Figure 33D). Although γH2AX levels were reduced in DEN-injected RIPK1^{LPC-KO} mice RIPK1 deficiency did not considerably affect p53 signaling suggesting a p53-independent role of RIPK1 in reducing γH2AX levels after DEN injection.
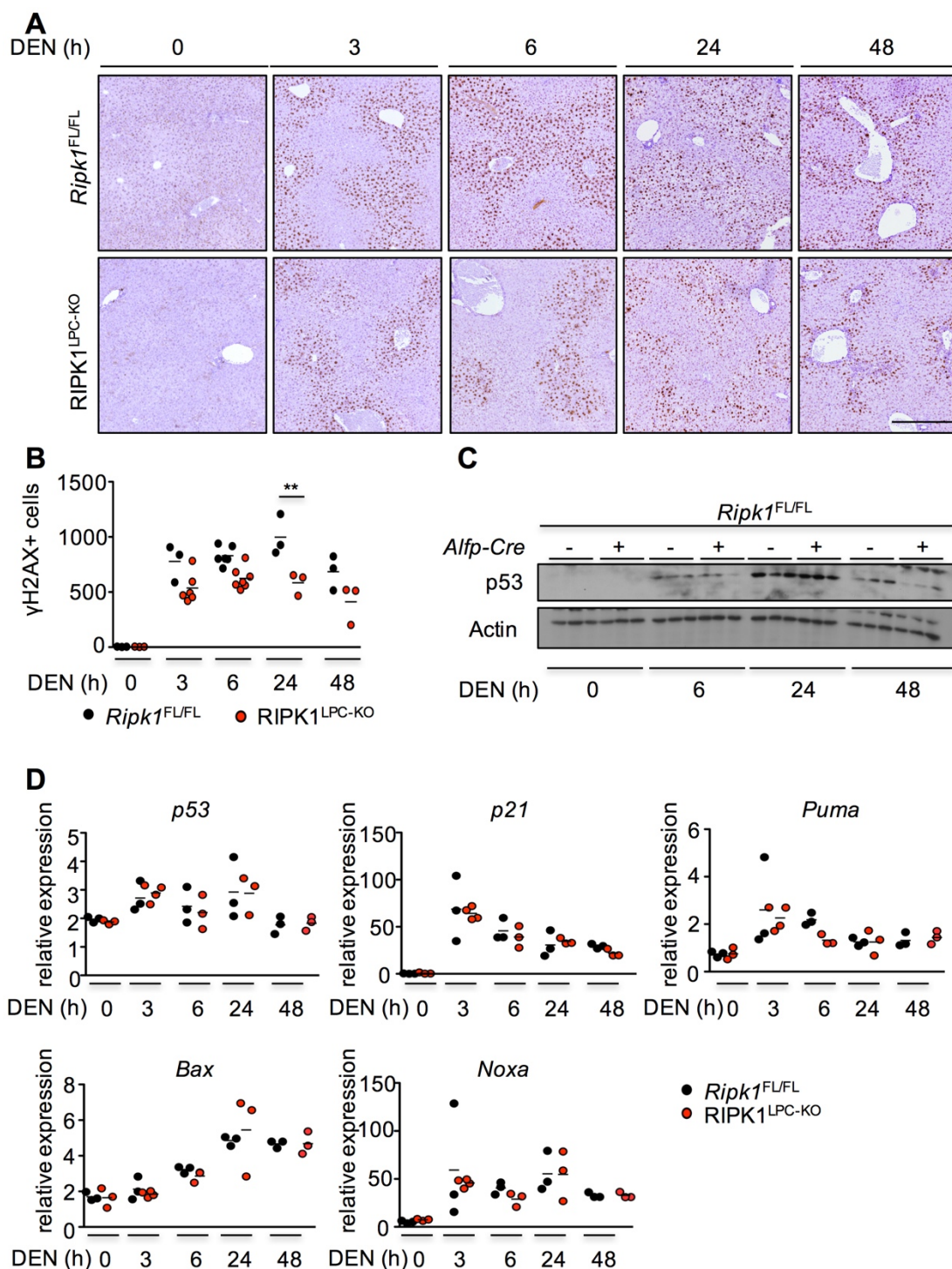
Figure 33. RIPK1^{LPC-KO} mice showed reduced γH2AX levels but similar p53 signaling compared to *Ripk1^{FL/FL}* mice upon an acute dose of DEN

(A-B) Representative images of livers of non-injected or with an acute dose of DEN-injected 6-week old *Ripk1^{FL/FL}* and RIPK1^{LPC-KO} mice stained for γH2AX. Scale bar, 100 µm (A) and quantification of γH2AX+ cells (mean of 5 fields per animal, n= 3-7 mice, **$P<0.01$) (B). (C) Immunoblot analysis for p53 in *Ripk1^{FL/FL}* and RIPK1^{LPC-KO} mice after 100 mg/kg of BW DEN injection for depicted periods of time. Actin was used as loading control. (D) qRT-PCR analysis of gene expression levels of *p53* and p53 target genes in *Ripk1^{FL/FL}* and RIPK1^{LPC-KO} mice after DEN injection for indicated timeperiods. Graphs show relative mRNA expression normalized to *Tbp*.

3.3.4. RIPK1^{LPC-KO} livers display highly elevated Caspase-3 cleavage after DEN injection

Loss of RIPK1 in LPCs revealed increased sensitivity of hepatocytes to apoptosis *in vitro* (Figure 20) and *in vivo* in response to LPS (Figure 16) suggesting a pro-survival function of RIPK1 in the liver. Given this high sensitivity of cells to TNF-induced apoptosis in absence of RIPK1, the level of hepatocyte apoptosis was assessed in response to an acute dose of DEN. After acute DEN injection, analysis of ALT in the sera of DEN-injected mice revealed elevated levels at 6 and 24h after DEN injection in RIPK1^{LPC-KO} mice indicative for increased liver damage (Figure 34A). Staining for CC3 and subsequently the quantification of positive cells in these mice showed strongly elevated levels of CC3+ cells starting at 3h, peaked at 6h and declined at 48h after acute DEN injection in RIPK1^{LPC-KO} mice (Figure 34B, C). In contrast to RIPK1^{LPC-KO} mice, *Ripk1^{FL/FL}* mice did not reveal positively stained cells at 3h or 6h but began to show CC3+ cells at 24h (Figure 34B, C). At 24h *Ripk1^{FL/FL}* mice displayed similar CC3+ cells compared to RIPK1^{LPC-KO} mice and continued at 48h with a slightly higher level of CC3+ cells than in RIPK1^{LPC-KO} mice (Figure 34B, C). Similarly, immunoblot analysis for CC3 revealed high levels 6h after DEN injection in RIPK1^{LPC-KO} mice but not in *Ripk1^{FL/FL}* mice (Figure 34D). However, at 24h high levels of CC3 were detected in *Ripk1^{FL/FL}* but not in RIPK1^{LPC-KO} protein lysates although staining for CC3 showed strong staining for CC3 in both RIPK1^{LPC-KO} and *Ripk1^{FL/FL}* mice (Figure 34D). This discrepancy between IHC and immunoblot could be explained by the instability and the degradation of the CC3 fragment. Furthermore, the IHC for CC3 already showed cell rupture and the release of CC3 suggesting the loss of the CC3 fragment during protein isolation. Nevertheless, these results together reveal a high sensitivity of RIPK1-deficient hepatocytes to DEN-induced apoptosis.
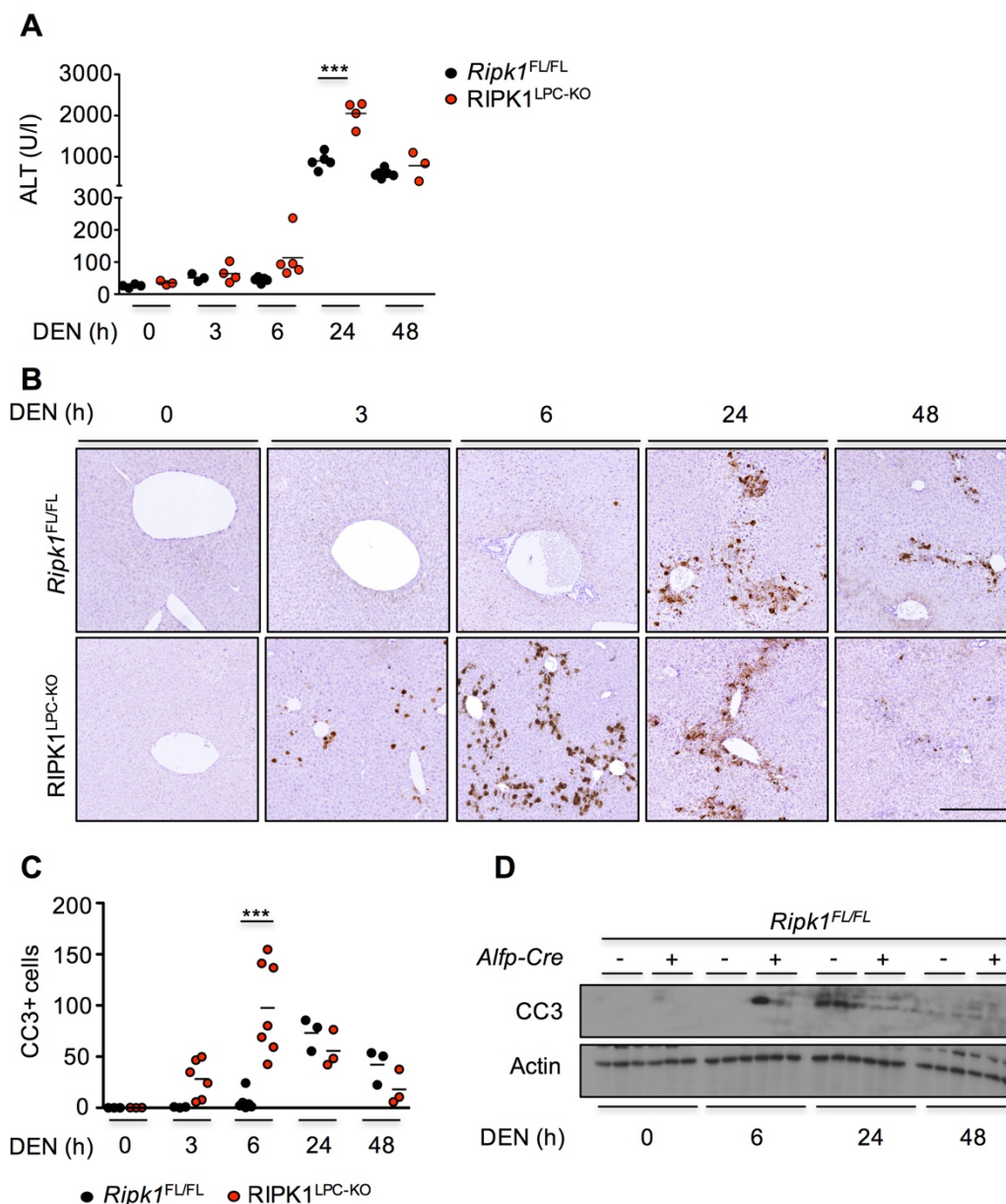
Figure 34. LPC-specific deficiency of RIPK1 sensitized hepatocytes to DEN-induced apoptosis
(A) Graph depicting serum ALT levels of 6-week-old $Ripk1^{FL/FL}$ and RIPK1^{LPC-KO} mice upon DEN injection for indicated timeperiods (***P<0.005). (B) Representative images of livers of non-injected or with an acute dose of DEN injected 6-week-old $Ripk1^{FL/FL}$ and RIPK1^{LPC-KO} mice stained for CC3. Scale bar, 100 μm. (C) Quantification of CC3+ cells in livers of $Ripk1^{FL/FL}$ and RIPK1^{LPC-KO} mice after DEN injection (mean of 5 fields per animal, n= 3-7 mice) (***P<0.005). (D) Immunoblot analysis for CC3 in protein lysates of livers from $Ripk1^{FL/FL}$ and RIPK1^{LPC-KO} mice after 100mg/kg of BW DEN injection for depicted timeperiods. Actin was used as loading control.

3.3.5. Increased hepatocyte apoptosis correlates with reduced levels of γH2AX+ cells

LPC-specific hepatocytes were highly prone to DEN-induced apoptosis (Figure 34) and IHC analysis revealed reduced γH2AX levels suggesting clearance of DNA damaged cells by apoptosis (Figure 33). To proof this hypothesis and to analyze whether death

of hepatocytes is DNA-damage-dependent in RIPK1^{LPC-KO} mice, liver sections of *Ripk1$^{FL/FL}$* and RIPK1^{LPC-KO} mice were co-stained for CC3 and γH2AX. Co-staining for CC3 and γH2AX revealed the presence of CC3 not only in γH2AX+ cells but also in γH2AX- cells, consistently not all γH2AX+ hepatocytes showed CC3 staining at the indicated timepoints (Figure 35). Nontheless, death of hepatocytes also occurred in γH2AX+ cells suggesting that reduced number of γH2AX+ cells might be a result of extensive apoptosis especially 6h after DEN in RIPK1^{LPC-KO} mice (Figure 35). Together these data suggest that hepatocyte apoptosis happens mostly independent of DNA-damage and hint at the presence of another stimulus in addition to DNA-damage in response to DEN.

Cleaved caspase 3   γH2AX   Dapi
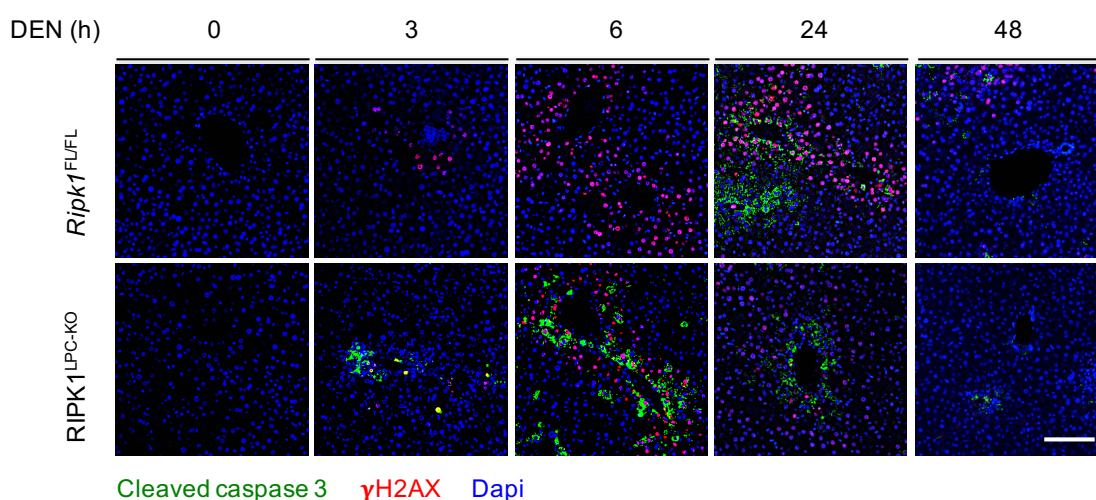
Figure 35. DEN-induced apoptosis happened in a DNA-damage-independent manner
Representative images of livers of non-injected or with an acute dose of DEN injected 6-week-old *Ripk1$^{FL/FL}$* and RIPK1^{LPC-KO} mice co-stained for CC3 and γH2AX. Scale bar, 100 μm.

3.3.6. LPC-specific deficiency of RIPK1 results in extensive Caspase-8- and Caspase-9-mediated hepatocyte apoptosis

To identify the mediator for DEN-induced Caspase-3 activation, the levels of Caspase-8, the initiator Caspase of extrinsic apoptosis, and Caspase-9, the initiator Caspase of intrinsic apoptosis, were assessed. IHC analysis for cleaved Caspase-8 (CC8) revealed elevated CC8+ cells 3h and 6h after DEN injection (Figure 36A,C) resembling the previously shown CC3+ levels (Figure 34B,C). Unlike CC3 and CC8, cleaved Caspase-9 (CC9) levels were not elevated at 3h but increased 6h after DEN injection (Figure 36B, C). Together, these results suggest the presence of Caspase-8-dependent extrinsic apoptosis 3h after DEN-injection. However, the apoptotic death at 6h after DEN injection either depends on Caspase-8-BID-mediated or on DNA-damage-induced Caspase-9 activation.
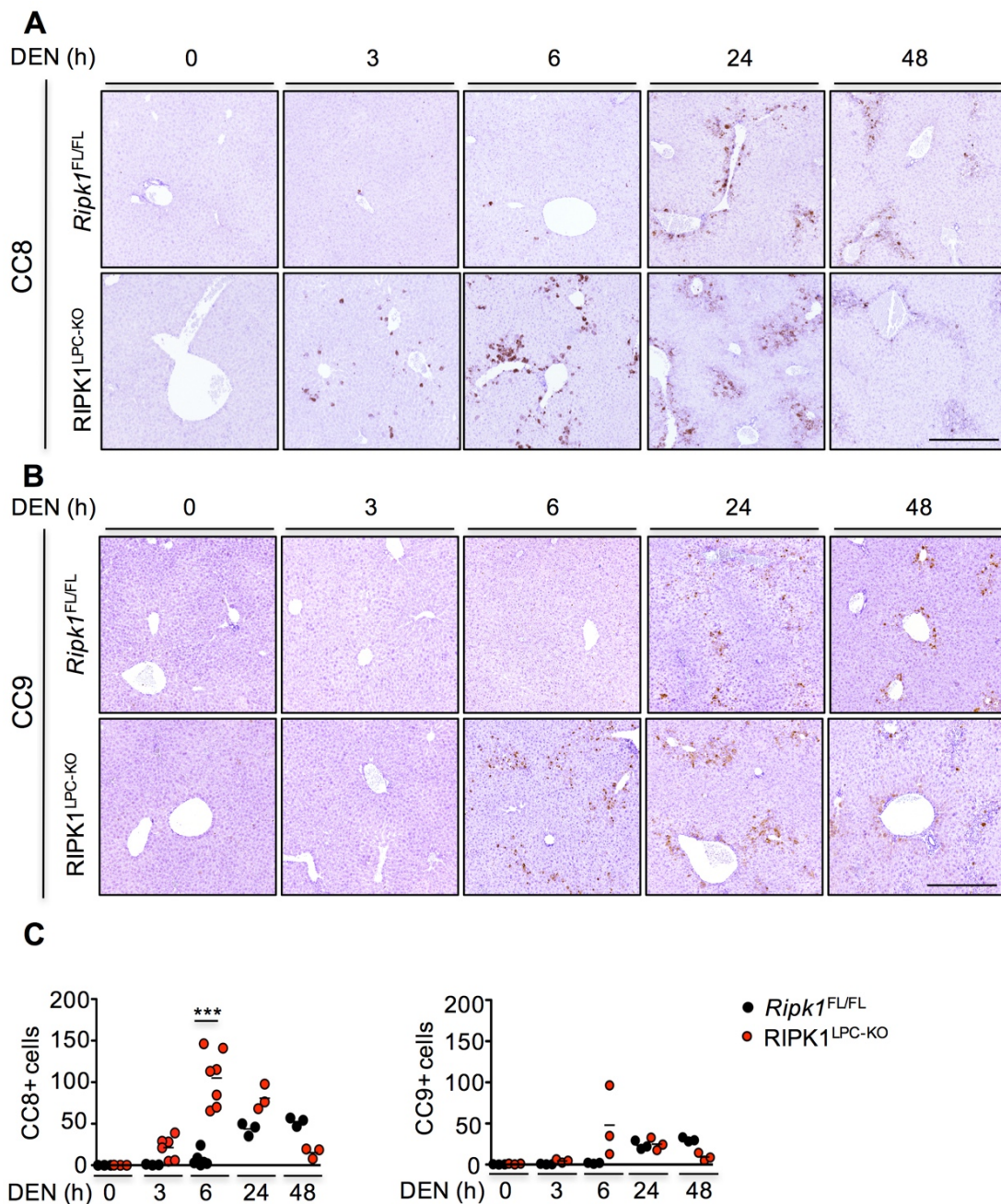
Figure 36. DEN-injection induced Caspase-8- and Caspase-9-dependent apoptosis in mice
(A-B) Representative images of livers of non-injected or with an acute dose of DEN injected 6-week-old *Ripk1*^{FL/FL} and RIPK1^{LPC-KO} mice stained for CC8 (A) and CC9 (B) (Scale bar, 100 µm) and graphs depicting the quantification of CC8+ cells and CC9+ cells (mean of 5 fields per animal, n= 3-7 mice) (***P<0.005) (C).

3.3.7. LPC-specific deficiency of RIPK1 does not affect hepatocyte proliferation in response to acute DEN

Maeda et al. reported that extensive apoptosis correlated with high compensatory proliferation of hepatocytes resulting in DEN-induced tumorigenesis (Maeda et al. 2005). Unlike the report of Maeda et al., apoptotic death in the liver of RIPK1LPC-KO mice was not accompanied by compensatory proliferation of hepatocytes when using

an acute dose of DEN indicated by similar Ki-67 staining between *Ripk1^{FL/FL}* and RIPK1^{LPC-KO} mice (Figure 37). This result emphasizes that loss of RIPK1 did not affect hepatocyte proliferation which could have explained the reduced induction of DEN-induced HCC development in RIPK1^{LPC-KO} mice.
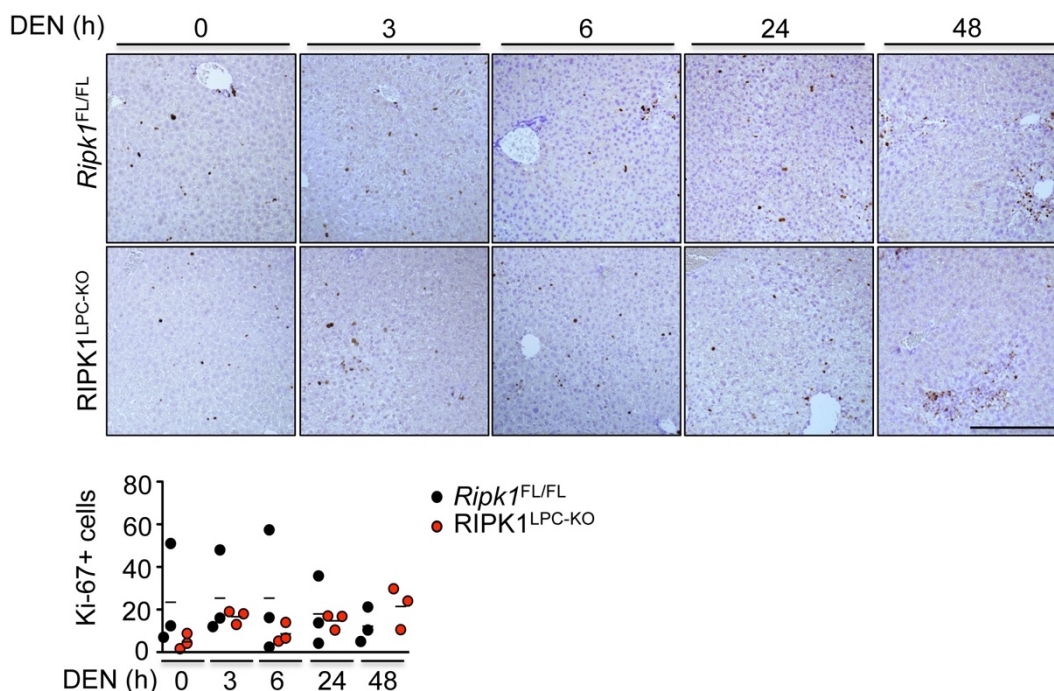
Figure 37. LPC-specific ablation of RIPK1 did not affect hepatocyte proliferation
Representative images of livers of non-injected or with an acute dose of DEN injected 6-week-old *Ripk1^{FL/FL}* and RIPK1^{LPC-KO} mice stained for Ki-67 (Scale bar, 100 μm). Quantification of Ki-67+ cells in *Ripk1^{FL/FL}* and RIPK1^{LPC-KO} mice after DEN injection (mean of 5 fields per animal, n= 3).

3.3.8. LPC-specific deficiency of RIPK1 does not promote cytokine induction

In a previous report, increased hepatocyte death and compensatory proliferation in IKK2^{Δhep} mice was accompanied by an inflammatory response (Maeda et al. 2005). Gene expression analysis of *Il1b* levels in RIPK1^{LPC-KO} mice compared to *Ripk1^{FL/FL}* mice upon acute DEN did not reveal major inductions suggesting that a single injection of an acute dose of DEN did not induce a strong inflammatory response (Figure 38).
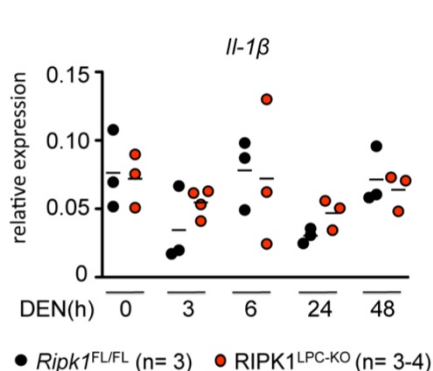
Figure 38. LPC-specific ablation of RIPK1 did not increase *Il1b* gene expression levels upon acute DEN qRT-PCR analysis of gene expression levels of *Il1b* in *Ripk1^{FL/FL}* and RIPK1^{LPC-KO} mice after DEN injection for indicated timeperiods. Graphs show relative mRNA expression normalized to *Tbp*.

3.3.9. Kinase-inactive RIPK1 mice do not show elevated DEN-induced hepatocyte apoptosis

Unlike LPC-specific full-length deficiency of RIPK1, deficiency of RIPK1 kinase activity did not affect DEN-induced HCC development *in vivo* indicating a kinase-activity-independent function of RIPK1 in mediating DEN-induced HCC (Figure 32). To address the kinase-dependent function of RIPK1 in response to an acute dose of DEN, 6-week old male *Ripk1*$^{FL/D138N}$ and RIPK1$^{LPC-KO/D138N}$ mice were injected with an acute dose of DEN. In contrast to RIPK1^{LPC-KO} mice, RIPK1$^{LPC-KO/D138N}$ did not show elevated serum ALT levels (Figure 39A) and did not reveal increased CC3+, CC8+ and CC9+ levels in the liver at 3, 6 and 24h upon acute DEN injection (Figure 39B-E) suggesting that loss of RIPK1 scaffolding function promoted DEN-induced hepatocyte apoptosis. These data highlight a potential correlation between the lack of early apoptosis and the tumor formation at 36-weeks of age.
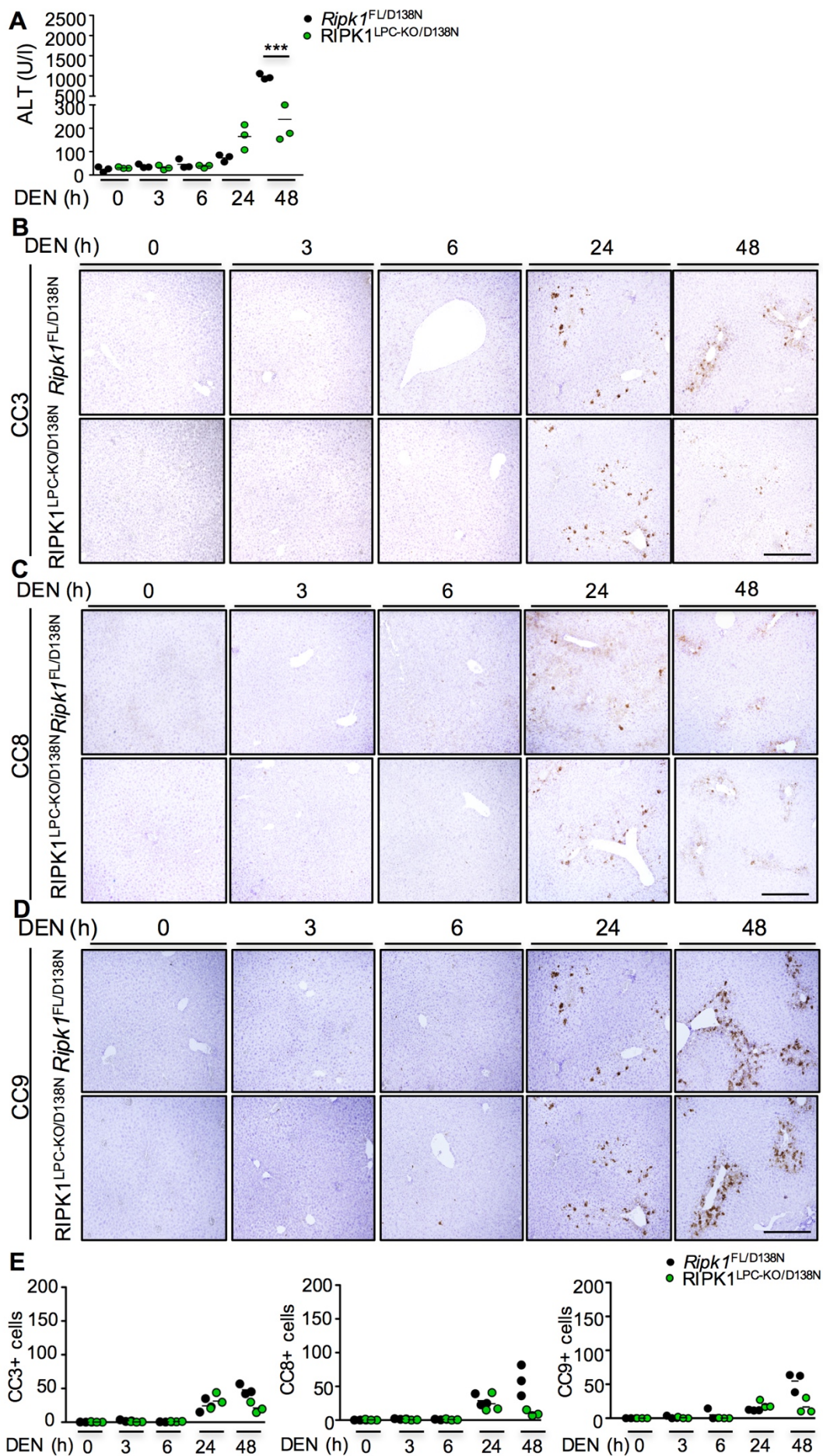
Figure 39. Deficiency of RIPK1 kinase activity prevented DEN-induced apoptosis
(A) Graph depicting serum ALT levels in *Ripk1*$^{FL/D138N}$ and RIPK1$^{LPC-KO/D138N}$ mice after an acute dose of DEN for indicated time periods. (B-D) Representative images of livers of non-injected or with an acute dose of DEN injected 6-week-old *Ripk1*$^{FL/D138N}$ and RIPK1$^{LPC-KO/D138N}$ mice stained for CC3 (B), CC8 (C) and CC9 (D) (Scale bar, 100 μm). (E) Quantification of CC3+, CC8+ and CC9+ cells in *Ripk1*$^{FL/D138N}$ and RIPK1$^{LPC-KO/D138N}$ mice after DEN injection. Quantification was performed in 5 fields per animal (mean of 5 fields per animal, n= 3).

3.3.10. Loss of RIPK1 kinase activity does not affect DEN-induced DNA-damage

LPC-specific deletion of RIPK1 resulted in reduced levels of γH2AX independent of p53 signaling presumably due to extensive apoptosis early after acute DEN (Figure 33). In contrast to RIPK1^{LPC-KO} mice, RIPK1$^{LPC-KO/D138N}$ mice did not display pronounced apoptosis (Figure 39). IHC analysis for γH2AX in RIPK1$^{LPC-KO/D138N}$ mice revealed similar levels of γH2AX+ cells compared to levels in *Ripk1*$^{FL/D138N}$ littermates implying a correlation between DNA-damage and cell death levels upon DEN (Figure 40).
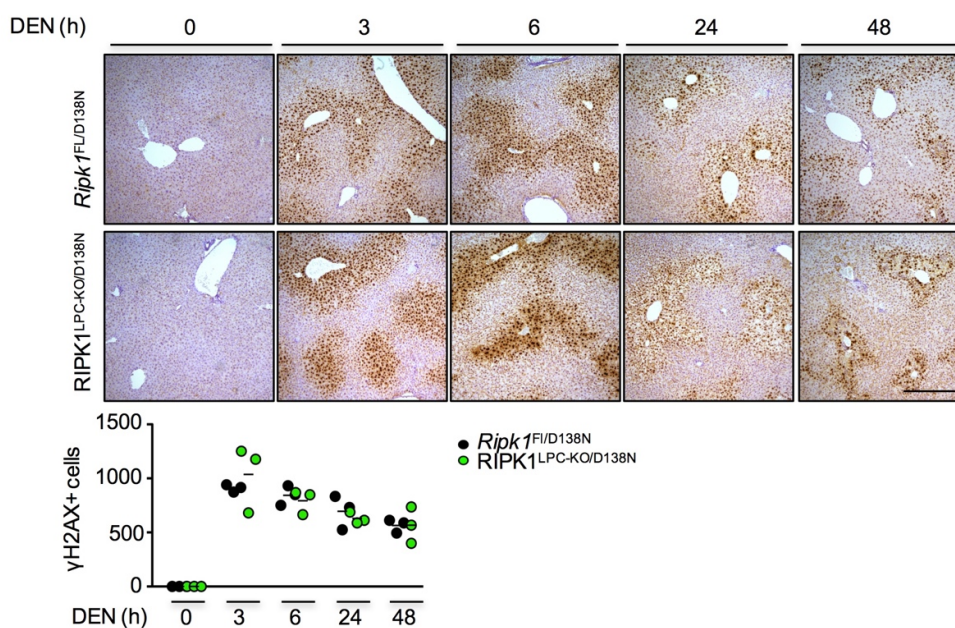
Figure 40. Loss of RIPK1 kinase activity did not affect γH2AX levels
Representative images of livers of non-injected or with an acute dose of DEN injected 6-week-old *Ripk1*$^{FL/D138N}$ and RIPK1$^{LPC-KO/D138N}$ mice stained for γH2AX (Scale bar, 100 μm). Quantification of γH2AX+ cells in *Ripk1*$^{FL/D138N}$ and RIPK1$^{LPC-KO/D138N}$ mice after DEN injection was performed in 5 fields per animal (mean of 5 fields per animal, n= 3).

3.3.11. Injection with an acute dose of DEN results in the induction of *Tnf* and *Trail* gene expression

To elucidate whether DR signaling is important for RIPK1-mediated HCC, gene expression levels of DRs and their ligands were measured 3, 6, 24 and 48h after an acute dose of DEN. Gene expression analysis revealed no considerable differences

between RIPK1^{LPC-KO} and *Ripk1$^{FL/FL}$* mice (Figure 41). However, in *Ripk1$^{FL/FL}$* and RIPK1^{LPC-KO} mice an induction in *Tnf* and *Trail* gene expression level was detected after DEN injection (Figure 41). Since previous results presented in this study showed higher sensitivity of RIPK1-deficient hepatocyte to DR-induced death these results emphasize a TNF or TRAIL-dependent role in RIPK1-deficient hepatocyte death in response to acute DEN.

● *Ripk1$^{FL/FL}$* (n= 3) ● RIPK1^{LPC-KO} (n= 3-4)
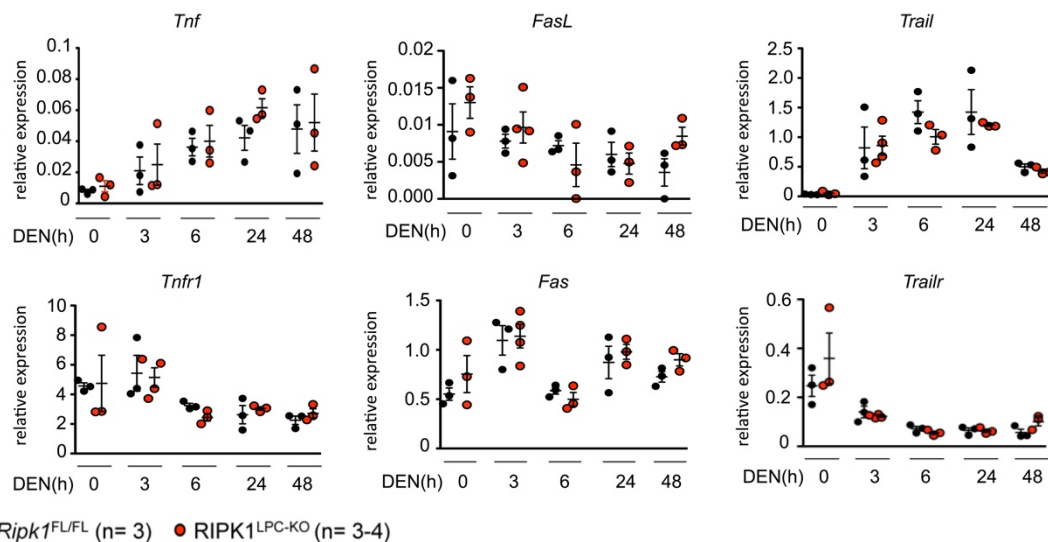
Figure 41. LPC-specific loss of RIPK1 did not alter gene expression patterns of DRs and their ligands in response to DEN
qRT-PCR analysis of gene expression levels of DRs and their ligands in *Ripk1$^{FL/FL}$* and RIPK1^{LPC-KO} mice after DEN injection for indicated timeperiods. Graphs show relative mRNA expression normalized to *Tbp*.

3.3.12. TNFR1 signaling promotes apoptotic death 3h after acute DEN injection

Since gene expression levels of DRs and IHC analysis for cleaved Caspase-8 indicated an important role of DR signaling in the regulation of hepatocyte apoptosis in RIPK1^{LPC-KO} mice, RIPK1^{LPC-KO} TNFR1^{LPC-KO} mice were generated by crossing *Ripk1$^{FL/FL}$ Alfp-Cre* transgenic mice with *Tnfr1$^{FL/FL}$* mice. To investigate the role of TNFR1 signaling in DEN-induced DNA-damage and cell death, male *Ripk1$^{FL/FL}$ Tnfr1$^{FL/FL}$* and RIPK1^{LPC-KO} TNFR1^{LPC-KO} mice were injected at 6 weeks of age with an acute dose of DEN. In contrast to RIPK1^{LPC-KO} mice, RIPK1^{LPC-KO} TNFR1^{LPC-KO} mice did not show considerable elevated levels of ALT and AST levels 24h after acute DEN injection (Figure 42A). In addition, IHC analysis for CC3 and CC8 showed similar levels between *Ripk1$^{FL/FL}$ Tnfr1$^{FL/FL}$* and RIPK1^{LPC-KO} TNFR1^{LPC-KO} mice at 3h after acute DEN injection (Figure 42B, C, E). However, 6h after acute DEN injection serum ALT and AST levels as well as CC3 and CC8 levels were still elevated but slightly lower compared to levels in RIPK1^{LPC-KO} mice (Figure 42A-C, E) while CC9 levels remained

unaffected by LPC-specific loss of TNFR1 (Figure 42D, E). Together these results suggest that predominantly the early onset of apoptotic death 3h after DEN injection is TNFR1-dependent.

A ALT (U/l)

● *Ripk1*^FL/FL *Tnfr1*^FL/FL
● RIPK1^LPC-KO TNFR1^LPC-KO

DEN (h) 0   3   6   24   48

B DEN (h)   0   3   6   24   48

CC3 *Ripk1*^FL/FL *Tnfr1*^FL/FL
CC3 RIPK1^LPC-KO TNFR1^LPC-KO

C DEN (h)   0   3   6   24   48

CC8 *Ripk1*^FL/FL *Tnfr1*^FL/FL
CC8 RIPK1^LPC-KO TNFR1^LPC-KO

D DEN (h)   0   3   6   24   48

CC9 *Ripk1*^FL/FL *Tnfr1*^FL/FL
CC9 RIPK1^LPC-KO TNFR1^LPC-KO

E   ● *Ripk1*^FL/FL *Tnfr1*^FL/FL   ● RIPK1^LPC-KO TNFR1^LPC-KO

CC3+ cells   DEN (h) 0   3   6   24   48
CC8+ cells   DEN (h) 0   3   6   24   48
CC9+ cells   DEN (h) 0   3   6   24   48

Figure 42. Loss of TNFR1 reduced CC3 and CC8 levels 3h after DEN injection
(A) Graph depicting serum ALT levels in *Ripk1*^{FL/FL} *Tnfr1*^{FL/FL} and RIPK1^{LPC-KO} TNFR1^{LPC-KO} mice after acute DEN injection for indicated timeperiods. (B-D) Representative images of livers of non-injected or with an acute dose of DEN injected 6-week-old *Ripk1*^{FL/FL} *Tnfr1*^{FL/FL} and RIPK1^{LPC-KO} TNFR1^{LPC-KO} mice stained for CC3 (B), CC8 (C) and CC9 (D) (Scale bar, 100 μm). (E) Quantification of CC3+, CC8+ and CC9+ cells in *Ripk1*^{FL/FL} *Tnfr1*^{FL/FL} and RIPK1^{LPC-KO} TNFR1^{LPC-KO} mice after DEN injection was performed in 5 fields per animal (mean of 5 fields per animal, n= 3).

3.3.13. LPC-specific deficiency of TNFR1 restores γH2AX levels in RIPK1^{LPC-KO} mice upon acute DEN.

To analyze the correlation between DEN-induced cell death and γH2AX levels in 6-week-old *Ripk1*^{FL/FL} *Tnfr1*^{FL/FL} and RIPK1^{LPC-KO} TNFR1^{LPC-KO} mice, mice were injected with an acute dose of DEN for 3, 6, 24 and 48h and subsequently IHC analysis for γH2AX was performed in their livers. In contrast to RIPK1^{LPC-KO} mice, RIPK1^{LPC-KO} TNFR1^{LPC-KO} mice showed similar γH2AX+ cell levels comparable to their control littermates suggesting a strong correlation between TNF-induced apoptotic death at 3h and γH2AX levels after acute DEN injection (Figure 43).
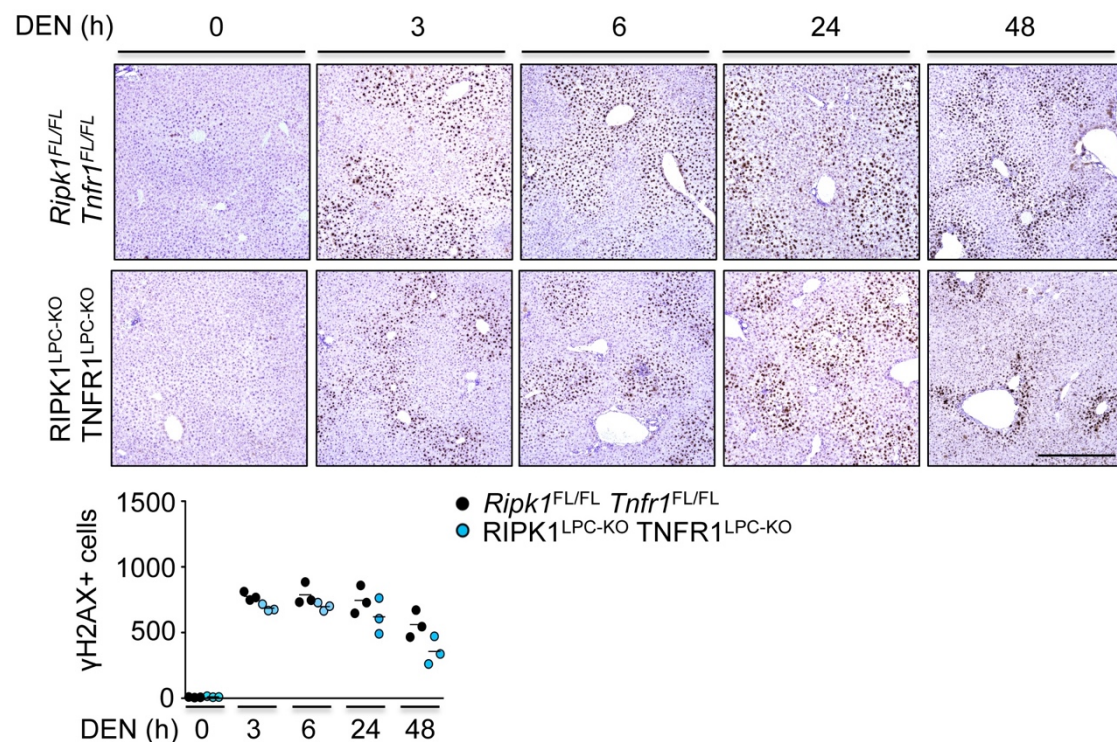
Figure 43. RIPK1^{LPC-KO} TNFR1^{LPC-KO} mice showed similar γH2AX+ levels compared to *Ripk1*^{FL/FL} *Tnfr1*^{FL/FL} mice upon acute DEN injection
Representative images of livers of non-injected or with an acute dose of DEN injected 6-week-old *Ripk1*^{FL/FL} *Tnfr1*^{FL/FL} and RIPK1^{LPC-KO} TNFR1^{LPC-KO} mice stained for γH2AX (Scale bar, 100 μm). Quantification of γH2AX+ cells in *Ripk1*^{FL/FL} *Tnfr1*^{FL/FL} and RIPK1^{LPC-KO} TNFR1^{LPC-KO} mice after DEN injection was performed in 5 fields per animal (mean of 5 fields per animal, n= 3).

3.3.14. TNFR1 signaling mediates the protective effect in RIPK1^{LPC-KO} mice in response to DEN-induced carcinogenesis

To assess whether early hepatocyte death is indeed the cause for reduced HCC development in RIPK1^{LPC-KO} mice, groups of *Ripk1$^{FL/FL}$Tnfr1$^{FL/FL}$*, RIPK1^{LPC-KO} TNFR1$^{LPC-KO/WT}$ and RIPK1^{LPC-KO} TNFR1^{LPC-KO} mice were injected at 2 weeks of age with DEN and tumor development was evaluated at 36 weeks of age. RIPK1^{LPC-KO} TNFR1^{LPC-KO} mice showed similar bodyweight gain, serum ALT and AST levels and liver to bodyweight ratio compared to their control littermates at the age of 36 weeks (Figure 44A, B, F). Macroscopic assessment of livers revealed similar tumor incidences, numbers and size in RIPK1^{LPC-KO} TNFR1^{LPC-KO} mice compared to their control littermates (Figure 44C-E). Strikingly, heterozygous deletion of TNFR1 in RIPK1^{LPC-KO} fully restored tumor growth in those mice as efficient as in homozygously deleted TNFR1 mice (Figure 44C-E). Together, these data suggest a RIPK1 pro-survival function downstream of TNFR1 in regulating DEN-induced HCC underscoring an early anti-apoptosis-dependent role of RIPK1 in promoting tumor induction and growth.
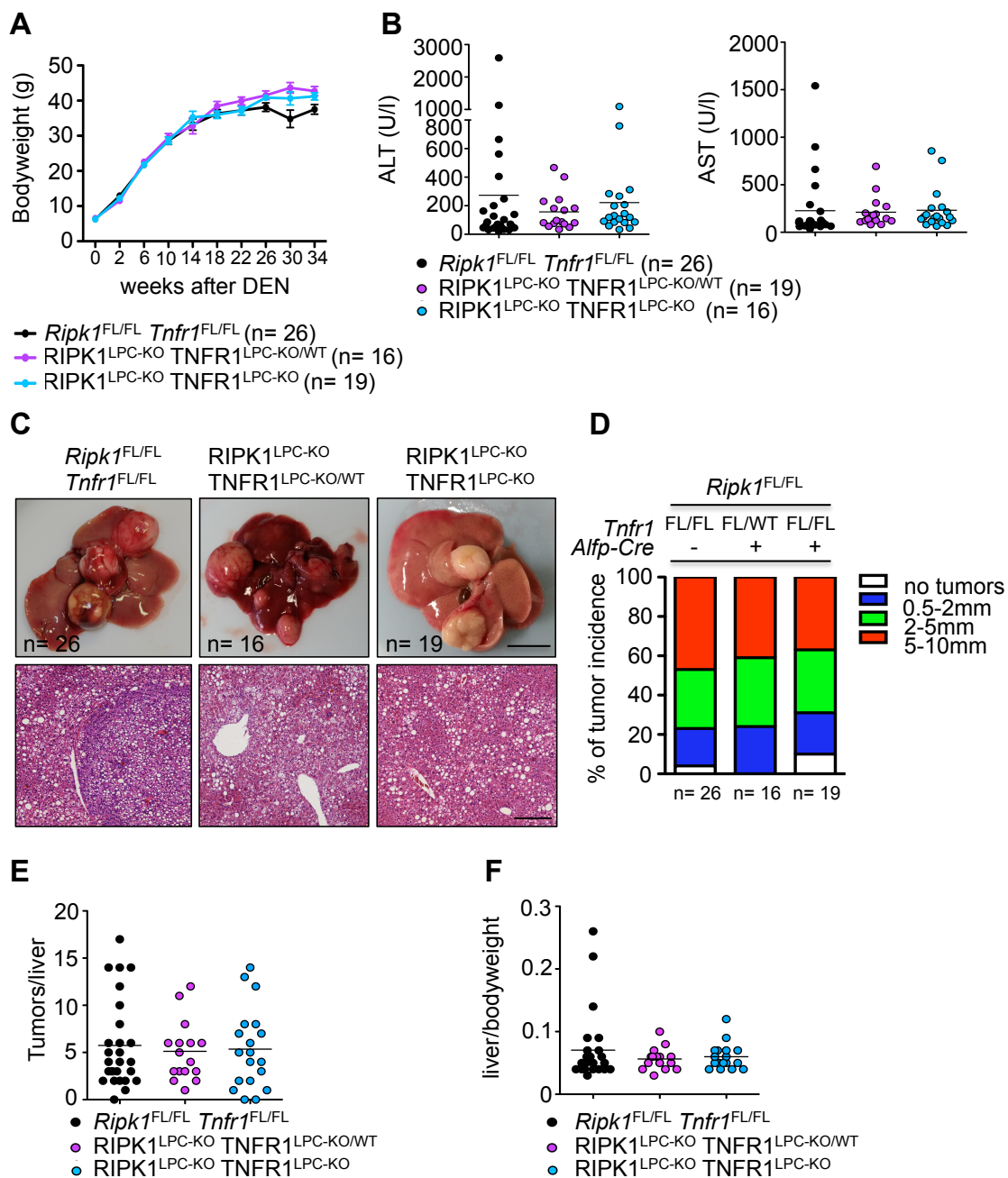
Figure 44. Loss of TNFR1 signaling promoted DEN-induced liver tumorigenesis
(A) Bodyweight curve of DEN-injected *Ripk1*$^{FL/FL}$ *Tnfr1*$^{FL/FL}$, *Ripk1*$^{LPC-KO}$ TNFR1$^{LPC-KO/WT}$ and RIPK1^{LPC-KO} TNFR1^{LPC-KO} mice starting from DEN injection until the age of 36 weeks (mean ± SEM). (B) Graph depicting serum ALT and AST levels of 36-week-old *Ripk1*$^{FL/FL}$ *Tnfr1*$^{FL/FL}$, *Ripk1*$^{LPC-KO}$ TNFR1$^{LPC-KO/WT}$ and RIPK1^{LPC-KO} TNFR1^{LPC-KO} mice upon DEN injection. (C) Representative pictures of livers (Scale bar: 1cm) and H&E stained liver sections from DEN-injected *Ripk1*$^{FL/FL}$ *Tnfr1*$^{FL/FL}$, *Ripk1*$^{LPC-KO}$ TNFR1$^{LPC-KO/WT}$ and RIPK1^{LPC-KO} TNFR1^{LPC-KO} mice at the age of 36 weeks. Scale bar, 100 µm. * indicates the tumor area. (D) Tumor load in 36-week-old *Ripk1*$^{FL/FL}$ *Tnfr1*$^{FL/FL}$, *Ripk1*$^{LPC-KO}$ TNFR1$^{LPC-KO/WT}$ and RIPK1^{LPC-KO} TNFR1^{LPC-KO} mice as estimated by quantification of the tumor size distribution. (E, F) Graphs depicting the number of tumors per liver (E) and the liver/bodyweight ratio (F) in 36-week-old mice injected with DEN.

3.3.15. LPC-specific deficiency of RIPK1 ameliorates obesity-induced liver carcinogenesis

Genetic or HFD-induced obesity aggravates DEN-induced liver carcinogenesis in a TNFR1-dependent manner (Uysal et al. 1997). To address the role of RIPK1 in obesity-mediated liver carcinogenesis, groups of male RIPK1^{LPC-KO} and *Ripk1$^{FL/FL}$* mice were injected with DEN at 2 weeks of age and subsequently divided in two groups, one receiving high-fat-diet (HFD) starting from the age of 4 weeks and a control group receiving normal-chow-diet (NCD). RIPK1^{LPC-KO} showed similar bodyweight gain, serum ALT and LDL-C levels compared to *Ripk1$^{FL/FL}$* mice under NCD- and HFD-fed conditions (Figure 45A-C). Furthermore, RIPK1^{LPC-KO} showed similar response to glucose at 12 and 24 weeks compared to *Ripk1$^{FL/FL}$* mice suggesting that LPC-specific RIPK1 deficiency does not affect the promotion of HFD-induced obesity and the maintenance of glucose metabolism (Figure 45D). Macroscopic assessment of tumor development at 36 weeks of age revealed reduced tumor incidences, tumor size and tumor numbers in HFD-fed RIPK1^{LPC-KO} mice compared to HFD-fed *Ripk1$^{FL/FL}$* littermates although the protective effect induced by RIPK1 deficiency was not as pronounced as in mice fed a NCD (Figure 45E-G). In summary, these results suggest a TNFR1-dependent role for RIPK1 in regulating DEN/obesity-induced HCC supporting data shown in figure 44.
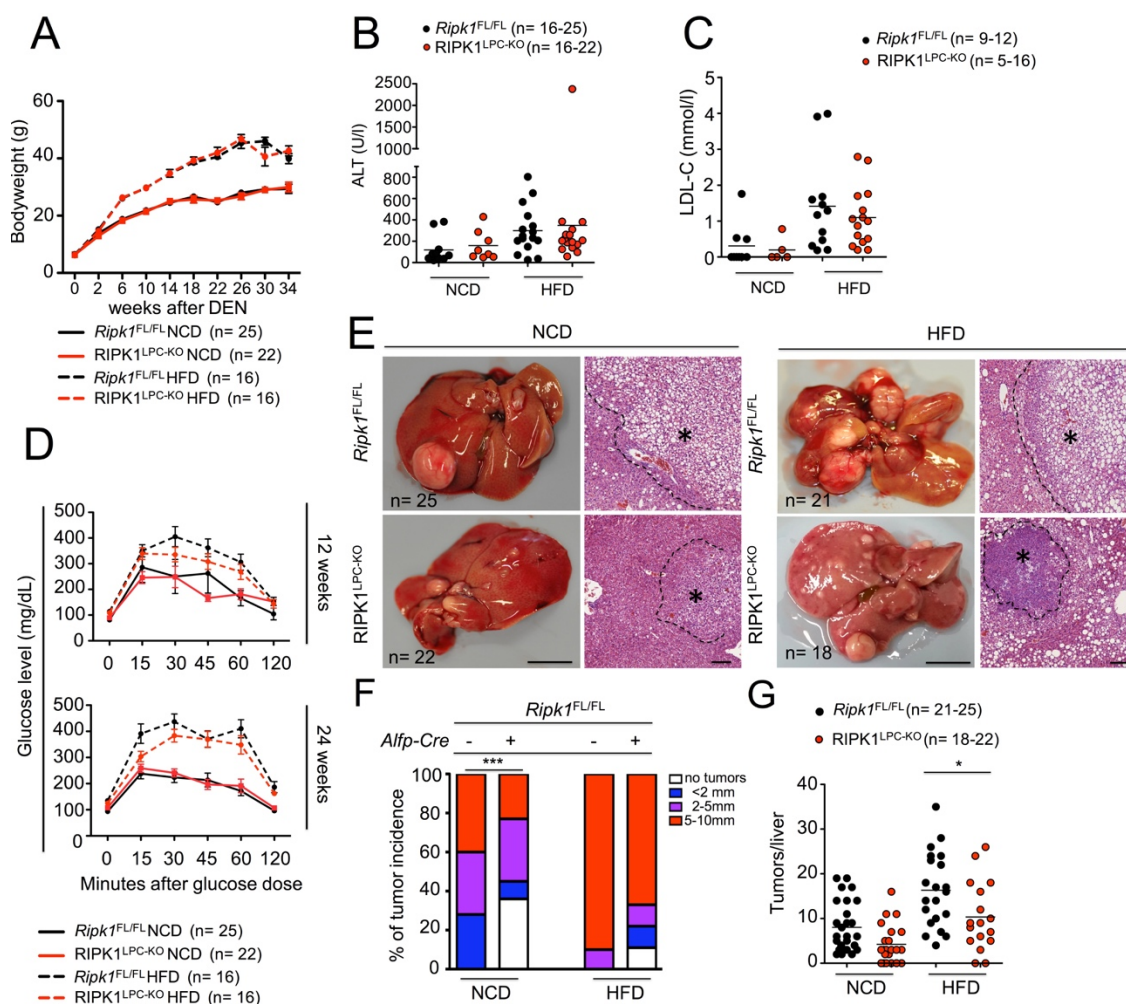
Figure 45. LPC-specific deficiency of RIPK1 mildly reduced obesity-induced liver carcinogenesis

(A) Bodyweight curve of NCD- or HFD-fed DEN-injected *Ripk1*^FL/FL and RIPK1^LPC-KO mice starting from DEN injection until the age of 36 weeks (mean ± SEM). (B, C) Graph depicting serum ALT (B) and serum LDL-C levels (C) of NCD- or HFD-fed 36-week-old *Ripk1*^FL/FL and RIPK1^LPC-KO mice upon DEN injection. (D) Graphs depicting blood glucose level after glucose administration in NCD- or HFD-fed *Ripk1*^FL/FL and RIPK1^LPC-KO mice at 12 and 24 weeks of age (mean ± SEM). (E) Representative pictures of livers (Scale bar: 1cm) from DEN-injected *Ripk1*^FL/FL and RIPK1^LPC-KO mice at the age of 36 weeks after NCD or HFD feeding. Scale bar, 100 μm. (F) Tumor load in NCD- or HFD-fed 36-week-old *Ripk1*^FL/FL and RIPK1^LPC-KO mice as estimated by quantification of the tumor size distribution (***$P < 0.005$). (G) Graphs depicting the number of tumors per liver in NCD- or HFD-fed 36-week old mice injected with DEN (*$P < 0.05$).

4. Discussion

4.1. RIPK1, a crucial regulator of cell survival *in vivo* and *in vitro*

RIPK1 has emerged as an important regulator of inflammation and cell death in response to TNFR1- and TLR-signaling. Therefore, tight regulation of RIPK1-signaling is of high importance to maintain tissue homeostasis. Indeed, full body ablation of RIPK1 resulted in perinatal lethality of the mice due to increased apoptotic death in multiple tissues including the intestine and the liver (Kelliher et al. 1998; Dillon et al. 2014; Kaiser et al. 2014). Consistently, epithelial cell-specific ablation of RIPK1 resulted in early postnatal death with increased apoptotic and necroptotic cell death in the intestine or the skin (Dannappel et al. 2014; Takahashi et al. 2014).

In sharp contrast to RIPK1^{IEC-KO} or RIPK1^{E-KO} mice, RIPK1^{LPC-KO} mice were viable, fertile and reached adulthood without considerable morphological liver pathology suggesting the existence of a RIPK1-independent mechanism in liver development and the regulation of liver homeostasis under basal conditions. In line with recent studies, our results revealed normal hepatocyte proliferation and death in RIPK1^{LPC-KO} mice (Suda et al. 2016; Filliol et al. 2016; Dara et al. 2015; Schneider et al. 2017). However, our detailed IHC analysis revealed focal immune cell patches in RIPK1^{LPC-KO} mice, which did not trigger an immune response indicated by gene expression analysis of *Tnf* and *Il1b*. Unlike hepatocytes in *Ripk1$^{-/-}$* mice, which might be constantly in contact with DAMPs/PAMPs due to intestinal barrier rupture, hepatocytes of RIPK1^{LPC-KO} mice *in vivo* have only minimal contact with DAMPs or PAMPs since the intestinal barrier is intact and prevents the translocation of large amounts of PAMPs/DAMPs to the liver. Taken together, RIPK1^{LPC-KO} mice do not show spontaneous liver pathology and premature death due to the fact that hepatocytes might have an additional or redundant RIPK1-independent pro-survival mechanisms to sustain the low level of immune cell infiltration and liver damage. Therefore, this low amount of bacterial components might not reach a specific threshold that would be sufficient to trigger extensive hepatocyte death or an inflammatory response but only result in local recruitment of additional macrophages, B and T cells. Future studies using co-depletion of RIPK1 specifically in IECs and hepatocytes would shed light on the importance of microbiota-dependent effects on *Ripk1$^{-/-}$* liver pathology. Noteworthy, in contrast to *Ripk1$^{-/-}$* mice, in RIPK1^{LPC-KO} mice *Alfp*-Cre-dependent recombination does not affect RIPK1 expression in KCs. Future studies are needed to unravel the effect of KCs on disease onset and progression in *Ripk1$^{-/-}$* mice.

Although RIPK1^{LPC-KO} mice did not display obvious abnormalities in the liver, RIPK1-deficient primary hepatocytes isolated from RIPK1^{LPC-KO} mice died spontaneously in

culture. Using a TNF inhibitor directly after isolation or additional LPC-specific deficiency of TNFR1 was sufficient to reduce up to 50% of the spontaneous death of primary RIPK1-deficient hepatocytes in culture. Consistent with recent reports, RIPK1-deficient primary hepatocytes were highly sensitive to TNF-induced apoptosis suggesting either an autocrine TNF release or a small contamination with immune cells during the process of hepatocyte isolation that results in the production of TNF (Filliol et al. 2016; Schneider et al. 2017; Suda et al. 2016). Given the fact that TNFR1 signaling inhibition did not fully prevent spontaneous hepatocyte death additional triggers for apoptosis are likely to be present during isolation. The result in this study pointed to a FasL-independent mechanism of apoptosis since culturing primary hepatocytes in presence of a neutralizing antibody for FasL did not prevent apoptosis. However, it remains to be elucidated whether signaling through other DRs such as TRAILR or DR3/6 or TLR-signaling could be involved in the spontaneous death of RIPK1-deficient primary hepatocytes. Another possibility would be that TNFR1-independent death was caused by stress associated with the mechanical and enzymatic disruption of the liver architecture.

Taken together, the data presented in this work reveal that under homeostatic conditions RIPK1 is largely dispensable for normal liver homeostasis while under stressed conditions RIPK1 displays a pro-survival function in primary hepatocytes.

4.2. RIPK1, a regulator of NF-κB activation in hepatocytes

Ablation of RIPK1 in various tissues sensitized cells to death *in vitro* and *in vivo* pointing to a crucial pro-survival role of RIPK1. However, the mechanism how RIPK1 maintains cell survival remains still highly controversial mainly due to contradictory studies on its role in TNF-induced NF-κB activation. First, Kelliher et al. suggested a major RIPK1-dependent role in mediating NF-κB activation (Kelliher et al. 1998), which was challenged by a later study suggesting a dispensable role of RIPK1 in NF-κB activation in various cell types (Wong et al. 2010). Likewise, recent studies revealed no impairment of NF-κB activation in RIPK1-deficient IECs and keratinocytes (Dannappel et al. 2014; Takahashi et al. 2014). Nevertheless, in our study RIPK1 ablation in hepatocytes impaired TNF-induced NF-κB activation demonstrated by diminished IκBα phosphorylation and degradation. Moreover, absence of RIPK1 abrogated nuclear translocation of p65 and significantly reduced NF-κB target gene expression emphasizing a crucial role of RIPK1 in mediating NF-κB activation in primary hepatocytes. On the contrary, recent reports revealed high sensitivity of RIPK1 deficient hepatocytes to death independent of NF-κB activation (Filliol et al. 2016; Schneider et al. 2017; Suda et al. 2016). In contrast to these studies, RIPK1-deficient

primary hepatocytes used in this work were cultured over night in the presence of zVAD-fmk to analyze TNF-mediated NF-κB activation whereas other studies stimulated within 3h with TNF or injected mice with LPS. Given the fact that hepatocyte isolation is still a highly sensitive method using a wide variety of reagents and different isolation protocols, small differences in the protocol or in the culturing procedure might affect the outcome of the experiments. An ultimate proof for RIPK1-dependent NF-κB activation would be to restore NF-κB signaling in RIPK1-deficient hepatocytes by expressing e.g. a constitutive active form of IKK2 to elucidate whether restored NF-κB signaling is able to prevent spontaneous hepatocyte death.

Since in our study primary RIPK1-deficient hepatocytes showed impaired NF-κB activation *in vitro*, *in vivo* NF-κB activation was assessed to analyze the higher susceptibility of RIPK1^{LPC-KO} mice to LPS. Expressing a constitutive active form of IKK2 in fact protected 80% of RIPK1^{LPC-KO} mice from LPS-induced liver injury demonstrating a crucial role for NF-κB signaling in regulating TNF-induced cell death in the absence of RIPK1. However, reconstituting NF-κB signaling was not sufficient to fully prevent liver injury but efficiently prevented early death of RIPK1^{LPC-KO} mice. These results suggest an important IKK2-dependent role in the regulation of liver damage upon LPS by reducing the liver injury level to a certain extent allowing hepatocyte recovery. Recently, a NF-κB-independent function of IKK1 and IKK2 has been identified (Dondelinger et al. 2015). It was reported that IKKs phosphorylate RIPK1 in order to restrain RIPK1 in complex-I to protect cells from RIPK1 kinase-dependent death. Given this fact, we hypothesize that expression of a constitutive active form of IKK2 in RIPK1^{LPC-KO} mice might reduce liver injury to some extent by NF-κB-dependent mechanisms but might not fully prevent hepatocyte apoptosis and liver injury since in absence of RIPK1 IKK2 could not prevent cell death by its NF-κB-independent mechanisms. This might result in the destabilization of complex-I leading to complex-IIa-dependent apoptosis. Noteworthy, in LPS-injected RIPK1^{LPC-KO} IKK2Ca^{LPC} mice, ALT and AST levels were decreasing with time and it remains to be elucidated whether this might be due increased regenerative capacity of hepatocytes or decreased hepatocyte death with time. On the same token, NF-κB signaling is highly activated after expression of a constitutive active form of IKK2 and therefore might increase cFLIP levels with time resulting in the inhibition of Caspase-8 oligomerization and consequently apoptosis. Together, these results argue for two pathways operating in parallel to ensure hepatocyte survival during endotoxin-mediated liver injury, a NF-κB-dependent and -independent pathway.

In addition to canonical NF-κB activation, the stabilization of cIAPs and TRAF2 proteins by RIPK1 was suggested to prevent hepatocyte death (Feoktistova et al. 2011). Accordingly, RIPK1[IEC-KO] and RIPK1[E-KO] mice revealed reduced TRAF2 and cIAP1 protein levels and consequently higher sensitivity of cells to death (Dannappel et al. 2014). Unlike in RIPK1[IEC-KO] and RIPK1[E-KO] mice, in RIPK1[LPC-KO] mice no considerable changes in gene and protein expression of pro-survival proteins such as TRAF2 and cIAP1 were detected even after LPS injection. This result suggests a cell-type specific role of RIPK1 in stabilizing these pro-survival proteins and it underscores the presence of another protein stabilizing cIAPs and TRAF2 in hepatocytes. In contrast to our study, it was recently reported that deficiency of RIPK1 resulted in TRAF2 downregulation, which did not affect canonical NF-κB activation but sensitized hepatocytes to apoptotic death (Schneider et al. 2017; Filliol et al. 2016; Gentle et al. 2011). The discrepancy between our study and the recent studies remains to be investigated, however, we assume that RIPK1 deficiency could be compensated by TRADD, since TRADD has been shown to mediate the recruitment of cIAPs and TRAF2. Moreover, TRADD deficiency in MEFs and macrophages abrogates NF-κB activation (Ermolaeva et al. 2008). However, TRADD-mediated NF-κB activation was supported only to a certain extent since our *in vitro* treatment of RIPK1-deficient hepatocytes with TNF still resulted in reduced NF-κB activation and increased hepatocyte apoptosis.

Moreover, assuming that TRADD could compensate the deficiency of RIPK1 in term of NF-κB activation and the stabilization of pro-survival proteins it remains unclear why TRADD might not compensate the reduction of TRAF2 and cIAP1 protein level in RIPK1-deficient IECs or keratinocytes. Combined, this suggests a cell-type specific function of TRADD probably due to different expression levels of TRADD in different tissues.

Although RIPK1 and TRAF2 alone were not sufficient to trigger spontaneous liver pathology, combined deficiency in LPCs triggered spontaneous hepatocyte apoptosis, cholestasis and chronic hepatitis resulting in HCC development (Schneider et al. 2017). Deficiency of RIPK1 and TRAF2 resulted in the instability of cIAP1/2, TRAF2 and cFLIP and reduced NF-κB activation, which correlated with chronic hepatocyte TRADD-dependent apoptosis that consequently resulted in liver injury and HCC formation (Schneider et al. 2017). However, the link between instability of pro-survival proteins and cell death was challenged by the fact that cFLIP_L levels remained low in RIPK1[LPC-KO] TRAF2[LPC-KO] Caspase-8[LPC-KO] mice, which was attributed to the observed NF-κB inhibition (Schneider et al. 2017). Conversely, Kondylis et al. reported restored

cFLIP$_L$ levels in NEMO^{LPC-KO} *Ripk1$^{D138N/D138N}$* mice independent of NF-κB activation (Kondylis et al. 2015).

Together these results suggest the presence of contributing proteins that are needed for NF-κB activation and that RIPK1 and TRAF2 display redundant or independent pro-survival functions. It remains to be seen how RIPK1 synergizes with other members of complex-I to prevent complex-II formation.

4.3. RIPK1 as a key regulator of cell death in response to LPS-induced toxicity

To mimic the microbiota dependent effect, we employed the LPS-mediated liver injury model to explore the role of TLR4- and TNFR1-dependent signaling in RIPK1^{LPC-KO} mice. Indeed, RIPK1^{LPC-KO} mice were highly susceptible to a low dose of LPS displaying liver injury resulting in early death of mice (Figure 46). Importantly, LPC-specific deficiency of TNFR1 protected RIPK1^{LPC-KO} mice from early LPS-induced death. Consistent with LPC-specific deficiency of TNFR1 in our study, pre-treatment with etanercept, a TNF decoy receptor, fully protected RIPK1^{LPC-KO} mice from LPS-induced liver injury (Filliol et al. 2017). Since in our study RIPK1-deficient primary hepatocytes showed impaired NF-κB activation it strongly suggests that TNF is expressed by KCs in response to LPS. Accordingly, Filliol et al. reported an amelioration of liver injury in RIPK1^{LPC-KO} mice challenged with LPS after depletion of KCs due to reduced serum TNF levels in LPS-injected mice (Filliol et al. 2017). Together these results strongly suggest that LPS activates TLR4, mainly present on KCs, which induces the release of TNF resulting in massive apoptotic hepatocyte death and liver injury in the absence of RIPK1 leading to liver failure and consequently death of the mice due to impaired liver functions.

Using the kinase-inactive mutant of RIPK1 (*Ripk1$^{D138N/D138N}$*) we demonstrated that RIPK1 scaffolding function rather than its kinase activity prevents LPS-induced liver injury. This finding is in line with recent studies revealing similar kinase-independent scaffolding function of RIPK1 in preventing ConA-mediated hepatitis and αGalCer-mediated liver injury (Suda et al. 2016; Filliol et al. 2016). Employing the LPS/D-GalN model, which triggers TNFR1-dependent cell death (Wroblewski et al. 2016), the kinase activity of RIPK1 was shown to mediate to a certain extent LPS/D-GalN-induced death. This partial protection seen after LPS/D-GalN injection in this study could be a dose-dependent effect or a compensatory effect by TRADD-mediated pro-death function. In summary, RIPK1 exhibits kinase-independent scaffolding function to prevent LPS-induced liver injury but kinase-dependent functions facilitating LPS/D-GalN induced cell death.

LPC-specific deficiency of FADD or TRADD fully protected RIPK1[LPC-KO] mice from LPS-induced liver injury emphasizing a crucial role of apoptosis in mediating the early death of RIPK1[LPC-KO] mice in response to low doses of LPS. In line with our data, Caspase-8 deficiency was sufficient to prevent increased liver injury in RIPK1[LPC-KO] mice (Schneider et al. 2017). In our study, ablation of RIPK1 sensitized to LPS/TNF-induced TRADD-dependent apoptosis. Both RIPK1 and TRADD are able to interact with Caspase-8 in complex-II in response to TNF, but although complex-IIa and –IIb are considered as two independent complexes, this has not been fully demonstrated yet.

In summary, the sensitivity of RIPK1[LPC-KO] mice to LPS resembles largely the high TRIF/TNFR1-dependent sensitivity of *Ripk1*^{-/-} mice to cell death emphasizing a crucial role of PAMPs/DAMPs in mediating hepatocyte death in *Ripk1*^{-/-} mice (Dillon et al. 2014). Importantly, our results together with other studies demonstrate a kinase-independent scaffolding function of RIPK1 in preventing apoptosis of hepatocytes in LPS/TNF-mediated liver injury. In addition, our LPS/D-GalN result emphasizes the importance of the kinase-dependent function of RIPK1 in mediating apoptosis, which supports the data of Dondelinger et al. (Dondelinger et al. 2015).
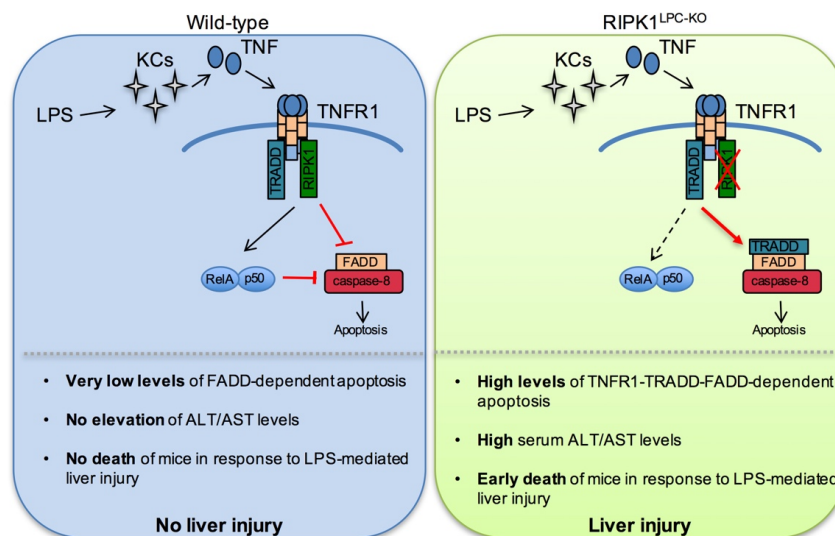
Figure 46. RIPK1 prevents LPS-induced liver injury
LPS administration induces KC dependent release of the cytokine TNF, which triggers the activation of TNFR1-signaling. In WT hepatocytes, LPS administration triggers TNFR1-dependent canonical NF-κB activation which prevents high levels of TNF-mediated apoptosis resulting in the protection of mice against LPS-induced liver injury. On the contrary, LPC-specific deletion of RIPK1 sensitizes hepatocytes to LPS/TNF-mediated TRADD-FADD-Caspase-8-dependent apoptosis due to impaired NF-κB activation. Elevated levels of apoptotic hepatocyte death results in increased liver damage indicated by increased serum ALT/AST levels which consequently resulted in early death of mice in response to LPS-mediated liver injury

4.4. Apoptosis as the preferable mechanism of hepatocyte death

LPC-specific RIPK1 deficiency sensitized primary hepatocytes to TNF-induced apoptosis whereas necroptosis seemed to be dispensable since culturing cells in presence of zVAD-fmk or LPC-specific FADD or TRADD deficiency fully protected hepatocytes from death *in vitro* and in response to LPS-induced toxicity *in vivo*. In line with our data, IECs deficient for RIPK1 undergo predominantly FADD-mediated apoptosis. Only under condition of apoptosis inhibition, death of IECs switched to RIPK3-dependent necroptosis (Dannappel et al. 2014). In RIPK1[E-KO] mice, keratinocytes died in an apoptosis- and necroptosis-dependent manner (Dannappel et al. 2014). Likewise, in *Ripk1^{-/-}* mice neither FADD/Caspase-8 nor RIPK3/MLKL alone could rescue the early perinatal lethality. Only a combined deficiency of Caspase-8/RIPK3 or FADD/RIPK3 could rescue *Ripk1^{-/-}* mice until adulthood without aberrant pathology. How tissue-specific deletion of RIPK1 affects the mechanism of cell death remains unclear. One important aspect is the tissue-specific expression of RIPK3, which was suggested to influence the induction of necroptosis (He et al. 2009). Strikingly, Dannappel et al. reported slightly higher RIPK3 levels in IEC protein extracts compared to keratinocyte protein extracts from RIPK1[IEC-KO] and RIPK1[E-KO] mice, respectively (Dannappel et al. 2014). However, as mentioned already above, IECs deficient for RIPK1 undergo predominantly FADD-mediated apoptosis while *in vivo* the keratinocyte death was primarily RIPK3-driven suggesting a RIPK3-level independent role in determining the mechanism of cell death (Dannappel et al. 2014). Unlike in the gut or the skin, the occurrence of necroptosis in the liver remains highly controversial. Several independent studies revealed low levels of RIPK3 in whole liver lysates under basal conditions. This suggests that hepatocytes barely undergo necroptosis but preferably Caspase-dependent apoptosis which is in line with our data that RIPK1[LPC-KO] FADD[LPC-KO] mice were fully protected in response to LPS. Highly contradictory were the results from various liver injury studies using acetaminophen, αGalCer, ConA or from chronic liver injury models such as alcoholic steatohepatitis (ASH) and non-alcoholic-steatohepatitis (Dara et al. 2016). Studies revealing a protection using *Ripk3^{-/-}* mice indicated a RIPK3 induction upon APAP, ConA and aGalCer (Ramachandran et al. 2011; Jouan-Lanhouet et al. 2012; Deutsch et al. 2015; An et al. 2013; Zhou et al. 2013; Arshad et al. 2015; Suda et al. 2016; Zhang et al. 2014). In contrast to these studies, several other independent reports showed no protection in *Ripk3^{-/-}* mice in liver injury models (Dara et al. 2015; Weinlich et al. 2013; Gunther et al. 2016, Schneider et al. 2017). The discrepancies between these studies could be attributed to the specificity problems that have been reported for the commercially available RIPK3 antibodies. Moreover, in a well-controlled study it was shown that RIPK3 is very

strongly expressed in immune cells rather than in hepatocytes. Therefore, future studies using conditional RIPK3 knockout mice would help deciphering the hepatocyte specific effect of RIPK3 in these liver injury models.

Furthermore, there are contrasting results about the implication of other necroptosis-inducing proteins such as RIPK1 and MLKL in mediating liver injury in these different studies (Dara et al. 2016). It is worth mentioning that all these studies were performed under different experimental settings. Furthermore, studies were performed using different concentrations of APAP and ConA and in different animal facilities. In conclusion, inconsistencies in protection in these liver injury models using $Ripk3^{-/-}$ mice emphasized a minor role of necroptosis in the liver. Moreover, deficiency of RIPK3 did not prevent HCC development in NEMO^{LPC-KO} mice with NEMO^{LPC-KO} $Ripk3^{-/-}$ mice revealing increased liver damage due to increased hepatocyte apoptosis (Kondylis et al. 2015). This result demonstrated that RIPK3-dependent necroptosis does not contribute to spontaneous HCC development in NEMO^{LPC-KO} mice. These results together with our own results strongly suggest a negligible impact of RIPK3-mediated necroptosis in hepatocytes due to very low levels of RIPK3 in the liver.

4.5. The pro-survival scaffolding function of RIPK1 promotes DEN-induced hepatocarcinogenesis

Given the fact that RIPK1 displays dual-functions in regulating cell survival and cell death it could be a promising target for new therapeutic strategies against HCC. Our *in vivo* results revealed a delay in DEN-induced HCC development in RIPK1^{LPC-KO} mice, which could be a consequence of extensive apoptotic death early after DEN injection (Figure 47). Immunohistological analysis revealed extensive hepatocyte apoptosis already 3 and 6h after acute DEN. Interestingly, LPC-specific TNFR1 deficiency strongly reduced the level of Caspase-8-dependent apoptosis 3h after acute DEN while at 6h Caspase-8-dependent death was only mildly affected suggesting the presence of an additional trigger for Caspase-8-dependent apoptosis. Since our analysis revealed also an induction in *Trail* gene expression levels it is likely that TRAIL is involved in mediating Caspase-8-dependent apoptosis 6h after DEN. However, it remains to be analyzed whether Caspase-9-dependent apoptosis is mediated by Caspase-8 signaling or by DNA-damage 6h after DEN. Strikingly, the level of DNA-damage was significantly reduced in RIPK1^{LPC-KO} but not in RIPK1^{LPC-KO} TNFR1^{LPC-KO} mice. Accordingly, additional LPC-specific TNFR1 ablation restored tumor growth and tumor numbers 34 weeks after DEN injection in RIPK1^{LPC-KO} TNFR1^{LPC-KO} mice. Together these results pointed to a crucial TNFR1-dependent role in triggering

cell death 3h after acute DEN resulting in clearance of DNA damaged cells, less tumor initiation and less HCC development.

In line with this, the loss of RIPK1 mildly reduced obesity-induced liver carcinogenesis which was reported to induce liver carcinogenesis in a TNFR1-dependent manner (Park et al. 2010). Presumably due to the clearance of DNA-damaged cells at 2 weeks of age, RIPK1^{LPC-KO} mice showed less tumor initiation after DEN injection. But at 4 weeks of age HFD feeding started and promoted a constant inflammatory basis with elevated TNF expression. Constant TNF production might cause constant hepatocyte death in RIPK1^{LPC-KO} mice. However, at the same time constant cell death might induce compensatory proliferation promoting tumorigenesis and, therefore, would explain the lower protective effect of RIPK1 deficiency on obesity-mediated DEN-induced tumorigenesis compared to the effect seen in DEN-injected NCD-fed mice (Figure 47).
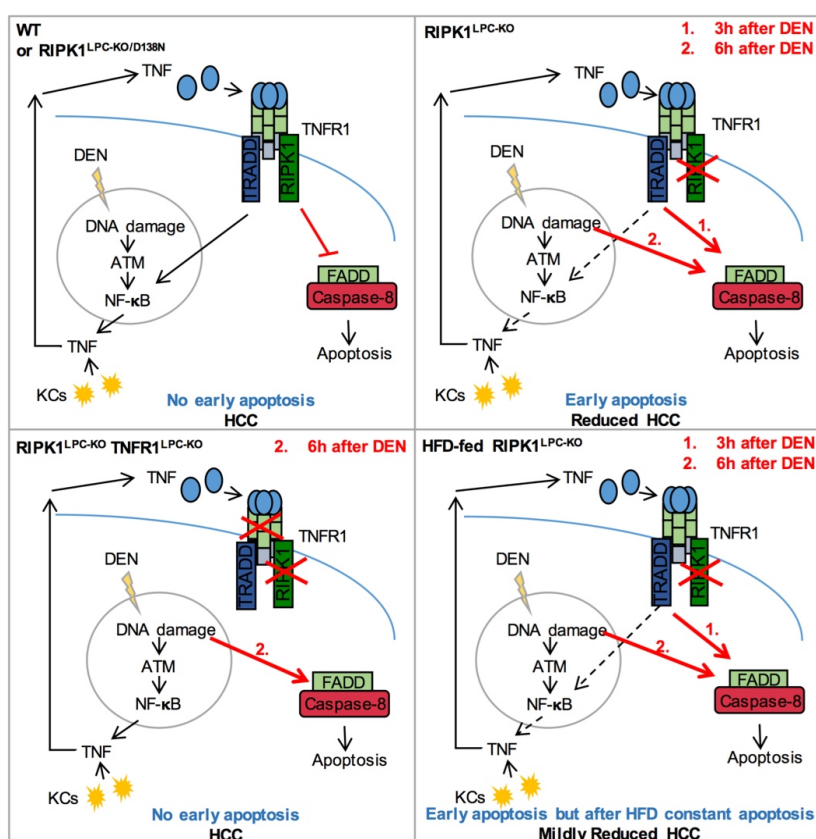
Figure 47. RIPK1 promotes DEN-induced HCC development by preventing early TNF-mediated apoptotic death

Metabolized DEN leads to DNA damage by alkylation that is recognized by ATM. ATM in turn induces NF-κB activation resulting in TNF expression. Subsequently TNF mediates TNFR1-dependent NF-κB activation or apoptosis. (A) In WT hepatocytes or in hepatocytes lacking the kinase activity of RIPK1 DEN triggers DEN/TNF-dependent NF-κB activation which blocks TNF- and DNA-damage-dependent apoptosis early after DEN injection resulting in DEN-mediated HCC development. (B) However, the absence of RIPK1 sensitizes hepatocytes 3h after acute DEN injection to TNFR1 induced TRADD-FADD-Caspase-8-dependent apoptosis and to DNA-damage-driven apoptosis 6h after DEN injection resulting in reduced HCC development. (C) Additional ablation of TNFR1 blocks hepatocyte death 3h after acute DEN injection and restores tumor formation in RIPK1^{LPC-KO} TNFR1^{LPC-KO} mice to similar extent as in their floxed

littermates. (D) Prior to HFD feeding RIPK1^{LPC-KO} mice, display early apoptosis as in (B) resulting in the reduction of DNA-damaged cells. Once fed with HFD, RIPK1-deficient hepatocytes expressed enhanced levels of TNF that could result in higher levels of TRADD-FADD-Caspase-8-dependent apoptosis inducing compensatory proliferation.

In previous reports, early extensive cell death is considered to increase cytokine-induced compensatory proliferation of hepatocytes which may have sustained DNA damage consequently inducing tumorigenesis (Koch et al. 2009; Maeda et al. 2005; Sakurai et al. 2008; Sakurai et al. 2006). Accordingly, hepatocyte-specific ablation of IKK2 resulted in increased HCC development showing increased hepatocyte apoptosis correlating with significantly increased mRNA levels of cellular proliferation markers including cyclin D1, hepatocyte growth factor (HGF) and proliferating cell nuclear antigen (PCNA) early on. Furthermore, IKK2$^{\Delta hep}$ mice displayed liver inflammation indicated by elevated IL-1α, IL-1β, TNF and IL-6 early after acute DEN injection (Maeda et al. 2005). Consistently, BID^{LPC-KO}, $Jnk1^{-/-}$ and $Puma^{-/-}$ mice revealed attenuated DEN-induced HCC development and consistently showed reduced hepatocyte death, cyclin D1 and PCNA mRNA expression levels and no inflammatory response (Sakurai et al. 2006; Yu et al. 2016; Qiu et al. 2011). Our analysis of hepatocyte proliferation in RIPK1^{LPC-KO} livers did not show increased proliferation indicated by similar Ki-67 staining early after DEN injection compared to $Ripk1^{FL/FL}$ mice although extensive apoptotic death was present early on. Moreover, inhibition of the kinase activity of RIPK1 resulted in reduced apoptotic death early after DEN injection and in similar tumor formation between RIPK1$^{LPC-KO/D138N}$ and $Ripk1^{FL/FL}$ mice. In contrast to partial hepatectomy or other models of severe acute liver injury (Martin, Theruvath and Neuhaus 2008), the overall number of apoptotic hepatocytes in the livers of DEN-injected RIPK1^{LPC-KO} is relatively small and it might not be sufficient to trigger compensatory proliferation. The divergence between RIPK1^{LPC-KO} and IKK2$^{\Delta hep}$ mice in response to DEN suggests a IKK2/ NF-κB-independent mechanism for RIPK1 in regulating DEN-induced HCC development but future studies are needed to unravel the mechanism of RIPK1 and IKK2 in regulating DEN-induced HCC development.

Our results implicated a key role of early apoptotic death in preventing HCC development regulated by RIPK1 scaffolding functions which seems to be contradictory to previous studies. As described above, in other models elevated levels of apoptosis correlated with increased HCC formation after DEN. However, the timepoint of apoptosis occurrence after acute DEN was reported to occur later then in our study. Wree *et al.* reported considerable TUNEL, Ki-67 and PCNA staining and increased cytokine expression levels in the liver of $Bid^{FL/FL}$ mice compared to Bid$^{\Delta hep}$ at 48h after acute DEN injection. Furthermore, Qiu et al. reported reduced apoptotic

levels in *Puma*^{-/-} mice 3-10 days after acute DEN injection. Moreover, Maeda et al. and Sakurai et al. showed elevated apoptosis in IKK2[Δhep] and *Jnk1*^{-/-} mice 24-48h after 25mg/kg BW DEN injection (Maeda et al. 2005; Sakurai et al. 2006). Taken only these studies into account, there are inconsistencies in term of DEN dosage and the timepoint of analysis. Importantly, cell death can also induce tumorigenesis by activating the inflammatory response as reported in a previous report (Maeda et al 2005). Unlike IKK2[Δhep] mice, RIPK1[LPC-KO] mice did not show an elevated inflammatory response early after acute DEN injection indicated by low *Il1b* gene expression levels and at 32- and 36-weeks of age judged by IHC analysis consistent with *Ripk1*[FL/FL] littermates. The strongest discrepancy between the previous studies compared to our study is the fact that after 5mg/kg injection of DEN, mutant but also WT mice died rapidly, which was not present in our study using 25mg/kg BW of DEN suggesting compound differences (Maeda et al. 2005; Sakurai et al. 2006). Taken all these discrepancies into account, it is difficult to compare the effects on DEN-induced HCC seen in their studies and in our study. Importantly, under our conditions early hepatocyte apoptosis reduced DEN-induced HCC formation independent of any effects on hepatocyte proliferation.

4.6. The role of RIPK1 in spontaneous HCC formation

Although NEMO and RIPK1 are both involved in TNF-induced complex-I signaling, it is still unclear why NEMO[LPC-KO] and RIPK1[LPC-KO] mice display distinct phenotypes as NEMO[LPC-KO] mice develop spontaneously HCC whereas RIPK1[LPC-KO] mice do not show spontaneous HCC formation but even delays tumorigenesis upon DEN treatment (Kondylis et al. 2015). NEMO[LPC-KO] mice show extensive hepatocyte apoptosis resulting in HCC formation while early hepatocyte apoptosis in RIPK1[LPC-KO] mice results in reduction of DEN-induced HCC. One major difference between spontaneous HCC and DEN-induced HCC is the occurrence of cell death. Unlike spontaneous HCC, a single injection of DEN resulted in induction of DNA-damage and cell death during a short and early period after injection while LPC-specific NEMO ablation induced sustained cell death and constant compensatory hepatocyte proliferation throughout their lives. Moreover, ablation of NEMO induced an extensive inflammatory response, increased cell death, compensatory proliferation and strong fibrosis (Kondylis et al. 2015). Extensive and chronic apoptosis as key factors for HCC development in NEMO[LPC-KO] mice was validated using NEMO[LPC-KO] FADD[LPC-KO] mice that displayed abrogated levels of apoptosis preventing HCC development (Ehlken et al. 2014). In contrast to LPC-specific deficiency of RIPK1, deficiency of its kinase activity alone strongly inhibited hepatocyte apoptosis, chronic liver disease and liver tumorigenesis in

NEMO[LPC-KO] mice suggesting that LPC-specific deficiency of NEMO predominantly result in RIPK1 kinase activity-dependent apoptosis. However, RIPK1 scaffolding function is needed to block TRADD-dependent complex IIa-mediated apoptosis. Accordingly, blocking key mediators of either complex IIa (TRADD) or complex IIb (RIPK1) dependent apoptosis was not sufficient in preventing HCC development but rather combined LPC-specific deficiency of NEMO, RIPK1 and TRADD (Kondylis et al. 2015).

Impaired or inhibited NF-κB activation is thought to sensitize hepatocytes to cell death, therefore, inhibited or attenuated NF-κB activation and increased hepatocyte death in NEMO[LPC-KO] and RIPK1[LPC-KO] mice supports the current model. However, surprisingly, p65/RelA[LPC-KO] mice or RelA/RelB/c-Rel[LPC-KO] mice do not phenocopy the liver pathology of NEMO[LPC-KO] mice suggesting independent functions of NEMO and NF-κB in mediating HCC development (Kondylis et al. 2015). Interestingly, combined LPC-specific deficiency of RelA and RIPK1, which independently do not show spontaneous HCC development, results in spontaneous HCC development similar to NEMO[LPC-KO] mice suggesting that NEMO or the IKK complex inhibits RIPK1 dependent extrinsic apoptosis independently of NF-κB activation (unpublished, *Van et al. 2017*). Significantly, as mentioned before combined LPC-specific ablation of RIPK1 and TRAF2 displayed multiple tumors at 52-weeks of age with increased apoptosis and proliferation consistent with TRAF2/IKK2[LPC-KO] mice (Schneider et al. 2017). The difference in the pathogenesis of these spontaneous hepatic phenotypes is indicative for NF-κB-independent functions of complex-I members. Interestingly, Dondelinger et al. reported that IKK-dependent phosphorylation of RIPK1 restrains RIPK1 in complex-I preventing RIPK1 kinase-dependent cell death independent of its function in NF-κB activation (Dondelinger et al. 2015). IKK1/2[LPC-KO] mice show similar liver damage as NEMO[LPC-KO] mice but on the contrary reveal a cholastatic phenotype (Luedde et al. 2008). Supporting the finding of Dondelinger et al., LPC-specific deficiency of RIPK1 prevented cholestasis and HCC development in IKK1/2[LPC-KO] mice (Koppe et al. 2016). Together these results suggest a combined role for NF-κB-dependent and -independent signaling in regulating tissue homeostasis and tumorigenesis. Future studies will help further understanding the discrepancies between NEMO, NF-κB and RIPK1 in HCC development.

4.7. RIPK1 in human cancer

Several studies revealed a potential role of RIPK1 in human cancer. Interestingly, Wang et al. reported that RIPK1 was overexpressed in 80% of tested human HCC

(172/210 patients) which correlated with worse prognosis (Wang et al. 2016). Furthermore, they identified a correlation between enhanced expression of RIPK1 and supressed cell apoptosis which promoted cell growth in HCC. Accordingly, knockdown of RIPK1 restored cell apoptosis resulting in growth arrest of HCC cells (Wang et al. 2016). Consistently, Liu et al. reported an upregulation in *RIPK1* expression in human melanoma via DNA copy-number gain and constitutive TNF-mediated ubiquitination. Mechanistically, RIPK1 was shown to promote cell proliferation in a NF-κB dependent manner (Liu et al. 2015) and through the activation of autophagy (Luan et al. 2015). In addition, RIPK1 was implicated in the promotion of breast cancer metastasis through NF-κB activation (Bist et al. 2011) and the survival of pancreatic cancer cells against TRAIL-induced apoptosis (Wang et al. 2007). Together with our results, these studies support a crucial role of RIPK1 in promoting tumorigenesis and metastasis by preventing apoptotic death in mouse and most importantly in human indicating that RIPK1 might be a promising target for cancer therapy. However, contrary to these studies, Schneider et al. emphasized that loss of RIPK1 in human HCC correlated with worse prognosis and increasing evidence pointed towards downregulation of RIPK1 in many cancer cell lines including metastatic HNSCC (Schneider et al. 2017). These data were supported by the finding of Koppe et al. which found RIPK1 downregulation in a subgroup of HCC patients with undefined characteristics suggesting an anti-carcinogenic role of RIPK1 independent of its kinase activity in the liver (Koppe et al. 2016).

Given these contradictory data, future studies are essential to help understanding the pro- and anti-carcinogenic function of RIPK1 in humans to provide more evidence for specific RIPK1 targeting for cancer therapy.

4.8. Concluding Remarks

Collectively, the data presented in this work demonstrated a pro-survival kinase-independent scaffolding-function of RIPK1 in regulating liver cell survival, LPS-induced acute liver damage and DEN-induced HCC development. Thus, our data demonstrated a pivotal pro-survival role of RIPK1 highlighting RIPK1 on the one hand as a potent protector from ALF but on the other hand as a potent driver of HCC development by preventing massive hepatocyte apoptosis. Our data on LPS-induced liver injury are in agreement with recently published studies while our data on DEN-induced HCC revealed a novel crucial role of early short-term apoptosis in reducing HCC development by reducing the amount of DNA-damaged cells. Future studies will help to further unravel the molecular mechanism of RIPK1 in regulating TNF-mediated cell

survival and cell death allowing the design of specific therapeutic strategies for ALF and HCC by considering RIPK1 as a specific target.

5. References

Abdel-Misih, S. R., and M. Bloomston. 2010. 'Liver anatomy', *Surg Clin North Am*, 90: 643-53.

Akira, S., K. Takeda, and T. Kaisho. 2001. 'Toll-like receptors: critical proteins linking innate and acquired immunity', *Nat Immunol*, 2: 675-80.

Akira, S., S. Uematsu, and O. Takeuchi. 2006. 'Pathogen recognition and innate immunity', *Cell*, 124: 783-801.

Alvarez-Diaz, S., C. P. Dillon, N. Lalaoui, M. C. Tanzer, D. A. Rodriguez, A. Lin, M. Lebois, R. Hakem, E. C. Josefsson, L. A. O'Reilly, J. Silke, W. S. Alexander, D. R. Green, and A. Strasser. 2016. 'The Pseudokinase MLKL and the Kinase RIPK3 Have Distinct Roles in Autoimmune Disease Caused by Loss of Death-Receptor-Induced Apoptosis', *Immunity*, 45: 513-26.

Bantel, H., and K. Schulze-Osthoff. 2012. 'Mechanisms of cell death in acute liver failure', *Front Physiol*, 3: 79.

Baud, V., and M. Karin. 2001. 'Signal transduction by tumor necrosis factor and its relatives', *Trends Cell Biol*, 11: 372-7.

Bautista, A. P., N. Skrepnik, M. R. Niesman, and G. J. Bagby. 1994. 'Elimination of macrophages by liposome-encapsulated dichloromethylene diphosphonate suppresses the endotoxin-induced priming of Kupffer cells', *J Leukoc Biol*, 55: 321-7.

Bianchini, F., R. Kaaks, and H. Vainio. 2002. 'Overweight, obesity, and cancer risk', *Lancet Oncol*, 3: 565-74.

Bieging, K. T., S. S. Mello, and L. D. Attardi. 2014. 'Unravelling mechanisms of p53-mediated tumour suppression', *Nat Rev Cancer*, 14: 359-70.

Bisgaard, H. C., and S. S. Thorgeirsson. 1996. 'Hepatic regeneration. The role of regeneration in pathogenesis of chronic liver diseases', *Clin Lab Med*, 16: 325-39.

Biton, S., and A. Ashkenazi. 2011. 'NEMO and RIP1 control cell fate in response to extensive DNA damage via TNF-alpha feedforward signaling', *Cell*, 145: 92-103.

Boess, F., M. Bopst, R. Althaus, S. Polsky, S. D. Cohen, H. P. Eugster, and U. A. Boelsterli. 1998. 'Acetaminophen hepatotoxicity in tumor necrosis factor/lymphotoxin-alpha gene knockout mice', *Hepatology*, 27: 1021-9.

Bonnet, M. C., D. Preukschat, P. S. Welz, G. van Loo, M. A. Ermolaeva, W. Bloch, I. Haase, and M. Pasparakis. 2011. 'The adaptor protein FADD protects epidermal keratinocytes from necroptosis in vivo and prevents skin inflammation', *Immunity*, 35: 572-82.

Bosanac, I., I. E. Wertz, B. Pan, C. Yu, S. Kusam, C. Lam, L. Phu, Q. Phung, B. Maurer, D. Arnott, D. S. Kirkpatrick, V. M. Dixit, and S. G. Hymowitz. 2010. 'Ubiquitin binding to A20 ZnF4 is required for modulation of NF-kappaB signaling', *Mol Cell*, 40: 548-57.

Bradham, C. A., J. Plumpe, M. P. Manns, D. A. Brenner, and C. Trautwein. 1998. 'Mechanisms of hepatic toxicity. I. TNF-induced liver injury', *Am J Physiol*, 275: G387-92.

Brockhaus, M., H. J. Schoenfeld, E. J. Schlaeger, W. Hunziker, W. Lesslauer, and H. Loetscher. 1990. 'Identification of two types of tumor necrosis factor receptors on human cell lines by monoclonal antibodies', *Proc Natl Acad Sci U S A*, 87: 3127-31.

Cai, Z., S. Jitkaew, J. Zhao, H. C. Chiang, S. Choksi, J. Liu, Y. Ward, L. G. Wu, and Z. G. Liu. 2014. 'Plasma membrane translocation of trimerized MLKL protein is required for TNF-induced necroptosis', *Nat Cell Biol*, 16: 55-65.

Calle, E. E., and R. Kaaks. 2004. 'Overweight, obesity and cancer: epidemiological evidence and proposed mechanisms', *Nat Rev Cancer*, 4: 579-91.

Chan, F. K., N. F. Luz, and K. Moriwaki. 2015. 'Programmed necrosis in the cross talk of cell death and inflammation', *Annu Rev Immunol*, 33: 79-106.

Chen, L.F. and W.C. Greene. 2004. 'Shaping the nuclear action of NF-kappaB', *Nat Rev Mol Cell Biol,* 5(5):392-401.

Chen, W., Z. Zhou, L. Li, C. Q. Zhong, X. Zheng, X. Wu, Y. Zhang, H. Ma, D. Huang, W. Li, Z. Xia, and J. Han. 2013. 'Diverse sequence determinants control human and mouse receptor interacting protein 3 (RIP3) and mixed lineage kinase domain-like (MLKL) interaction in necroptotic signaling', *J Biol Chem*, 288: 16247-61.

Cho, Y. S., S. Challa, D. Moquin, R. Genga, T. D. Ray, M. Guildford, and F. K. Chan. 2009. 'Phosphorylation-driven assembly of the RIP1-RIP3 complex regulates programmed necrosis and virus-induced inflammation', *Cell*, 137: 1112-23.

Cusson-Hermance, N., S. Khurana, T. H. Lee, K. A. Fitzgerald, and M. A. Kelliher. 2005. 'Rip1 mediates the Trif-dependent toll-like receptor 3- and 4-induced NF-{kappa}B activation but does not contribute to interferon regulatory factor 3 activation', *J Biol Chem*, 280: 36560-6.

Dannappel, M., K. Vlantis, S. Kumari, A. Polykratis, C. Kim, L. Wachsmuth, C. Eftychi, J. Lin, T. Corona, N. Hermance, M. Zelic, P. Kirsch, M. Basic, A. Bleich, M. Kelliher, and M. Pasparakis. 2014. 'RIPK1 maintains epithelial homeostasis by inhibiting apoptosis and necroptosis', *Nature*, 513: 90-4.

Dara, L., H. Johnson, J. Suda, S. Win, W. Gaarde, D. Han, and N. Kaplowitz. 2015. 'Receptor interacting protein kinase 1 mediates murine acetaminophen toxicity independent of the necrosome and not through necroptosis', *Hepatology*, 62: 1847-57.

Dara, L.,Z.X., Liu, N., Kaplowitz. 2016.'Questions and controversies: The role of necroptosis in liver disease', *Cell death Discov,*5;2:16089.

de Almagro, M. C., T. Goncharov, A. Izrael-Tomasevic, S. Duttler, M. Kist, E. Varfolomeev, X. Wu, W. P. Lee, J. Murray, J. D. Webster, K. Yu, D. S. Kirkpatrick, K. Newton, and D. Vucic. 2017. 'Coordinated ubiquitination and phosphorylation of RIP1 regulates necroptotic cell death', *Cell Death Differ*, 24: 26-37.

de Almagro, M. C., T. Goncharov, K. Newton, and D. Vucic. 2015. 'Cellular IAP proteins and LUBAC differentially regulate necrosome-associated RIP1 ubiquitination', *Cell Death Dis*, 6: e1800.

Degterev, A., J. Hitomi, M. Germscheid, I. L. Ch'en, O. Korkina, X. Teng, D. Abbott, G. D. Cuny, C. Yuan, G. Wagner, S. M. Hedrick, S. A. Gerber, A. Lugovskoy, and J. Yuan. 2008. 'Identification of RIP1 kinase as a specific cellular target of necrostatins', *Nat Chem Biol*, 4: 313-21.

Degterev, A., Z. Huang, M. Boyce, Y. Li, P. Jagtap, N. Mizushima, G. D. Cuny, T. J. Mitchison, M. A. Moskowitz, and J. Yuan. 2005. 'Chemical inhibitor of nonapoptotic cell death with therapeutic potential for ischemic brain injury', *Nat Chem Biol*, 1: 112-9.

Dembic, Z., H. Loetscher, U. Gubler, Y. C. Pan, H. W. Lahm, R. Gentz, M. Brockhaus, and W. Lesslauer. 1990. 'Two human TNF receptors have similar extracellular, but distinct intracellular, domain sequences', *Cytokine*, 2: 231-7.

Depuydt, B., G. van Loo, P. Vandenabeele, and W. Declercq. 2005. 'Induction of apoptosis by TNF receptor 2 in a T-cell hybridoma is FADD dependent and blocked by Caspase-8 inhibitors', *J Cell Sci*, 118: 497-504.

Dietschy, J. M., S. D. Turley, and D. K. Spady. 1993. 'Role of liver in the maintenance of cholesterol and low density lipoprotein homeostasis in different animal species, including humans', *J Lipid Res*, 34: 1637-59.

Dillon, C. P., A. Oberst, R. Weinlich, L. J. Janke, T. B. Kang, T. Ben-Moshe, T. W. Mak, D. Wallach, and D. R. Green. 2012. 'Survival function of the FADD-CASPASE-8-cFLIP(L) complex', *Cell Rep*, 1: 401-7.

Dillon, C. P., R. Weinlich, D. A. Rodriguez, J. G. Cripps, G. Quarato, P. Gurung, K. C. Verbist, T. L. Brewer, F. Llambi, Y. N. Gong, L. J. Janke, M. A. Kelliher, T. D. Kanneganti, and D. R. Green. 2014. 'RIPK1 blocks early postnatal lethality mediated by Caspase-8 and RIPK3', *Cell*, 157: 1189-202.

Dondelinger, Y., M. A. Aguileta, V. Goossens, C. Dubuisson, S. Grootjans, E. Dejardin, P. Vandenabeele, and M. J. Bertrand. 2013. 'RIPK3 contributes to TNFR1-mediated RIPK1 kinase-dependent apoptosis in conditions of cIAP1/2 depletion or TAK1 kinase inhibition', *Cell Death Differ*, 20: 1381-92.

Dondelinger, Y., W. Declercq, S. Montessuit, R. Roelandt, A. Goncalves, I. Bruggeman, P. Hulpiau, K. Weber, C. A. Sehon, R. W. Marquis, J. Bertin, P. J. Gough, S. Savvides, J. C. Martinou, M. J. Bertrand, and P. Vandenabeele. 2014. 'MLKL compromises plasma membrane integrity by binding to phosphatidylinositol phosphates', *Cell Rep*, 7: 971-81.

Dondelinger, Y., S. Jouan-Lanhouet, T. Divert, E. Theatre, J. Bertin, P. J. Gough, P. Giansanti, A. J. Heck, E. Dejardin, P. Vandenabeele, and M. J. Bertrand. 2015. 'NF-kappaB-Independent Role of IKKalpha/IKKbeta in Preventing RIPK1 Kinase-Dependent Apoptotic and Necroptotic Cell Death during TNF Signaling', *Mol Cell*, 60: 63-76.

Draber, P., S. Kupka, M. Reichert, H. Draberova, E. Lafont, D. de Miguel, L. Spilgies, S. Surinova, L. Taraborrelli, T. Hartwig, E. Rieser, L. Martino, K. Rittinger, and H. Walczak. 2015. 'LUBAC-Recruited CYLD and A20 Regulate Gene Activation and Cell Death by Exerting Opposing Effects on Linear Ubiquitin in Signaling Complexes', *Cell Rep*, 13: 2258-72.

Dynek, J. N., T. Goncharov, E. C. Dueber, A. V. Fedorova, A. Izrael-Tomasevic, L. Phu, E. Helgason, W. J. Fairbrother, K. Deshayes, D. S. Kirkpatrick, and D. Vucic. 2010. 'c-IAP1 and UbcH5 promote K11-linked polyubiquitination of RIP1 in TNF signalling', *EMBO J*, 29: 4198-209.

Ea, C. K., L. Deng, Z. P. Xia, G. Pineda, and Z. J. Chen. 2006. 'Activation of IKK by TNFalpha requires site-specific ubiquitination of RIP1 and polyubiquitin binding by NEMO', *Mol Cell*, 22: 245-57.

Ehlken, H., S. Krishna-Subramanian, L. Ochoa-Callejero, V. Kondylis, N. E. Nadi, B. K. Straub, P. Schirmacher, H. Walczak, G. Kollias, and M. Pasparakis. 2014. 'Death receptor-independent FADD signalling triggers hepatitis and hepatocellular carcinoma in mice with liver parenchymal cell-specific NEMO knockout', *Cell Death Differ*, 21: 1721-32.

El-Serag, H. B. 2011. 'Hepatocellular carcinoma', *N Engl J Med*, 365: 1118-27.

Fausto, N. 2004. 'Liver regeneration and repair: hepatocytes, progenitor cells, and stem cells', *Hepatology*, 39: 1477-87.

Feoktistova, M., P. Geserick, B. Kellert, D. P. Dimitrova, C. Langlais, M. Hupe, K. Cain, M. MacFarlane, G. Hacker, and M. Leverkus. 2011. 'cIAPs block Ripoptosome formation, a RIP1/Caspase-8 containing intracellular cell death complex differentially regulated by cFLIP isoforms', *Mol Cell*, 43: 449-63.

Festjens, N., T. Vanden Berghe, S. Cornelis, and P. Vandenabeele. 2007. 'RIP1, a kinase on the crossroads of a cell's decision to live or die', *Cell Death Differ*, 14: 400-10.

Freudenberg, M. A., D. Keppler, and C. Galanos. 1986. 'Requirement for lipopolysaccharide-responsive macrophages in galactosamine-induced sensitization to endotoxin', *Infect Immun*, 51: 891-5.

Fu, T. M., Y. Li, A. Lu, Z. Li, P. R. Vajjhala, A. C. Cruz, D. B. Srivastava, F. DiMaio, P. A. Penczek, R. M. Siegel, K. J. Stacey, E. H. Egelman, and H. Wu. 2016. 'Cryo-EM Structure of Caspase-8 Tandem DED Filament Reveals Assembly and Regulation Mechanisms of the Death-Inducing Signaling Complex', *Mol Cell*, 64: 236-50.

Ghosh, S., and M. S. Hayden. 2008. 'New regulators of NF-kappaB in inflammation', *Nat Rev Immunol*, 8: 837-48.

Green, D. R., T. Ferguson, L. Zitvogel, and G. Kroemer. 2009. 'Immunogenic and tolerogenic cell death', *Nat Rev Immunol*, 9: 353-63.

Gross, A., X. M. Yin, K. Wang, M. C. Wei, J. Jockel, C. Milliman, H. Erdjument-Bromage, P. Tempst, and S. J. Korsmeyer. 1999. 'Caspase cleaved BID targets mitochondria and is required for cytochrome c release, while BCL-XL

prevents this release but not tumor necrosis factor-R1/Fas death', *J Biol Chem*, 274: 1156-63.

Gruber, S., B. K. Straub, P. J. Ackermann, C. M. Wunderlich, J. Mauer, J. M. Seeger, H. Buning, L. Heukamp, H. Kashkar, P. Schirmacher, J. C. Bruning, and F. T. Wunderlich. 2013. 'Obesity promotes liver carcinogenesis via Mcl-1 stabilization independent of IL-6Ralpha signaling', *Cell Rep*, 4: 669-80.

Guicciardi, M. E., H. Malhi, J. L. Mott, and G. J. Gores. 2013. 'Apoptosis and necrosis in the liver', *Compr Physiol*, 3: 977-1010.

Gunther, C., G. W. He, A. E. Kremer, J. M. Murphy, E. J. Petrie, K. Amann, P. Vandenabeele, A. Linkermann, C. Poremba, U. Schleicher, C. Dewitz, S. Krautwald, M. F. Neurath, C. Becker, and S. Wirtz. 2016. 'The pseudokinase MLKL mediates programmed hepatocellular necrosis independently of RIPK3 during hepatitis', *J Clin Invest*, 126: 4346-60.

Hakem, R., A. Hakem, G. S. Duncan, J. T. Henderson, M. Woo, M. S. Soengas, A. Elia, J. L. de la Pompa, D. Kagi, W. Khoo, J. Potter, R. Yoshida, S. A. Kaufman, S. W. Lowe, J. M. Penninger, and T. W. Mak. 1998. 'Differential requirement for Caspase 9 in apoptotic pathways in vivo', *Cell*, 94: 339-52.

Haas, T. L., C. H. Emmerich, B. Gerlach, A. C. Schmukle, S. M. Cordier, E. Rieser, R. Feltham, J. Vince, U. Warnken, T. Wenger, R. Koschny, D. Komander, J. Silke, and H. Walczak. 2009. 'Recruitment of the linear ubiquitin chain assembly complex stabilizes the TNF-R1 signaling complex and is required for TNF-mediated gene induction', *Mol Cell*, 36: 831-44.

Hayden, M. S., and S. Ghosh. 2008. 'Shared principles in NF-kappaB signaling', *Cell*, 132: 344-62.

———. 2012. 'NF-kappaB, the first quarter-century: remarkable progress and outstanding questions', *Genes Dev*, 26: 203-34.

Hayden, M. S., and S. Ghosh. 2014. 'Regulation of NF-kappaB by TNF family cytokines', *Semin Immunol*, 26: 253-66.

He, S., Y. Liang, F. Shao, and X. Wang. 2011. 'Toll-like receptors activate programmed necrosis in macrophages through a receptor-interacting kinase-3-mediated pathway', *Proc Natl Acad Sci U S A*, 108: 20054-9.

He, S., L. Wang, L. Miao, T. Wang, F. Du, L. Zhao, and X. Wang. 2009. 'Receptor interacting protein kinase-3 determines cellular necrotic response to TNF-alpha', *Cell*, 137: 1100-11.

Hill-Baskin, A. E., M. M. Markiewski, D. A. Buchner, H. Shao, D. DeSantis, G. Hsiao, S. Subramaniam, N. A. Berger, C. Croniger, J. D. Lambris, and J. H. Nadeau. 2009. 'Diet-induced hepatocellular carcinoma in genetically predisposed mice', *Hum Mol Genet*, 18: 2975-88.

Hinson, J. A., N. R. Pumford, and D. W. Roberts. 1995. 'Mechanisms of acetaminophen toxicity: immunochemical detection of drug-protein adducts', *Drug Metab Rev*, 27: 73-92.

Hoshino, K., O. Takeuchi, T. Kawai, H. Sanjo, T. Ogawa, Y. Takeda, K. Takeda, and S. Akira. 1999. 'Cutting edge: Toll-like receptor 4 (TLR4)-deficient mice are hyporesponsive to lipopolysaccharide: evidence for TLR4 as the Lps gene product', *J Immunol*, 162: 3749-52.

Hsu, H., J. Huang, H. B. Shu, V. Baichwal, and D. V. Goeddel. 1996. 'TNF-dependent recruitment of the protein kinase RIP to the TNF receptor-1 signaling complex', *Immunity*, 4: 387-96.

Hsu, H., H. B. Shu, M. G. Pan, and D. V. Goeddel. 1996. 'TRADD-TRAF2 and TRADD-FADD interactions define two distinct TNF receptor 1 signal transduction pathways', *Cell*, 84: 299-308.

Hsu, H., J. Xiong, and D. V. Goeddel. 1995. 'The TNF receptor 1-associated protein TRADD signals cell death and NF-kappa B activation', *Cell*, 81: 495-504.

Hughes, M. A., I. R. Powley, R. Jukes-Jones, S. Horn, M. Feoktistova, L. Fairall, J. W. Schwabe, M. Leverkus, K. Cain, and M. MacFarlane. 2016. 'Co-operative and

Hierarchical Binding of c-FLIP and Caspase-8: A Unified Model Defines How c-FLIP Isoforms Differentially Control Cell Fate', *Mol Cell*, 61: 834-49.

Hur, G. M., J. Lewis, Q. Yang, Y. Lin, H. Nakano, S. Nedospasov, and Z. G. Liu. 2003. 'The death domain kinase RIP has an essential role in DNA damage-induced NF-kappa B activation', *Genes Dev*, 17: 873-82.

Ikeda, F., Y. L. Deribe, S. S. Skanland, B. Stieglitz, C. Grabbe, M. Franz-Wachtel, S. J. van Wijk, P. Goswami, V. Nagy, J. Terzic, F. Tokunaga, A. Androulidaki, T. Nakagawa, M. Pasparakis, K. Iwai, J. P. Sundberg, L. Schaefer, K. Rittinger, B. Macek, and I. Dikic. 2011. 'SHARPIN forms a linear ubiquitin ligase complex regulating NF-kappaB activity and apoptosis', *Nature*, 471: 637-41.

Janeway, C. A., Jr., and R. Medzhitov. 2002. 'Innate immune recognition', *Annu Rev Immunol*, 20: 197-216.

Jaworski, M., A. Buchmann, P. Bauer, O. Riess, and M. Schwarz. 2005. 'B-raf and Ha-ras mutations in chemically induced mouse liver tumors', *Oncogene*, 24: 1290-5.

Kaiser, W. J., and M. K. Offermann. 2005. 'Apoptosis induced by the toll-like receptor adaptor TRIF is dependent on its receptor interacting protein homotypic interaction motif', *J Immunol*, 174: 4942-52.

Kaiser, W. J., J. W. Upton, A. B. Long, D. Livingston-Rosanoff, L. P. Daley-Bauer, R. Hakem, T. Caspary, and E. S. Mocarski. 2011. 'RIP3 mediates the embryonic lethality of Caspase-8-deficient mice', *Nature*, 471: 368-72.

Kanayama, A., R. B. Seth, L. Sun, C. K. Ea, M. Hong, A. Shaito, Y. H. Chiu, L. Deng, and Z. J. Chen. 2004. 'TAB2 and TAB3 activate the NF-kappaB pathway through binding to polyubiquitin chains', *Mol Cell*, 15: 535-48.

Kawai, T., and S. Akira. 2010. 'The role of pattern-recognition receptors in innate immunity: update on Toll-like receptors', *Nat Immunol*, 11: 373-84.

Kelliher, M. A., S. Grimm, Y. Ishida, F. Kuo, B. Z. Stanger, and P. Leder. 1998. 'The death domain kinase RIP mediates the TNF-induced NF-kappaB signal', *Immunity*, 8: 297-303.

Keppler, D. O., J. Pausch, and K. Decker. 1974. 'Selective uridine triphosphate deficiency induced by D-galactosamine in liver and reversed by pyrimidine nucleotide precursors. Effect on ribonucleic acid synthesis', *J Biol Chem*, 249: 211-6.

Kerr, J. F., A. H. Wyllie, and A. R. Currie. 1972. 'Apoptosis: a basic biological phenomenon with wide-ranging implications in tissue kinetics', *Br J Cancer*, 26: 239-57.

Kim, E. Y., and H. S. Teh. 2001. 'TNF type 2 receptor (p75) lowers the threshold of T cell activation', *J Immunol*, 167: 6812-20.

Kmiec, Z. 2001. 'Cooperation of liver cells in health and disease', *Adv Anat Embryol Cell Biol*, 161: III-XIII, 1-151.

Koch, K. S., S. Maeda, G. He, M. Karin, and H. L. Leffert. 2009. 'Targeted deletion of hepatocyte Ikkbeta confers growth advantages', *Biochem Biophys Res Commun*, 380: 349-54.

Kondylis, V., A. Polykratis, H. Ehlken, L. Ochoa-Callejero, B. K. Straub, S. Krishna-Subramanian, T. M. Van, H. M. Curth, N. Heise, F. Weih, U. Klein, P. Schirmacher, M. Kelliher, and M. Pasparakis. 2015. 'NEMO Prevents Steatohepatitis and Hepatocellular Carcinoma by Inhibiting RIPK1 Kinase Activity-Mediated Hepatocyte Apoptosis', *Cancer Cell*, 28: 582-98.

Kono, H., and K. L. Rock. 2008. 'How dying cells alert the immune system to danger', *Nat Rev Immunol*, 8: 279-89.

Koppe, C., P. Verheugd, J. Gautheron, F. Reisinger, K. Kreggenwinkel, C. Roderburg, L. Quagliata, L. Terracciano, N. Gassler, R. H. Tolba, Y. Boege, A. Weber, M. Karin, M. Luedde, U. P. Neumann, R. Weiskirchen, F. Tacke, M. Vucur, C. Trautwein, B. Luscher, C. Preisinger, M. Heikenwalder, and T. Luedde. 2016. 'IkappaB kinasealpha/beta control biliary homeostasis and

hepatocarcinogenesis in mice by phosphorylating the cell-death mediator receptor-interacting protein kinase 1', *Hepatology*, 64: 1217-31.

Krysko, D. V., T. Vanden Berghe, K. D'Herde, and P. Vandenabeele. 2008. 'Apoptosis and necrosis: detection, discrimination and phagocytosis', *Methods*, 44: 205-21.

Kuida, K., T. S. Zheng, S. Na, C. Kuan, D. Yang, H. Karasuyama, P. Rakic, and R. A. Flavell. 1996. 'Decreased apoptosis in the brain and premature lethality in CPP32-deficient mice', *Nature*, 384: 368-72.

Lamkanfi, M., and V. M. Dixit. 2010. 'Manipulation of host cell death pathways during microbial infections', *Cell Host Microbe*, 8: 44-54.

Lee, T. H., J. Shank, N. Cusson, and M. A. Kelliher. 2004. 'The kinase activity of Rip1 is not required for tumor necrosis factor-alpha-induced IkappaB kinase or p38 MAP kinase activation or for the ubiquitination of Rip1 by Traf2', *J Biol Chem*, 279: 33185-91.

Legarda-Addison, D., H. Hase, M. A. O'Donnell, and A. T. Ting. 2009. 'NEMO/IKKgamma regulates an early NF-kappaB-independent cell-death checkpoint during TNF signaling', *Cell Death Differ*, 16: 1279-88.

Legler, D. F., O. Micheau, M. A. Doucey, J. Tschopp, and C. Bron. 2003. 'Recruitment of TNF receptor 1 to lipid rafts is essential for TNFalpha-mediated NF-kappaB activation', *Immunity*, 18: 655-64.

Li, H., M. Kobayashi, M. Blonska, Y. You, and X. Lin. 2006. 'Ubiquitination of RIP is required for tumor necrosis factor alpha-induced NF-kappaB activation', *J Biol Chem*, 281: 13636-43.

Li, H., H. Zhu, C. J. Xu, and J. Yuan. 1998. 'Cleavage of BID by Caspase 8 mediates the mitochondrial damage in the Fas pathway of apoptosis', *Cell*, 94: 491-501.

Li, J., T. McQuade, A. B. Siemer, J. Napetschnig, K. Moriwaki, Y. S. Hsiao, E. Damko, D. Moquin, T. Walz, A. McDermott, F. K. Chan, and H. Wu. 2012. 'The RIP1/RIP3 necrosome forms a functional amyloid signaling complex required for programmed necrosis', *Cell*, 150: 339-50.

Li, N., S. Banin, H. Ouyang, G. C. Li, G. Courtois, Y. Shiloh, M. Karin, and G. Rotman. 2001. 'ATM is required for IkappaB kinase (IKKk) activation in response to DNA double strand breaks', *J Biol Chem*, 276: 8898-903.

Lin, J., S. Kumari, C. Kim, T. M. Van, L. Wachsmuth, A. Polykratis, and M. Pasparakis. 2016. 'RIPK1 counteracts ZBP1-mediated necroptosis to inhibit inflammation', *Nature*, 540: 124-28.

Lin, Y., A. Devin, Y. Rodriguez, and Z. G. Liu. 1999. 'Cleavage of the death domain kinase RIP by Caspase-8 prompts TNF-induced apoptosis', *Genes Dev*, 13: 2514-26.

Liu, L. M., J. X. Zhang, J. Luo, H. X. Guo, H. Deng, J. Y. Chen, and S. L. Sun. 2008. 'A role of cell apoptosis in lipopolysaccharide (LPS)-induced nonlethal liver injury in D-galactosamine (D-GalN)-sensitized rats', *Dig Dis Sci*, 53: 1316-24.

Liu, X.Y., F., Lai, X. G. Yan, C.C. Jiang, S. T. Guo, C. Y. Wang, A. Croft, H.Y. Tseng, J.
    S. Wilmott, R. A. Scolyer, L. Jin, X. D. Zhang. 2015.'RIP1 Kinase Is an Oncogenic
    Driver in Melanoma', *Cancer Res*,75(8): 1736-1748.

Locksley, R. M., N. Killeen, and M. J. Lenardo. 2001. 'The TNF and TNF receptor superfamilies: integrating mammalian biology', *Cell*, 104: 487-501.

Luan, Q., L. Jin, C. C. Jiang, K. H. Tay, F. Lai, X. Y. Liu, Y. L. Liu, S. T. Guo, C. Y. Li, X. G. Yan, H. Y. Tseng, and X. D. Zhang. 2015. 'RIPK1 regulates survival of human melanoma cells upon endoplasmic reticulum stress through autophagy', *Autophagy*, 11: 975-94.

Luedde, T., J. Heinrichsdorff, R. de Lorenzi, R. De Vos, T. Roskams, and M. Pasparakis. 2008. 'IKK1 and IKK2 cooperate to maintain bile duct integrity in the liver', *Proc Natl Acad Sci U S A*, 105: 9733-8.

Luedde, T., N. Kaplowitz, and R. F. Schwabe. 2014. 'Cell death and cell death responses in liver disease: mechanisms and clinical relevance', *Gastroenterology*, 147: 765-83 e4.

Luo, X., I. Budihardjo, H. Zou, C. Slaughter, and X. Wang. 1998. 'Bid, a Bcl2 interacting protein, mediates cytochrome c release from mitochondria in response to activation of cell surface death receptors', *Cell*, 94: 481-90.

Lukas, J., C. Lukas, and J. Bartek. 2011. 'More than just a focus: The chromatin response to DNA damage and its role in genome integrity maintenance', *Nat Cell Biol*, 13: 1161-9.

Luster, M. I., D. R. Germolec, T. Yoshida, F. Kayama, and M. Thompson. 1994. 'Endotoxin-induced cytokine gene expression and excretion in the liver', *Hepatology*, 19: 480-8.

Maeda, S., H. Kamata, J. L. Luo, H. Leffert, and M. Karin. 2005. 'IKKbeta couples hepatocyte death to cytokine-driven compensatory proliferation that promotes chemical hepatocarcinogenesis', *Cell*, 121: 977-90.

Mahoney, D. J., H. H. Cheung, R. L. Mrad, S. Plenchette, C. Simard, E. Enwere, V. Arora, T. W. Mak, E. C. Lacasse, J. Waring, and R. G. Korneluk. 2008. 'Both cIAP1 and cIAP2 regulate TNFalpha-mediated NF-kappaB activation', *Proc Natl Acad Sci U S A*, 105: 11778-83.

Martich, G. D., A. J. Boujoukos, and A. F. Suffredini. 1993. 'Response of man to endotoxin', *Immunobiology*, 187: 403-16.

Martins, P. N., T. P. Theruvath, and P. Neuhaus. 2008. 'Rodent models of partial hepatectomies', *Liver Int*, 28: 3-11.

Mc Guire, C., T. Volckaert, U. Wolke, M. Sze, R. de Rycke, A. Waisman, M. Prinz, R. Beyaert, M. Pasparakis, and G. van Loo. 2010. 'Oligodendrocyte-specific FADD deletion protects mice from autoimmune-mediated demyelination', *J Immunol*, 185: 7646-53.

McQuade, T., Y. Cho, and F. K. Chan. 2013. 'Positive and negative phosphorylation regulates RIP1- and RIP3-induced programmed necrosis', *Biochem J*, 456: 409-15.

Medema, J. P., C. Scaffidi, F. C. Kischkel, A. Shevchenko, M. Mann, P. H. Krammer, and M. E. Peter. 1997. 'FLICE is activated by association with the CD95 death-inducing signaling complex (DISC)', *EMBO J*, 16: 2794-804.

Medema, J. P., R. E. Toes, C. Scaffidi, T. S. Zheng, R. A. Flavell, C. J. Melief, M. E. Peter, R. Offringa, and P. H. Krammer. 1997. 'Cleavage of FLICE (Caspase-8) by granzyme B during cytotoxic T lymphocyte-induced apoptosis', *Eur J Immunol*, 27: 3492-8.

Mercurio, F., H. Zhu, B. W. Murray, A. Shevchenko, B. L. Bennett, J. Li, D. B. Young, M. Barbosa, M. Mann, A. Manning, and A. Rao. 1997. 'IKK-1 and IKK-2: cytokine-activated IkappaB kinases essential for NF-kappaB activation', *Science*, 278: 860-6.

Mevissen, T. E., M. K. Hospenthal, P. P. Geurink, P. R. Elliott, M. Akutsu, N. Arnaudo, R. Ekkebus, Y. Kulathu, T. Wauer, F. El Oualid, S. M. Freund, H. Ovaa, and D. Komander. 2013. 'OTU deubiquitinases reveal mechanisms of linkage specificity and enable ubiquitin chain restriction analysis', *Cell*, 154: 169-84.

Micheau, O., and J. Tschopp. 2003. 'Induction of TNF receptor I-mediated apoptosis via two sequential signaling complexes', *Cell*, 114: 181-90.

Mitchell, J. R., D. J. Jollow, W. Z. Potter, D. C. Davis, J. R. Gillette, and B. B. Brodie. 1973. 'Acetaminophen-induced hepatic necrosis. I. Role of drug metabolism', *J Pha*

Mitchell, S., J. Vargas, and A. Hoffmann. 2016. 'Signaling via the NFkappaB system', *Wiley Interdiscip Rev Syst Biol Med*, 8: 227-41.

Mizuhara, H., E. O'Neill, N. Seki, T. Ogawa, C. Kusunoki, K. Otsuka, S. Satoh, M. Niwa, H. Senoh, and H. Fujiwara. 1994. 'T cell activation-associated hepatic injury: mediation by tumor necrosis factors and protection by interleukin 6', *J Exp Med*, 179: 1529-37.

Mitchell, S., J. Vargas, and A. Hoffmann. 2016. 'Signaling via the NFkappaB system', *Wiley Interdiscip Rev Syst Biol Med*, 8: 227-41.

Mollah, S., I. E. Wertz, Q. Phung, D. Arnott, V. M. Dixit, and J. R. Lill. 2007. 'Targeted mass spectrometric strategy for global mapping of ubiquitination on proteins', *Rapid Commun Mass Spectrom*, 21: 3357-64.

Moulin, M., H. Anderton, A. K. Voss, T. Thomas, W. W. Wong, A. Bankovacki, R. Feltham, D. Chau, W. D. Cook, J. Silke, and D. L. Vaux. 2012. 'IAPs limit activation of RIP kinases by TNF receptor 1 during development', *EMBO J*, 31: 1679-91.

Moquin, D. M., T. McQuade, and F. K. Chan. 2013. 'CYLD deubiquitinates RIP1 in the TNFalpha-induced necrosome to facilitate kinase activation and programmed necrosis', *PLoS One*, 8: e76841.

Morikawa, A., T. Sugiyama, Y. Kato, N. Koide, G. Z. Jiang, K. Takahashi, Y. Tamada, and T. Yokochi. 1996. 'Apoptotic cell death in the response of D-galactosamine-sensitized mice to lipopolysaccharide as an experimental endotoxic shock model', *Infect Immun*, 64: 734-8.

Murphy, J. M., P. E. Czabotar, J. M. Hildebrand, I. S. Lucet, J. G. Zhang, S. Alvarez-Diaz, R. Lewis, N. Lalaoui, D. Metcalf, A. I. Webb, S. N. Young, L. N. Varghese, G. M. Tannahill, E. C. Hatchell, I. J. Majewski, T. Okamoto, R. C. Dobson, D. J. Hilton, J. J. Babon, N. A. Nicola, A. Strasser, J. Silke, and W. S. Alexander. 2013. 'The pseudokinase MLKL mediates necroptosis via a molecular switch mechanism', *Immunity*, 39: 443-53.

Naugler, W. E., T. Sakurai, S. Kim, S. Maeda, K. Kim, A. M. Elsharkawy, and M. Karin. 2007. 'Gender disparity in liver cancer due to sex differences in MyD88-dependent IL-6 production', *Science*, 317: 121-4.

Nelson, S. D. 1990. 'Molecular mechanisms of the hepatotoxicity caused by acetaminophen', *Semin Liver Dis*, 10: 267-78.

Newton, K., D. L. Dugger, K. E. Wickliffe, N. Kapoor, M. C. de Almagro, D. Vucic, L. Komuves, R. E. Ferrando, D. M. French, J. Webster, M. Roose-Girma, S. Warming, and V. M. Dixit. 2014. 'Activity of protein kinase RIPK3 determines whether cells die by necroptosis or apoptosis', *Science*, 343: 1357-60.

Newton, K., K. E. Wickliffe, A. Maltzman, D. L. Dugger, A. Strasser, V. C. Pham, J. R. Lill, M. Roose-Girma, S. Warming, M. Solon, H. Ngu, J. D. Webster, and V. M. Dixit. 2016. 'RIPK1 inhibits ZBP1-driven necroptosis during development', *Nature*, 540: 129-33.

Ni, H. M., M. R. McGill, X. Chao, B. L. Woolbright, H. Jaeschke, and W. X. Ding. 2016. 'Caspase Inhibition Prevents Tumor Necrosis Factor-alpha-Induced Apoptosis and Promotes Necrotic Cell Death in Mouse Hepatocytes in Vivo and in Vitro', *Am J Pathol*, 186: 2623-36.

O'Donnell, M. A., D. Legarda-Addison, P. Skountzos, W. C. Yeh, and A. T. Ting. 2007. 'Ubiquitination of RIP1 regulates an NF-kappaB-independent cell-death switch in TNF signaling', *Curr Biol*, 17: 418-24.

Onizawa, M., S. Oshima, U. Schulze-Topphoff, J. A. Oses-Prieto, T. Lu, R. Tavares, T. Prodhomme, B. Duong, M. I. Whang, R. Advincula, A. Agelidis, J. Barrera, H. Wu, A. Burlingame, B. A. Malynn, S. S. Zamvil, and A. Ma. 2015. 'The ubiquitin-modifying enzyme A20 restricts ubiquitination of the kinase RIPK3 and protects cells from necroptosis', *Nat Immunol*, 16: 618-27.

Park, E. J., J. H. Lee, G. Y. Yu, G. He, S. R. Ali, R. G. Holzer, C. H. Osterreicher, H. Takahashi, and M. Karin. 2010. 'Dietary and genetic obesity promote liver inflammation and tumorigenesis by enhancing IL-6 and TNF expression', *Cell*, 140: 197-208.

Park, S. M., J. B. Yoon, and T. H. Lee. 2004. 'Receptor interacting protein is ubiquitinated by cellular inhibitor of apoptosis proteins (c-IAP1 and c-IAP2) in vitro', *FEBS Lett*, 566: 151-6.

Pasparakis, M., and P. Vandenabeele. 2015. 'Necroptosis and its role in inflammation', *Nature*, 517: 311-20.

Pearson, G., F. Robinson, T. Beers Gibson, B. E. Xu, M. Karandikar, K. Berman, and M. H. Cobb. 2001. 'Mitogen-activated protein (MAP) kinase pathways: regulation and physiological functions', *Endocr Rev*, 22: 153-83.

Piret, B., S. Schoonbroodt, and J. Piette. 1999. 'The ATM protein is required for sustained activation of NF-kappaB following DNA damage', *Oncogene*, 18: 2261-71.

Poltorak, A., X. He, I. Smirnova, M. Y. Liu, C. Van Huffel, X. Du, D. Birdwell, E. Alejos, M. Silva, C. Galanos, M. Freudenberg, P. Ricciardi-Castagnoli, B. Layton, and B. Beutler. 1998. 'Defective LPS signaling in C3H/HeJ and C57BL/10ScCr mice: mutations in Tlr4 gene', *Science*, 282: 2085-8.

Polykratis, A., N. Hermance, M. Zelic, J. Roderick, C. Kim, T. M. Van, T. H. Lee, F. K. Chan, M. Pasparakis, and M. A. Kelliher. 2014. 'Cutting edge: RIPK1 Kinase inactive mice are viable and protected from TNF-induced necroptosis in vivo', *J Immunol*, 193: 1539-43.

Poon, I. K., C. D. Lucas, A. G. Rossi, and K. S. Ravichandran. 2014. 'Apoptotic cell clearance: basic biology and therapeutic potential', *Nat Rev Immunol*, 14: 166-80.

Pop, C., A. Oberst, M. Drag, B. J. Van Raam, S. J. Riedl, D. R. Green, and G. S. Salvesen. 2011. 'FLIP(L) induces Caspase 8 activity in the absence of interdomain Caspase 8 cleavage and alters substrate specificity', *Biochem J*, 433: 447-57.

Pobezinskaya, Y. L., Y. S. Kim, S. Choksi, M. J. Morgan, T. Li, C. Liu, and Z. Liu. 2008. 'The function of TRADD in signaling through tumor necrosis factor receptor 1 and TRIF-dependent Toll-like receptors', *Nat Immunol*, 9: 1047-54.

Qiu, W., X. Wang, B. Leibowitz, W. Yang, L. Zhang, and J. Yu. 2011. 'PUMA-mediated apoptosis drives chemical hepatocarcinogenesis in mice', *Hepatology*, 54: 1249-58.

Qureshi, S. T., L. Lariviere, G. Leveque, S. Clermont, K. J. Moore, P. Gros, and D. Malo. 1999. 'Endotoxin-tolerant mice have mutations in Toll-like receptor 4 (Tlr4)', *J Exp Med*, 189: 615-25.

Racanelli, V., and B. Rehermann. 2006. 'The liver as an immunological organ', *Hepatology*, 43: S54-62.

Rahighi, S., F. Ikeda, M. Kawasaki, M. Akutsu, N. Suzuki, R. Kato, T. Kensche, T. Uejima, S. Bloor, D. Komander, F. Randow, S. Wakatsuki, and I. Dikic. 2009. 'Specific recognition of linear ubiquitin chains by NEMO is important for NF-kappaB activation', *Cell*, 136: 1098-109.

Rajewsky, K., H. Gu, R. Kuhn, U. A. Betz, W. Muller, J. Roes, and F. Schwenk. 1996. 'Conditional gene targeting', *J Clin Invest*, 98: 600-3.

Rajput, A., A. Kovalenko, K. Bogdanov, S. H. Yang, T. B. Kang, J. C. Kim, J. Du, and D. Wallach. 2011. 'RIG-I RNA helicase activation of IRF3 transcription factor is negatively regulated by Caspase-8-mediated cleavage of the RIP1 protein', *Immunity*, 34: 340-51.

Rao, K. V., and S. D. Vesselinovitch. 1973. 'Age- and sex-associated diethylnitrosamine dealkylation activity of the mouse liver and hepatocarcinogenesis', *Cancer Res*, 33: 1625-7.

Rebsamen, M., L. X. Heinz, E. Meylan, M. C. Michallet, K. Schroder, K. Hofmann, J. Vazquez, C. A. Benedict, and J. Tschopp. 2009. 'DAI/ZBP1 recruits RIP1 and RIP3 through RIP homotypic interaction motifs to activate NF-kappaB', *EMBO Rep*, 10: 916-22.

Ritorto, M. S., R. Ewan, A. B. Perez-Oliva, A. Knebel, S. J. Buhrlage, M. Wightman, S. M. Kelly, N. T. Wood, S. Virdee, N. S. Gray, N. A. Morrice, D. R. Alessi, and M. Trost. 2014. 'Screening of DUB activity and specificity by MALDI-TOF mass spectrometry', *Nat Commun*, 5: 4763.

Rothwarf, D. M., and M. Karin. 1999. 'The NF-kappa B activation pathway: a paradigm in information transfer from membrane to nucleus', *Sci STKE*, 1999: RE1.

Sabio, G., and R. J. Davis. 2014. 'TNF and MAP kinase signalling pathways', *Semin Immunol*, 26: 237-45.

Sakurai, H., H. Miyoshi, J. Mizukami, and T. Sugita. 2000. 'Phosphorylation-dependent activation of TAK1 mitogen-activated protein kinase kinase kinase by TAB1', *FEBS Lett*, 474: 141-5.

Sakurai, T., S. Maeda, L. Chang, and M. Karin. 2006. 'Loss of hepatic NF-kappa B activity enhances chemical hepatocarcinogenesis through sustained c-Jun N-terminal kinase 1 activation', *Proc Natl Acad Sci U S A*, 103: 10544-51.

Sakurai, T., G. He, A. Matsuzawa, G. Y. Yu, S. Maeda, G. Hardiman, and M. Karin. 2008. 'Hepatocyte necrosis induced by oxidative stress and IL-1 alpha release mediate carcinogen-induced compensatory proliferation and liver tumorigenesis', *Cancer Cell*, 14: 156-65.

Sasaki, Y., E. Derudder, E. Hobeika, R. Pelanda, M. Reth, K. Rajewsky, and M. Schmidt-Supprian. 2006. 'Canonical NF-kappaB activity, dispensable for B cell development, replaces BAFF-receptor signals and promotes B cell proliferation upon activation', *Immunity*, 24: 729-39.

Sato, Y., E. Goto, Y. Shibata, Y. Kubota, A. Yamagata, S. Goto-Ito, K. Kubota, J. Inoue, M. Takekawa, F. Tokunaga, and S. Fukai. 2015. 'Structures of CYLD USP with Met1- or Lys63-linked diubiquitin reveal mechanisms for dual specificity', *Nat Struct Mol Biol*, 22: 222-9.

Sauer, B., and N. Henderson. 1988. 'Site-specific DNA recombination in mammalian cells by the Cre recombinase of bacteriophage P1', *Proc Natl Acad Sci U S A*, 85: 5166-70.

Schall, T. J., M. Lewis, K. J. Koller, A. Lee, G. C. Rice, G. H. Wong, T. Gatanaga, G. A. Granger, R. Lentz, H. Raab, and et al. 1990. 'Molecular cloning and expression of a receptor for human tumor necrosis factor', *Cell*, 61: 361-70.

Sen, R., and D. Baltimore. 1986a. 'Inducibility of kappa immunoglobulin enhancer-binding protein Nf-kappa B by a posttranslational mechanism', *Cell*, 47: 921-8.

———. 1986b. 'Multiple nuclear factors interact with the immunoglobulin enhancer sequences', *Cell*, 46: 705-16.

Senftleben, U., Y. Cao, G. Xiao, F. R. Greten, G. Krahn, G. Bonizzi, Y. Chen, Y. Hu, A. Fong, S. C. Sun, and M. Karin. 2001. 'Activation by IKKalpha of a second, evolutionary conserved, NF-kappa B signaling pathway', *Science*, 293: 1495-9.

Shariff, M. I., I. J. Cox, A. I. Gomaa, S. A. Khan, W. Gedroyc, and S. D. Taylor-Robinson. 2009. 'Hepatocellular carcinoma: current trends in worldwide epidemiology, risk factors, diagnosis and therapeutics', *Expert Rev Gastroenterol Hepatol*, 3: 353-67.

Shu, H. B., M. Takeuchi, and D. V. Goeddel. 1996. 'The tumor necrosis factor receptor 2 signal transducers TRAF2 and c-IAP1 are components of the tumor necrosis factor receptor 1 signaling complex', *Proc Natl Acad Sci U S A*, 93: 13973-8.

Silke, J., and E. L. Hartland. 2013. 'Masters, marionettes and modulators: intersection of pathogen virulence factors and mammalian death receptor signaling', *Curr Opin Immunol*, 25: 436-40.

Stanger, B. Z., P. Leder, T. H. Lee, E. Kim, and B. Seed. 1995. 'RIP: a novel protein containing a death domain that interacts with Fas/APO-1 (CD95) in yeast and causes cell death', *Cell*, 81: 513-23.

Su, L., B. Quade, H. Wang, L. Sun, X. Wang, and J. Rizo. 2014. 'A plug release mechanism for membrane permeation by MLKL', *Structure*, 22: 1489-500.

Sun, L., H. Wang, Z. Wang, S. He, S. Chen, D. Liao, L. Wang, J. Yan, W. Liu, X. Lei, and X. Wang. 2012. 'Mixed lineage kinase domain-like protein mediates necrosis signaling downstream of RIP3 kinase', *Cell*, 148: 213-27.

Sun, X., J. Yin, M. A. Starovasnik, W. J. Fairbrother, and V. M. Dixit. 2002. 'Identification of a novel homotypic interaction motif required for the phosphorylation of receptor-interacting protein (RIP) by RIP3', *J Biol Chem*, 277: 9505-11.

Takahashi, N., L. Vereecke, M. J. Bertrand, L. Duprez, S. B. Berger, T. Divert, A. Goncalves, M. Sze, B. Gilbert, S. Kourula, V. Goossens, S. Lefebvre, C. Gunther, C. Becker, J. Bertin, P. J. Gough, W. Declercq, G. van Loo, and P. Vandenabeele. 2014. 'RIPK1 ensures intestinal homeostasis by protecting the epithelium against apoptosis', *Nature*, 513: 95-9.

Takiuchi, T., T. Nakagawa, H. Tamiya, H. Fujita, Y. Sasaki, Y. Saeki, H. Takeda, T. Sawasaki, A. Buchberger, T. Kimura, and K. Iwai. 2014. 'Suppression of LUBAC-mediated linear ubiquitination by a specific interaction between LUBAC and the deubiquitinases CYLD and OTULIN', *Genes Cells*, 19: 254-72.

Teoh, N., P. Pyakurel, Y. Y. Dan, K. Swisshelm, J. Hou, C. Mitchell, N. Fausto, Y. Gu, and G. Farrell. 2010. 'Induction of p53 renders ATM-deficient mice refractory to hepatocarcinogenesis', *Gastroenterology*, 138: 1155-65 e1-2.

Thomas, C. 1961. '[On the morphology of diethylnitrosamine induced liver changes and tumors in rats]', *Z Krebsforsch*, 64: 224-33.

Tiegs, G., J. Hentschel, and A. Wendel. 1992. 'A T cell-dependent experimental liver injury in mice inducible by concanavalin A', *J Clin Invest*, 90: 196-203.

Togano, T., M. Nakashima, M. Watanabe, K. Umezawa, T. Watanabe, M. Higashihara, and R. Horie. 2012. 'Synergistic effect of 5-azacytidine and NF-kappaB inhibitor DHMEQ on apoptosis induction in myeloid leukemia cells', *Oncol Res*, 20: 571-7.

Tokunaga, F., T. Nakagawa, M. Nakahara, Y. Saeki, M. Taniguchi, S. Sakata, K. Tanaka, H. Nakano, and K. Iwai. 2011. 'SHARPIN is a component of the NF-kappaB-activating linear ubiquitin chain assembly complex', *Nature*, 471: 633-6.

Tokunaga, F., H. Nishimasu, R. Ishitani, E. Goto, T. Noguchi, K. Mio, K. Kamei, A. Ma, K. Iwai, and O. Nureki. 2012. 'Specific recognition of linear polyubiquitin by A20 zinc finger 7 is involved in NF-kappaB regulation', *EMBO J*, 31: 3856-70.

Tokunaga, F., S. Sakata, Y. Saeki, Y. Satomi, T. Kirisako, K. Kamei, T. Nakagawa, M. Kato, S. Murata, S. Yamaoka, M. Yamamoto, S. Akira, T. Takao, K. Tanaka, and K. Iwai. 2009. 'Involvement of linear polyubiquitylation of NEMO in NF-kappaB activation', *Nat Cell Biol*, 11: 123-32.

Tolba, R., T. Kraus, C. Liedtke, M. Schwarz, and R. Weiskirchen. 2015. 'Diethylnitrosamine (DEN)-induced carcinogenic liver injury in mice', *Lab Anim*, 49: 59-69.

Treisman, R. 1996. 'Regulation of transcription by MAP kinase cascades', *Curr Opin Cell Biol*, 8: 205-15.

Trompouki, E., E. Hatzivassiliou, T. Tsichritzis, H. Farmer, A. Ashworth, and G. Mosialos. 2003. 'CYLD is a deubiquitinating enzyme that negatively regulates NF-kappaB activation by TNFR family members', *Nature*, 424: 793-6.

Uysal, K. T., S. M. Wiesbrock, M. W. Marino, and G. S. Hotamisligil. 1997. 'Protection from obesity-induced insulin resistance in mice lacking TNF-alpha function', *Nature*, 389: 610-4.

Vail, M. E., R. H. Pierce, and N. Fausto. 2001. 'Bcl-2 delays and alters hepatic carcinogenesis induced by transforming growth factor alpha', *Cancer Res*, 61: 594-601.

van den Berghe, G. 1991. 'The role of the liver in metabolic homeostasis: implications for inborn errors of metabolism', *J Inherit Metab Dis*, 14: 407-20.

Van Dien, M., K. Takahashi, M. M. Mu, N. Koide, T. Sugiyama, I. Mori, T. Yoshida, and T. Yokochi. 2001. 'Protective effect of wogonin on endotoxin-induced lethal shock in D-galactosamine-sensitized mice', *Microbiol Immunol*, 45: 751-6.

Vanden Berghe, T., N. Vanlangenakker, E. Parthoens, W. Deckers, M. Devos, N. Festjens, C. J. Guerin, U. T. Brunk, W. Declercq, and P. Vandenabeele. 2010. 'Necroptosis, necrosis and secondary necrosis converge on similar cellular disintegration features', *Cell Death Differ*, 17: 922-30.

Van Hauwermeiren, F., M. Armaka, N. Karagianni, K. Kranidioti, R. E. Vandenbroucke, S. Loges, M. Van Roy, J. Staelens, L. Puimege, A. Palagani, W. V. Berghe, P. Victoratos, P. Carmeliet, C. Libert, and G. Kollias. 2013. 'Safe TNF-based

antitumor therapy following p55TNFR reduction in intestinal epithelium', *J Clin Invest*, 123: 2590-603.

Varfolomeev, E., T. Goncharov, A. V. Fedorova, J. N. Dynek, K. Zobel, K. Deshayes, W. J. Fairbrother, and D. Vucic. 2008. 'c-IAP1 and c-IAP2 are critical mediators of tumor necrosis factor alpha (TNFalpha)-induced NF-kappaB activation', *J Biol Chem*, 283: 24295-9.

Varfolomeev, E. E., M. Schuchmann, V. Luria, N. Chiannilkulchai, J. S. Beckmann, I. L. Mett, D. Rebrikov, V. M. Brodianski, O. C. Kemper, O. Kollet, T. Lapidot, D. Soffer, T. Sobe, K. B. Avraham, T. Goncharov, H. Holtmann, P. Lonai, and D. Wallach. 1998. 'Targeted disruption of the mouse Caspase 8 gene ablates cell death induction by the TNF receptors, Fas/Apo1, and DR3 and is lethal prenatally', *Immunity*, 9: 267-76.

Varfolomeev, E., and D. Vucic. 2016. 'Intracellular regulation of TNF activity in health and disease', *Cytokine*.

Verhelst, K., I. Carpentier, M. Kreike, L. Meloni, L. Verstrepen, T. Kensche, I. Dikic, and R. Beyaert. 2012. 'A20 inhibits LUBAC-mediated NF-kappaB activation by binding linear polyubiquitin chains via its zinc finger 7', *EMBO J*, 31: 3845-55.

Vivarelli, M. S., D. McDonald, M. Miller, N. Cusson, M. Kelliher, and R. S. Geha. 2004. 'RIP links TLR4 to Akt and is essential for cell survival in response to LPS stimulation', *J Exp Med*, 200: 399-404.

Vlantis, K., A. Wullaert, A. Polykratis, V. Kondylis, M. Dannappel, R. Schwarzer, P. Welz, T. Corona, H. Walczak, F. Weih, U. Klein, M. Kelliher, and M. Pasparakis. 2016. 'NEMO Prevents RIP Kinase 1-Mediated Epithelial Cell Death and Chronic Intestinal Inflammation by NF-kappaB-Dependent and -Independent Functions', *Immunity*, 44: 553-67.

Wachter, T., M. Sprick, D. Hausmann, A. Kerstan, K. McPherson, G. Stassi, E. B. Brocker, H. Walczak, and M. Leverkus. 2004. 'cFLIPL inhibits tumor necrosis factor-related apoptosis-inducing ligand-mediated NF-kappaB activation at the death-inducing signaling complex in human keratinocytes', *J Biol Chem*, 279: 52824-34.

Wajant, H. 2003. 'Death receptors', *Essays Biochem*, 39: 53-71.

Wang, C., L. Deng, M. Hong, G. R. Akkaraju, J. Inoue, and Z. J. Chen. 2001. 'TAK1 is a ubiquitin-dependent kinase of MKK and IKK', *Nature*, 412: 346-51.

Wang, C., B. Yao, M. Xu, and X. Zheng. 2016. 'RIP1 upregulation promoted tumor progression by activating AKT/Bcl-2/BAX signaling and predicted poor postsurgical prognosis in HCC', *Tumour Biol*, 37: 15305-13.

Wang, H., L. Sun, L. Su, J. Rizo, L. Liu, L. F. Wang, F. S. Wang, and X. Wang. 2014. 'Mixed lineage kinase domain-like protein MLKL causes necrotic membrane disruption upon phosphorylation by RIP3', *Mol Cell*, 54: 133-46.

Wang, L., F. Du, and X. Wang. 2008. 'TNF-alpha induces two distinct Caspase-8 activation pathways', *Cell*, 133: 693-703.

Wang, P., J. Zhang, A. Bellail, W. Jiang, J. Hugh, N. M. Kneteman, and C. Hao. 2007. 'Inhibition of RIP and c-FLIP enhances TRAIL-induced apoptosis in pancreatic cancer cells', *Cell Signal*, 19: 2237-46.

Weber, S. N., A. Bohner, D. H. Dapito, R. F. Schwabe, and F. Lammert. 2016. 'TLR4 Deficiency Protects against Hepatic Fibrosis and Diethylnitrosamine-Induced Pre-Carcinogenic Liver Injury in Fibrotic Liver', *PLoS One*, 11: e0158819.

Welz, P. S., A. Wullaert, K. Vlantis, V. Kondylis, V. Fernandez-Majada, M. Ermolaeva, P. Kirsch, A. Sterner-Kock, G. van Loo, and M. Pasparakis. 2011. 'FADD prevents RIP3-mediated epithelial cell necrosis and chronic intestinal inflammation', *Nature*, 477: 330-4.

Wertz, I. E., K. M. O'Rourke, H. Zhou, M. Eby, L. Aravind, S. Seshagiri, P. Wu, C. Wiesmann, R. Baker, D. L. Boone, A. Ma, E. V. Koonin, and V. M. Dixit. 2004. 'De-ubiquitination and ubiquitin ligase domains of A20 downregulate NF-kappaB signalling', *Nature*, 430: 694-9.

Wilson, N. S., V. Dixit, and A. Ashkenazi. 2009. 'Death receptor signal transducers: nodes of coordination in immune signaling networks', *Nat Immunol*, 10: 348-55.

Woronicz, J. D., X. Gao, Z. Cao, M. Rothe, and D. V. Goeddel. 1997. 'IkappaB kinase-beta: NF-kappaB activation and complex formation with IkappaB kinase-alpha and NIK', *Science*, 278: 866-9.

Wright, A., W. W. Reiley, M. Chang, W. Jin, A. J. Lee, M. Zhang, and S. C. Sun. 2007. 'Regulation of early wave of germ cell apoptosis and spermatogenesis by deubiquitinating enzyme CYLD', *Dev Cell*, 13: 705-16.

Wroblewski, R., M. Armaka, V. Kondylis, M. Pasparakis, H. Walczak, H.W. Mittruecker, C. Schramm, A.W. Lohse, G. Kollias, H. Ehlken. 2016.'Opposing role of tumor necrosis factor receptor 1 signaling in T-cell-mediated hepatitis and bacterial infection in mice', *Hepatology*, 10.1002/hep.28551.

Wu, C. J., D. B. Conze, T. Li, S. M. Srinivasula, and J. D. Ashwell. 2006. 'Sensing of Lys 63-linked polyubiquitination by NEMO is a key event in NF-kappaB activation [corrected]', *Nat Cell Biol*, 8: 398-406.

Wullaert, A., G. van Loo, K. Heyninck, and R. Beyaert. 2007. 'Hepatic tumor necrosis factor signaling and nuclear factor-kappaB: effects on liver homeostasis and beyond', *Endocr Rev*, 28: 365-86.

Xie, T., W. Peng, C. Yan, J. Wu, X. Gong, and Y. Shi. 2013. 'Structural insights into RIP3-mediated necroptotic signaling', *Cell Rep*, 5: 70-8.

Xiong, Q., K. Hase, Y. Tezuka, T. Namba, and S. Kadota. 1999. 'Acteoside inhibits apoptosis in D-galactosamine and lipopolysaccharide-induced liver injury', *Life Sci*, 65: 421-30.

Xu, M., B. Skaug, W. Zeng, and Z. J. Chen. 2009. 'A ubiquitin replacement strategy in human cells reveals distinct mechanisms of IKK activation by TNFalpha and IL-1beta', *Mol Cell*, 36: 302-14.

Yang, Y., F. Xia, N. Hermance, A. Mabb, S. Simonson, S. Morrissey, P. Gandhi, M. Munson, S. Miyamoto, and M. A. Kelliher. 2011. 'A cytosolic ATM/NEMO/RIP1 complex recruits TAK1 to mediate the NF-kappaB and p38 mitogen-activated protein kinase (MAPK)/MAPK-activated protein 2 responses to DNA damage', *Mol Cell Biol*, 31: 2774-86.

Yu, C., S. Yan, B. Khambu, X. Chen, Z. Dong, J. Luo, G. K. Michalopoulos, S. Wu, and X. M. Yin. 2016. 'Gene Expression Analysis Indicates Divergent Mechanisms in DEN-Induced Carcinogenesis in Wild Type and Bid-Deficient Livers', *PLoS One*, 11: e0155211.

Zhang, D., J. Lin, and J. Han. 2010. 'Receptor-interacting protein (RIP) kinase family', *Cell Mol Immunol*, 7: 243-9.

Zhang, D. W., J. Shao, J. Lin, N. Zhang, B. J. Lu, S. C. Lin, M. Q. Dong, and J. Han. 2009. 'RIP3, an energy metabolism regulator that switches TNF-induced cell death from apoptosis to necrosis', *Science*, 325: 332-6.

Zhang, Y. F., W. He, C. Zhang, X. J. Liu, Y. Lu, H. Wang, Z. H. Zhang, X. Chen, and D. X. Xu. 2014. 'Role of receptor interacting protein (RIP)1 on apoptosis-inducing factor-mediated necroptosis during acetaminophen-evoked acute liver failure in mice', *Toxicol Lett*, 225: 445-53.

Zhang, Y., S. S. Su, S. Zhao, Z. Yang, C. Q. Zhong, X. Chen, Q. Cai, Z. H. Yang, D. Huang, R. Wu, and J. Han. 2017. 'RIP1 autophosphorylation is promoted by mitochondrial ROS and is essential for RIP3 recruitment into necrosome', *Nat Commun*, 8: 14329.

Zhao, J., S. Jitkaew, Z. Cai, S. Choksi, Q. Li, J. Luo, and Z. G. Liu. 2012. 'Mixed lineage kinase domain-like is a key receptor interacting protein 3 downstream component of TNF-induced necrosis', *Proc Natl Acad Sci U S A*, 109: 5322-7.

Zheng, L., G. Fisher, R. E. Miller, J. Peschon, D. H. Lynch, and M. J. Lenardo. 1995. 'Induction of apoptosis in mature T cells by tumour necrosis factor', *Nature*, 377: 348-51.

Zhou, W., and J. Yuan. 2014. 'Necroptosis in health and diseases', *Semin Cell Dev Biol*, 35: 14-23.

Zilberman-Rudenko, J., L. M. Shawver, A. W. Wessel, Y. Luo, M. Pelletier, W. L. Tsai, Y. Lee, S. Vonortas, L. Cheng, J. D. Ashwell, J. S. Orange, R. M. Siegel, and E. P. Hanson. 2016. 'Recruitment of A20 by the C-terminal domain of NEMO suppresses NF-kappaB activation and autoinflammatory disease', *Proc Natl Acad Sci U S A*, 113: 1612-7.

6. Acknowledgement

7. Erklärung zur Dissertation

Ich versichere, dass ich die von mir vorgelegte Dissertation selbstständig angefertigt, die benutzten Quellen und Hilfsmittel vollständig angegeben und die Stellen der Arbeit-einschließlich Tabellen, Karten und Abbildungen-, die anderen Werken im Wortlaut oder dem Sinn nach entnommen sind, in jedem Einzelfall als Entlehnung kenntlich gemacht habe; dass diese Dissertation noch keiner anderen Fakultät oder Universität zur Prüfung vorgelegen hat; dass sie-abgesehen von unten angegebenen Teilpublikationen- noch nicht veröffentlich worden ist sowie, dass ich eine solche Veröffentlichung vor Abschluss des Promotionsverfahrens nicht vornehmen werde.

Die Bestimmungen dieser Promotionsordnung sind mir bekannt. Die von mir vorgelegte Dissertation ist von Prof. Dr. Manolis Pasparakis betreut worden.

23. Juni 2017   Trieu My Van

Teilpublikation

Teile dieser Doktorarbeit wurden in folgender Publikation veröffentlicht:

Van TM, Polykratis A, Straub BK, Kondylis V, Papadopoulou N, Pasparakis M, Kinase-independent functions of RIPK1 regulate hepatocyte survival and liver carcinogenesis. J Clin Invest. 2017 Jun 19. pii: 92508. doi: 10.1172/JCI92508.

RESEARCH ARTICLE

Kinase-independent functions of RIPK1 regulate hepatocyte survival and liver carcinogenesis

Trieu-My Van,[1,2,3] Apostolos Polykratis,[1,2,3] Beate Katharina Straub,[4] Vangelis Kondylis,[1,2,3] Nikoletta Papadopoulou,[5] and Manolis Pasparakis[1,2,3]

[1]Institute for Genetics, [2]Cologne Excellence Cluster on Cellular Stress Responses in Aging-Associated Diseases (CECAD), [3]Center for Molecular Medicine (CMMC), University of Cologne, Cologne, Germany. [4]Institute of Pathology, University of Mainz, Mainz, Germany. [5]Institute for Medical Microbiology, Immunology and Hygiene, Cologne, Germany.

The mechanisms that regulate cell death and inflammation play an important role in liver disease and cancer. Receptor-interacting protein kinase 1 (RIPK1) induces apoptosis and necroptosis via kinase-dependent mechanisms and exhibits kinase-independent prosurvival and proinflammatory functions. Here, we have used genetic mouse models to study the role of RIPK1 in liver homeostasis, injury, and cancer. While ablating either RIPK1 or RelA in liver parenchymal cells (LPCs) did not cause spontaneous liver pathology, mice with combined deficiency of RIPK1 and RelA in LPCs showed increased hepatocyte apoptosis and developed spontaneous chronic liver disease and cancer that were independent of TNF receptor 1 (TNFR1) signaling. In contrast, mice with LPC-specific knockout of *Ripk1* showed reduced diethylnitrosamine-induced (DEN-induced) liver tumorigenesis that correlated with increased DEN-induced hepatocyte apoptosis. Lack of RIPK1 kinase activity did not inhibit DEN-induced liver tumor formation, showing that kinase-independent functions of RIPK1 promote DEN-induced hepatocarcinogenesis. Moreover, mice lacking both RIPK1 and TNFR1 in LPCs displayed normal tumor formation in response to DEN, demonstrating that RIPK1 deficiency decreases DEN-induced liver tumor formation in a TNFR1-dependent manner. Therefore, these findings indicate that RIPK1 cooperates with NF-κB signaling to prevent TNFR1-independent hepatocyte apoptosis and the development of chronic liver disease and cancer, but acts downstream of TNFR1 signaling to promote DEN-induced liver tumorigenesis.

Introduction

Liver injury in response to immune deregulation and/or infection can result in acute liver failure or chronic liver disease. Chronic hepatocyte death coupled with compensatory hepatocyte proliferation greatly increases the risk of tumorigenesis. Indeed, hepatocellular carcinoma (HCC), the most frequent primary liver cancer, usually develops in the context of chronic liver injury and inflammation caused by hepatitis B virus (HBV) or HCV infections, alcoholic and nonalcoholic steatohepatitis, and aflatoxin-mediated toxicity (1). HCC is one of the most frequent and difficult to treat types of cancer, constituting the third most common cause of cancer-related death worldwide (1, 2).

Death receptors activate distinct signaling pathways controlling inflammation and cell death and are implicated in liver disease and cancer (3, 4). Receptor-interacting protein kinase 1 (RIPK1) is a key regulator of TNF receptor 1 (TNFR1) signaling (5). The kinase activity of RIPK1 triggers cell death by activating either caspase-8–mediated apoptosis or RIPK3-MLKL–dependent (where MLKL indicates mixed lineage kinase domain-like protein) necroptosis. In addition, RIPK1 induces prosurvival and proinflammatory responses via kinase-independent scaffolding functions (5). RIPK1 is recruited to the TNFR1 signaling complex together with TNFR1-associated death domain protein (TRADD),

the E3 ubiquitin ligases TNF receptor–associated factor 2 (TRAF2) and cellular inhibitors of apoptosis 1 (cIAP1) and cIAP2, and the linear ubiquitin chain assembly complex (LUBAC) (6, 7). RIPK1 contributes to the activation of NF-κB, but this function seems to be dependent on the cell types and experimental conditions studied (8–11). NF-κB signaling regulates immune and inflammatory responses and cell survival (12, 13) and is implicated in the pathogenesis of hepatitis and HCC (14, 15). Mice with liver parenchymal cell–specific (LPC-specific) ablation of NF-κB essential modulator (NEMO)/IκB kinase γ (IKKγ), the regulatory subunit of the IKK complex that is required for canonical NF-κB activation, developed spontaneously chronic hepatitis and HCC due to RIPK1 kinase activity–driven, FAS-associated death domain (FADD)/caspase-8–mediated hepatocyte apoptosis (16–19). In contrast, LPC-specific NF-κB deficiency did not cause spontaneous development of severe chronic liver disease and cancer, suggesting that NEMO regulates liver homeostasis by NF-κB–dependent and –independent functions (16).

Mice lacking RIPK1 specifically in LPCs (*Ripk1*^{fl/fl} *Alfp-Cre* mice, hereafter referred to as RIPK1[LPC-KO] mice) did not develop spontaneous liver disease, showing that RIPK1 is not required for normal liver homeostasis under steady-state conditions (16, 20–24). However, RIPK1[LPC-KO] mice were highly sensitive to concanavalin A–mediated (ConA-mediated) liver damage, which was partly induced by TNF-mediated hepatocyte apoptosis (24). Moreover, administration of LPS caused severe liver injury in RIPK1[LPC-KO] mice by inducing TNF-dependent hepatocyte apoptosis (20, 21). Interestingly, although LPC-specific deficiency of either RIPK1

Trieu My Van

Weisshausstr. 17, 50939 Cologne, Germany
tvan1@uni-koeln.de
+49 221 47884361
Linkedin: Trieu My Van
German, March 15, 1989

University Education

April 2013- May 2017	**Ph.D. thesis** titled 'The Role of RIPK1 signaling in liver injury and cancer', CECAD, Prof. Dr. Pasparakis, University of Cologne, Germany
April 2013	**Master thesis** titled 'The role of RIP kinases in liver homeostasis', CECAD, Prof. Dr. Pasparakis, University of Cologne, Germany **(Grade 1.4, excellent)**
September 2011	**Bachelor thesis** titled 'MicroRNA expression profiling during brown adipocyte differentiation', Institute for Genetics, Prof. Dr. Brüning, University of Cologne, Germany **(Grade 1.6, very good)**

Internships

July 2012	'Generation of GST-tagged RFC-1 peptides and characterization of polK-1 mutants and PCN1, RFC1 RNAi', Institute for Genetics, Prof. Dr. Schumacher, University of Cologne, Germany
February 2012	'Generation of antiserum', Institute for Genetics, Prof. Dr. Schumacher, University of Cologne, Germany
September 2011	Institute for Genetics, Prof. Dr. Pasparakis, University of Cologne, Germany
March 2011	'The adaptive immune system and the effects of superantigenes on the adaptive immune system', Institute of Molecular Medicine and Experimental Immunology, Dr. Andreas Limmer, University hospital Bonn, Germany

---

Publications

Van TM, Polykratis A, Straub BK, Kondylis V, Papadopoulou N, Pasparakis M, Kinase-independent functions of RIPK1 regulate hepatocyte survival and liver carcinogenesis. J Clin Invest. 2017 Jun 19. pii: 92508. doi: 10.1172/JCI92508.

Lin J, Kumari S, Kim C, **Van TM**, Wachsmuth L, Polykratis A, Pasparakis M, RIPK1 counteracts ZBP1-mediated necroptosis to inhibit inflammation., Nature. 2016 Dec 1;540(7631):124-128. doi: 10.1038/nature20558.

Oliverio M, Schmidt E, Mauer J, Baitzel C, Hansmeier N, Khani S, Konieczka S, Pradas-Juni M, Brodesser S, **Van TM**, Bartsch D, Brönneke HS, Heine M, Hilpert H, Tarcitano E, Garinis GA, Frommolt P, Heeren J, Mori MA, Brüning JC, Kornfeld JW., <u>Dicer1–miR-328–Bace1 signalling controls brown adipose tissue differentiation and function</u>, Nat Cell Biol. 2016 Mar;18(3):328-36. doi: 10.1038/ncb3316.

Kondylis V, Polykratis A, Ehlken H, Ochoa-Callejero L, Straub BK, Krishna-Subramanian S, **Van TM**, Curth HM, Heise N, Weih F, Klein U, Schirmacher P, Kelliher M, Pasparakis M., <u>NEMO Prevents Steatohepatitis and Hepatocellular Carcinoma by Inhibiting RIPK1 Kinase Activity-Mediated Hepatocyte Apoptosis.,</u> Cancer Cell. 2015 Nov 9;28(5):582-98. doi: 10.1016/j.ccell.2015.10.001.

Polykratis A, Hermance N, Zelic M, Roderick J, Kim C, **Van TM**, Lee TH, Chan FK, Pasparakis M, Kelliher MA., <u>Cutting edge: RIPK1 Kinase inactive mice are viable and protected from TNF-induced necroptosis in vivo.,</u> J Immunol. 2014 Aug 15;193(4):1539-43. doi: 10.4049/jimmunol.1400590.

Academic Fellowship

2013-2016	Full Ph.D. scholarship of the 'Cologne Graduate School of Ageing Research' (12 out of 400 applicants)

Scientific Conferences

Oral Presentations	- CECAD's 5th annual PhD/Post Doc Retreat, January 2016, Trier, Germany - CECAD's 4th annual PhD/Post Doc Retreat, March 2015, Maastricht, Netherlands
Poster presentation	- Keystone Symposia, Cell Death and Inflammation, April 2017, Dublin, Ireland - Cell Death, Inflammation and Immunity, May 2016, Crete, Greece - Cell Symposia: Cell death and immunity, November 2015, Berkeley, USA

Certified Courses and Soft Skill Courses

Science-related training

2016	- Short course on "Managing R&D Projects" - Short Course on "Entrepreneurial Introductory Translational Research (EITR)
2014	- Microbiology and Forensic Science, Open2Study - Biostatistics, Brain4hire, Cologne
2013	- Felasa B course, Cologne

Soft skill training

2015	- Negotiation and Conflict Resolution, Open2study - Figure making, Brain4hire, Cologne - Scientific writing, Dr. Ruth Willmott, Cologne - Principles of Project Management, Open2study

2014	- Carrier development training I-III, Dr. Ruth Willmott, Cologne
	- Scientific presentation, Dr. Ruth Willmott, Cologne
	- Poster presentation, Dr. Ruth Willmott, Vienna
	- PowerPoint presentation, Dr. Ruth Willmott, Cologne

Standard Methods and specialized techniques

| **Microbiological methods** | - Competent cell preparation and transformation |

DNA-specific	- DNA Isolation from cells and tissues
	- PCR
	- DNA cloning techniques

| **RNA-specific** | - RNA isolation from cells and tissues |
| | - qRT-PCR |

| **Protein-specific** | - Protein isolation from cells and tissues |
| | - Western Blot |

Cell/tissue-specific	- Isolation and culturing of primary hepatocytes
	- Isolation and culturing of keratinocytes
	- Isolation and differentiation of BMDMs
	- Isolation and culturing of primary MEFs
	- Cell cytotoxity tests (Neutral red, WST, LDH, PI staining)
	- Histopathological analysis (cutting and various stainings of liver, skin, lung and gut)

***In vivo*-specific**	- DEN-induced carcinogenesis
	- Glucose and Insulin-Tolerance test
	- Cheek Bleeding
	- Organ preparation (liver, skin, gut)

| **Microscopy** | - confocal microscopy |

Work-related Responsibilities

Supervision	Medical Student between March- May 2016
	Master Student between March- May 2016
	Medical Student between June - August 2014
	Bachelor Student between May- September 2013

| **Teaching** | Master practical course titled 'Mouse genetics', 20 Students for one week, July 2015 and 2016 |

Professional Membership

| **Since October 2015** | First of board of Management of btS Cologne e.V. |
| **Since March 2014** | Biotechnological student initiative (btS) Cologne e.V. |

Organizing Skills

| **March- November 2015** | -'Cologne graduate school of ageing research' Symposium, fund raiser |

March 2015- present	- Lecture Series for multiple biotech presentations in collaboration with btS Cologne

Languages

German	native speaker, bilingual
Vietnamese	native speaker, bilingual
English	fluent, written and oral
Latin	basic ('*Großes Latinum*')

Computer Skills

Operating systems	Windows XP/7, MAC OS
Software	MS office, Endnote,
Data analysis	Prism, Fiji

Trieu My Van   **Cologne, June 2017**